CUKUROVA UNIVERSITY

INSTITUTE OF NATURAL AND APPLIED SCIENCES

MSc THESIS

Detection Of Abnormal Skin Tissues With Impedance Mapping Approach Using EIT Techniques

Büşra OĞUZHAN

Biomedical Engineering Department

August, 2024

CUKUROVA UNIVERSITY

INSTITUTE OF NATURAL AND APPLIED SCIENCES

MSc THESIS APPROVAL

Detection Of Abnormal Skin Tissues With Impedance Mapping Approach Using EIT Techniques

---

Büşra OĞUZHAN

Biomedical Engineering Department

This Master's Thesis was evaluated by the following Jury Members on 16/08/2024 and was approved by unanimity / ~~majority~~ of votes.

Jury : Asst. Prof. Dr. Mustafa İSTANBULLU (Advisor) ……

: Prof. Dr. Mutlu AVCI ……

: Asst. Prof. Dr. Abdurrahman Özgür POLAT ……

This Thesis was written in the Department of Biomedical Engineering, Institute of Natural and Applied Sciences.
Thesis Number:

Prof. Dr. Sadık DİNÇER
Director
Institute of Natural and Applied Sciences

This work was supported by the Scientific Research Project Unit of Çukurova University.
Project ID: FYL-2022-15575

CONTENTS

CUKUROVA UNIVERSITY
INSTITUTE OF NATURAL AND APPLIED SCIENCES

MSc THESIS

Detection Of Abnormal Skin Tissues With Impedance Mapping Approach Using EIT Techniques

Büşra OĞUZHAN

Advisor: Assist. Prof. Dr. Mustafa İSTANBULLU

Department of Biomedical Engineering

ABSTRACT

The skin is an organ in the body that is in direct contact with the external environment and is most exposed to harmful external effects. Harmful effects cause abnormal tissue formation that can grow uncontrollably and undesirably on the skin. Early diagnosis and monitoring of these abnormal tissues, which exhibit different electrical properties than healthy skin tissue, are crucial. Electrical Impedance Tomography is one of the methods used for visualizing these abnormal tissues. This thesis presents an electrical impedance-based measurement and imaging system developed for the detection of abnormal tissues formed in the skin. Before experimental studies, the system was simulated on platforms such as COMSOL MULTIPHYSICS and EIDORS. A resistive phantom model representing healthy and abnormal tissue-containing skin models was created for the experimental study. A novel planar electrode array containing 32 electrodes in a circular arrangement was integrated with the electronic measurement system harware. The data obtained from the measurement was used in the image generation stage. It seeks to construct a high-resolution and precise image of the abnormal tissue from the data obtained from the proposed novel electrode design. Compatibility of simulation and experimental study results indicate that the proposed system could detect the location of abnormal tissue on the skin with high accuracy. The proposed system enables non-invasive, comfortable, and low-cost detection of abnormal tissues in the skin using an electrical impedance-based imaging technique.

Keywords: EIT, abnormal skin tissue detection, resistive phantom, EIDORS, COMSOL

ÇUKUROVA ÜNİVERSİTESİ
FEN BİLİMLERİ ENSTİTÜSÜ

YÜKSEK LİSANS TEZİ

EIT Tekniklerini Kullanarak Empedans Haritalama Yaklaşımı İle Anormal Cilt Dokularının Tespiti

Büşra OĞUZHAN

Danışman: Dr. Öğr. Üyesi Mustafa İSTANBULLU

Biyomedikal Mühendisliği Anabilim Dalı

ÖZ

Cilt yüzeyi dış ortamla doğrudan temas halinde olan ve zararlı dış etkilere en çok maruz kalan organdır. Zararlı etkiler ciltte istenmeyen ve kontrolsüz çoğalabilen anormal doku oluşumuna sebep olmaktadır. Sağlıklı cilt dokusundan farklı elektriksel özellikler sergileyen bu istenmeyen dokuların erken teşhisi ve takibi oldukça önemlidir. Elektriksel empedans tomografisi bu farklılaşmış dokuların görüntülenmesine yönelik kullanılan yöntemlerdendir. Bu tez, ciltte oluşan farklılaşmış dokuların tespitine yönelik geliştirilen elektriksel empedans temelli ölçüm ve görüntüleme sistemi sunmaktadır. Sistem, deneysel çalışmalar yapılmadan önce COMSOL MULTIPHYSICS ve EIDORS gibi platformlarda simüle edilmiştir. Deneysel çalışma için sağlıklı ve anormal doku bulunduran cilt modellerini temsil eden rezistif bir phantom modeli oluşturulmuştur. Özgün bir şekilde tasarlanan halkasal düzendeki 32 elektrotlu ölçüm sistemi elektronik donanım kısmı ile entegre edilmiştir. Ölçüm sonucu elde edilen veriler görüntü oluşturma aşamasında kullanılmıştır. Önerilen özgün elektrot tasarımı ile elde edilen verilerden anormal doku görüntüsünün yüksek çözünürlükte ve doğrulukta oluşturulması amaçlanmıştır. Simülasyonlardan ve deneysel çalışmalardan elde edilen sonuçlar karşılaştırılmış ve önerilen sistemin ciltte oluşan anormal bir dokunun yerinin tespitini yüksek doğrulukta yapabildiği sonucuna varılmıştır. Önerilen sistem, elektriksel empedans tabanlı görüntüleme tekniği ile ciltte oluşan anormal dokuların non-invaziv, konforlu ve az maliyetli olarak teşhisine olanak tanımaktadır.

Anahtar Kelimeler: EIT, anormal cilt doku tespiti, rezistif fantom, EIDORS, COMSOL

GENİŞLETİLMİŞ ÖZET

Ciltte oluşan anormal dokuların teşhisi ve analizi için invaziv olmayan tekniklerin geliştirilmesi, geleneksel biyopsi işlemlerininin konforsuz ve hasta için ağrılı bir süreç olduğu düşünülürse, tıbbi teşhislerde oldukça önemlidir. Cerrahi müdahaleye olan ihtiyacı ortadan kaldıran non-invaziv teşhis yöntemleri optik, fotodinamik, termal, ultrasonik ve elektriksel temellere dayanır. Bunlar arasında, Elektriksel Empedans Spektroskopisi (EIS) ve Elektriksel Empedans Tomografisi (EIT) gibi teknikler, yüksek hassasiyetleri, düşük maliyetli olmaları ve hasta konforu açısından bakıldığında önemli bir umut vadetmektedir.

EIS, farklı elektrot tasarımlarına sahip ölçüm sistemleri kullanılarak elektriksel biyoempedansı ölçen bir tekniktir. Bu yöntem, sağlıklı ve farklılaşmış dokular arasındaki elektriksel farklılığı tespit ederek cildin elektriksel özellikleri hakkında bilgi verir. Öte yandan EIT, ise yine elektriksel yöntemleri kullanarak organların veya dokuların tomografik görüntülerini elde etmeye yarayan bir tekniktir. Geleneksel bilgisayarlı tomografi görüntüleme yöntemleriyle karşılaştırıldığında, EIT, iyonlaştırıcı olmayan, radyasyon içermeyen, hızlı, taşınabilir ve az maliyetli bir yöntemdir. Bu özellikler, tıbbi ve biyomedikal mühendislik uygulamalarında yeni araştırma alanları açarak yenilikçi tanı teknikleri için önemli potansiyeller sunmaktadır.

Bu tezin temel bölümleri elektriksel empedansa dayalı görüntüleme tekniklerinin anlaşılmasını amaçlamaktadır. Cerrahi işlem gerektiren teşhis yöntemlerinin konforsuz ve ağrılı bir süreç içerdiği göz önünde bulundurulduğunda non-invaziv ve oldukça kolay teşhis sunan bu görüntüleme tekniği oldukça önemlidir. Tıbbi teşhisin daha güvenilir ve yüksek doğrulukta sonuçlar vermesi için elektriksel temelli bu sistemin kapsamında kullanılan tekniklerin geliştirilebilir olması bu çalışma için en önemli noktadır.

Tezin giriş kısmı cilt dokusunun yapısını ve elektriksel özelliklerini genel hatlarıyla vurgulamıştır. Bu kısımda sağlıklı ve farklılaşmış cilt dokularının elektriksel karakteristikleri, elektriksel empedans görüntüleme sistemi, önerilen sistemin tasarımı, donanımı ve bu sistemin simüle edileceği programlar ile ilgili ön bilgiler verilmiştir.

Bölüm 2, EIT tekniğinin kullanıldığı önceki çalışmalar ile tezin hedeflerini vurgulamak adına karşılaştırmalı genel bir bakış açısı sunmaktadır. EIT tekniği ile vücutta hangi organların ne amaç ile görüntülendiği ve tasarlanan çeşitli elektrot yapılarının kısa bilgilerini içeren ölçüm sistemleri de vurgulanmıştır. Kullanılan ölçüm sistemleri ve önerilen elektrot tasarımlarının özgünlüğü elde edilecek verilerin sayısını, doğruluğunu ve hassasiyetini etkilemektedir. Doğru ve tutarlı bir şekilde elde edilen veriler ise oluşturulacak görüntülerin çözünürlüğünün daha kaliteli olmasını sağlamaktadır. Dolayısıyla doku ve organ görüntülemesinin kalitesi ise yapılacak olan teşhis için daha güvenilir sonuçlar alınmasına olanak tanımaktadır. Bölüm bu anlamda EIT alanındaki çalışmaların bazı eksik ve araştırmaya ihtiyaç duyulan bölümlerini vurgulamayı amaçlamaktadır.

Bölüm 3, cildin sağlıklı ve patolojik durumlarda sergilediği elektriksel özellikleri incelemeyi hedeflemektedir. Bu bölümde öncelikle cildin fizyolojik yapısı daha sonra ise cildin elektriksel özellikleri hakkında bilgiler verilmiştir. Bu elektriksel özelliklerin farklı fizyolojik koşullarda, değişen frekanslarda farklı tepkiler gösterdiği vurgulanmıştır.

Bölüm 4, temel olarak EIT'nin çalışma prensibini anlatmaktadır. Elektriksel empedans tomografisini oluşturan temel kısımlar hakkında bilgiler verilmiştir. Daha sonra cilt üzerinden elde edilen elektriksel empedans ölçüm tekniği, elektrot tasarımları ve görüntü oluşturma teknikleri ayrıntılı bir şekilde vurgulanmıştır. Tezin sonraki bölümlerinin daha iyi anlaşılabilmesi için bu ön değerlendirmeler oldukça önemlidir.

Bölüm 5, COMSOL Multiphysics programı ile ilgili genel bilgiler sunmaktadır. Bu bölüm programın temel özellikleri ve ara yüzü hakkında kısa bilgiler içermektedir. Elektriksel Empendas Tomografisinin uygulanabilirliği**,** çeşitli fiziksel modellerin tasarlanmasına ve üzerinde elektriksel, termal, kimyasal ve yapısal analizler yapılmasına olanak tanıyan COMSOL Multiphysics programı kullanarak gözlemlenmiştir. Bu simülasyon programında cildin fizyolojik ve elektriksel özellikleri göz önünde bulundurularak gerçeğe yakın, katmanlı bir cilt modeli tasarlanmıştır. Daha sonra cilt yüzeyinden alınacak ölçümler için özgün bir elektrot modeli tasarlanmıştır. Bu elektrot modeli halkasal düzende iç içe geçmiş 32 adet elektrot içermektedir. Yüksek sayıda elektrotlarlayapılan ölçümler veri sayısını artıracak ve dolayısıyla oluşturulacak görüntünün çözünürlüğü de artacaktır. Böylece literatürde daha az sayıda elektrot ile yapılmış çalışmalardan elde edilen sonuçlar ile bu tez kapsamında elde edilen sonuçlar karşılaştırmaya açık olacaktır. Daha sonra bir sonraki aşamada kullanılacak ölçüm sistemi tanımlanmıştır. Önerilen ölçüm sistemi, tasarlanan özgün elektrot düzenine ek olarak, sinüzoidal bir uyartım işaretinin oluşturulması, gerilim kuvvetlendiricileri, gerilim kontrollü akım kaynağı, çıkış katı kuvvetlendiricisi ve enstrumantasyon kuvvetlendiricilerinden oluşmaktadır. 32 adet elektrot içeren elektrot dizisinde ise elektrotlardan iki tanesi akım enjekte edilecek elektrot çifti iken diğer tüm elektrotlar gerilim ölçüm elektrotlarıdır. Detayları ilgili bölümlerde verilecek olan bu özgün elektrot düzeni ve ölçüm yöntemi cilt yüzeyinin 360° taranmasını sağlamaktadır. Önerilen ölçüm sistemini test etmek amacıyla simülasyon programlarında sağlıklı cilt dokusu ve içinde farklılaşmış bir doku parçası olan hasta cilt dokusu modellenmiş ve önerilen elektrot düzeni ile ölçümler alınması sağlanmıştır. Sonuçta hem sağlıklı hem de hasta dokulardan 3D, 2D, 1D grafikler elde edilmiştir. Bu program tasarlanan sistemin deneysel çalışması yapılmadan önce sistemin doğruluğunu ve çalışabilir olmasının kontrolünü sağlaması açısından oldukça önemlidir.

Bölüm 6, EIT verilerini analiz etmek ve yeniden yapılandırmak amacıyla kullanılan MATLAB tabanlı EIDORS açık kaynaklı yazılım paketi ile ilgili temel bilgiler içermektedir. Bu paket kullanıcıların kendi tasarladıkları elektriksel empedans temelli sistemleri test etmeleri, özelleştirmeleri ve geliştirebilmeleri için olanak tanımaktadır. EIDORS'ta EIT çalışmalarını simüle etmek için sistem modelleme, elektrot konfigürasyonları, elektriksel akım tanımlamaları ve görüntü

yapılandırılmasında kullanılacak çeşitli yöntemler bu bölümde açıklanmıştır. Tasarlanan sistemin EIT özelinde çalışmalar sunan bir simülasyon programında da simüle edilmesi sistemin çalışabilirliği ve doğruluğunun yorumlanması için oldukça önemlidir.

Bölüm 7, tasarlanan ve iki farklı simülasyon programında simüle edilen elektriksel empedans yaklaşımlı görüntüleme sistemini deneysel olarak gerçekleme aşamalarını içermektedir. Öncelikle üzerinde ölçüm yapılacak sağlıklı, anormal dokuya sahip ve çok katmanlı yapıdaki cilt modellerini temsil eden rezistif fantom modelleri oluşturulmuştur. Modelde kullanılan direnç değerleri ve direnç yerleşim düzeninde yapılan farklılıklar ile gerçeğe yakın cilt modeli oluşturulması bu bölümün en önemli noktalarından bir tanesidir. Modeller ve tasarlanan elektrot düzeni PCB tekniği ile basılmıştır. Daha sonra diğer bir aşama olan elektronik donanım bünyesinde kullanılan devreler ile birlikte detaylı olarak açıklanmıştır. Oluşturulan cilt modeli fantomları ile yüzeye sabit akım sağlayacak elektronik donanım kısmı entegre edilmiştir. Belirlenen ölçüm yöntemine göre elde edilen veriler dijital ortamda kaydedilmiştir. Bu bölüm çalışmanın deneysel ortamda gerçeklenebilir olduğunu göstermektedir.

Bölüm 8, COMSOL Multiphysic, EIDORS ve oluşturulan rezistif fantomaların deneysel çalışmaların sonuçlarından elde edilen verilerin 3D, 2D ve 1D grafiklerinden, karşılaştırmalardan ve yorumlarından oluşan sonuç bölümüdür.

Sonuç olarak bu tezde, ciltte oluşan anormal dokuların tespitini yapabilecek EIT tabanlı, non-invaziv bir ölçüm sistemi üzerine çalışılmıştır. Elde edilen sonuçlar cerrahi müdahele gerektirmeyen bu yöntemin tıbbi teşhis ve takip süreçlerinde önemli bir rol alacağını göstermektedir. Çalışmada EIT sisteminin ciltte oluşan anormal dokuların tespiti için geliştirilen elektrot konfigürasyonu ve cilt modelleme tekniğinin özgünlüğü vurgulanmıştır. Önerilen tasarımın COMSOL ve EIDORS gibi farklı platformlarda modellenmesi ve simüle edilmesi çalışmanın önemli bir bölümünü oluşturmaktadır. Bu çalışmalar sistemin doğruluğunu ve tutarlılığını gözlemlemeye olanak tanımaktadır. Ayrıca çalışmanın diğer bir bölümü olan deneysel çalışmalar ve sonuçları için karşılaştırılabilir bir alan yaratmaktadır. Simüle edilen sistem verileri ile gerçek deneysel veriler karşılaştırıldığında ölçüm sonuçlarının tutarlı ve hassas bir tespit yaptığı görülmüştür. Sonuç olarak önerilen özgün elektrot modeli ile entegre edilen ölçüm sistemi, EIT tekniği için yenilikiçi ve güvenilir bir tıbbi tanı yöntemi sunmaktadır.

ACKNOWLEDGEMENTS

I would like to express my endless gratitude to my valuable advisor, Dr. Mustafa İSTANBULLU, who has increased my interest in academic studies since the first day I registered for this program, who has motivated me even in the most hopeless moments with his kind and patient nature, who has found original and logical solutions to every problem that occurs, who is always helpful and open to new ideas. I am grateful for the care and efforts he has shown to help me achieve my goals. I look forward to doing practical work with the valuable information I have learned from you on this path.

I would like to express my gratitude to my valuable teacher, Dr. Dilek SÖNMEZER AÇIKGÖZ, who has always been by my side, given me morale and motivation, has never withheld her help, and has enabled me to register for this program.

I would like to thank our valuable head of department, Prof. Dr. Mutlu AVCI, who guided us when we needed his helpful information.

I would like to thank my family, Hatice-Ahmet OĞUZHAN and my sisters Fatmagül, Beyza, and Betül, who stood behind me in every decision I made, who helped me get back on my feet when I was tired and started everything again and who always made me feel their support at every stage of my education.

I would like to thank my dear friends Esra YÜCEL, Elif Tuğba DEVECİ BAĞLAR, and Asiye ŞAHİN KOYUNCU for their friendship and support.

I dedicate this thesis to those who lost their lives in the February 6 Kahramanmaraş earthquake.

We all have both a bright and a dark side. What matters is which one we choose. This is what makes us who we are.

LIST OF TABLES

LIST OF FIGURES

SYMBOLS AND ABBREVIATIONS

UV	: Ultraviolet
COMSOL	: Computer Solution
EIDORS	: Electrical Impedance and Diffuse Optical Reconstruction Software
EIT	: Electrical Impedance Tomography
EIS	: Electrical Impedance Spectroscopy
MATLAB	: Matrix Laboratory
3D	: 3 Dimensional
2D	: 2 Dimensional
1D	: 1 Dimensional
DNA	: Deoxyribonucleic Acid
PCB	: Printed Circuit Board
ADC	: Analog to Digital Converter
SVM	: Support Vector Machine
ACE1	: Active Complex Electrode1
UST	: Ultrasonic Tomography
CO	: Cardiac Output
SV	: Stroke Volume
ECG	: Electrocardiogram
GS	: Gamma Scintigraphy
MIX	: Magnitude Index
IMIX	: Imaginary-part Index
FEM	: Finite Element Model
MRI	: Magnetic Resonance Imaging
AC	: Alternative Current
DC	: Direct Current
TUT	: Test Under Tissue
CT	: Computerized Tomography
FEA	: Finite Element Analysis
CEM	: Complete Electrode Model
CG	: Conjugate Gradient
TR	: Tikhonov Regularization
SVD	: Singular Value Decomposition
GREIT	: Graz consensus Reconstruction algorithm for EIT
TV	: Total Variation
PDEs	: Partial Differential Equations

EAGLE : Easy Applicable Graphical Layout Editor

PSPICE : Personal Simulation Program with Integrated Circuit Emphasis

TCAD : Technology Computer-Aided Design

VCCS : Voltage to Current Converter Source

DDS : Direct Digital Synthesizer

PIC : Programmable Integrated Circuit

SPI : Serial Peripheral Interface

BJT : Bipolar Junction Transistor

MOSFET : Metal Oxide Semi-conductor Field Effect Transistor

NPN : Negative-Positive-Negative

PNP : Positive-Negative-Positive

INA : Instrumentation Amplifiers

ES : Electrical Study

1. INTRODUCTION

The skin is the most exposed organ to environmental factors, such as ultraviolet (UV) radiation, chemical agents, and physical effects. These exposures can lead to various adverse effects on the skin, influencing both its health and surface appearance. The skin's structure comprises multiple layers with varying thicknesses and cellular compositions, each playing a critical role in maintaining the skin's overall function and resilience. Mutations in the DNA of cells within these layers can result in the formation of undesirable and rapidly proliferating abnormal lesions, which may be harmful or benign. The ability to accurately diagnose and analyze these lesions is essential for effective treatment and management.

Healthy and abnormal skin tissues exhibit distinct electrical properties. Abnormal skin tissue, characterized by a higher cell density and increased cytoplasmic fluid content compared to healthy skin tissue, exhibits lower electrical resistance due to the conductive nature of the cytoplasmic fluid. This electrical disparity is a key diagnostic marker, as it enables the differentiation between healthy and abnormal tissues. Understanding and leveraging these electrical properties can significantly enhance the accuracy and efficacy of non-invasive diagnostic techniques.

Traditional biopsy processes, even though effective in diagnosing skin conditions, are invasive and associated with inherent risks and discomforts for patients. Consequently, the development and utilization of non-invasive measurement techniques have gained significant attention. These non-invasive techniques include optical, photodynamic, thermal, ultrasonic, and electrical methods, each offering unique advantages and eliminating the need for surgical intervention. Among these, electrical impedance-based techniques such as Electrical Impedance Spectroscopy (EIS) and Electrical Impedance Tomography (EIT) have shown considerable promise due to their precision and practicality.

EIS is a technique that measures electrical bioimpedance using various electrode configurations placed on the skin. This method provides valuable data on the electrical properties of skin tissue, enabling the distinction between healthy and abnormal tissues. EIT, on the other hand, utilizes electrical methods to achieve tomographic imaging of organs or tissues. Compared to traditional computerized tomographic imaging methods, EIT offers several advantages, including being non-ionizing, radiation-free, fast, portable, and cost-effective. These attributes have opened new research areas in medical and biomedical engineering applications, expanding the potential for innovative diagnostic and therapeutic techniques.

This study aims to non-invasively obtain the impedance values of the skin from the skin surface then detect the abnormal tissues in the skin by analyzing the impedance data. The research is structured in multiple phases to ensure comprehensive and accurate results. In the initial phase, a novel electrode array is designed to ensure high precision and accuracy in the measurements obtained

from the tissue. This electrode array is produced as a printed circuit board (PCB), leveraging advanced manufacturing techniques to achieve the necessary specifications.

The second stage selects a specific electrode pair in the electrode array, applies a constant alternating current to these electrodes, and measures the resulting voltage. By applying Ohm's law, the impedance of the tissue under test will be calculated as a function of frequency. The collected data will then be digitized using an analog-to-digital converter (ADC) for further analysis. This step is crucial for ensuring that the data is accurately captured and stored for subsequent processing and interpretation.

In the final phase, the impedance difference data between healthy and abnormal tissues will be utilized to achieve three-dimensional imaging through reconstruction techniques. This approach aims to provide a detailed and accurate representation of the tissue structure, enabling more precise diagnosis and analysis of skin conditions. By comparing the electrical properties of healthy and abnormal tissues, this method can identify abnormalities and provide insights into the underlying causes of various skin conditions.

The development and application of non-invasive techniques for the diagnosis and analysis of skin tissues represent a significant advancement in medical diagnostics. This study's approach to utilizing electrical impedance measurements and three-dimensional imaging aims to provide a comprehensive and accurate method for identifying and analyzing differentiated skin tissues. By improving the precision and accessibility of these diagnostic methods, this research has the potential to greatly enhance clinical outcomes and patient care in dermatology and related fields. Furthermore, the non-invasive nature of these techniques ensures that patients experience minimal discomfort and risk, making them a preferred option for both clinicians and patients.

In summary, the innovative use of electrical impedance-based techniques for the non-invasive diagnosis and analysis of skin tissues offers significant potential for improving the detection and treatment of various skin conditions. This research not only aims to enhance the accuracy and efficacy of current diagnostic methods but also seeks to pave the way for future advancements in medical technology and patient care. Through meticulous design, rigorous testing, and comprehensive analysis, this study aspires to contribute valuable knowledge and tools to the field of dermatology and biomedical engineering.

2. PRELIMINARY WORK

Studies using electrical impedance techniques in the literature are directed towards monitoring brain activities, pulmonary ventilation, cardiac activities, and movements of the intestines and stomach, as well as the diagnosis of breast and skin cancers.

The resistant structure of the skull poses challenges for measuring intracranial impedance. Xuetao Shi and colleagues (Shi et al., 2018) developed a digital synthesis method to obtain higher precision data for detecting brain activities, creating a physical brain phantom for this purpose.

Barry McDermott and colleagues (McDermott et al., 2018) investigated Support Vector Machine (SVM) classifiers for detecting brain hemorrhages. They designed a two-layer head model with a hemorrhage and used electrodes placed on the skull to train and test linear SVM classifiers.

Michelle M. Mellenthin and colleagues (Mellenthin et al., 2019) presented the design of the Active Complex Electrode (ACE1) EIT system to obtain thoracic EIT chest ventilation and perfusion images. Unlike other studies in the literature, this system differs in terms of typical frame rates, frequencies of injected currents, and current patterns used.

The limited spatial resolution and the low number of electrodes leading to low resolution are among the disadvantages of EIT. Manuchehr Soleimani and colleagues (Soleimani and Rymarczyk, 2023) proposed Ultrasonic Tomography (UST) for pulmonary monitoring as a solution to this problem.

Measuring cardiac output (CO) and stroke volume (SV) non-invasively with EIT does not yield sufficient accuracy. Fabian Braun and colleagues (Braun et al., 2018) examined the effect of advanced image reconstruction approaches on EIT measurement accuracy, concluding that the main challenge in EIT-based SV monitoring is due to factors such as electrode contact impedance, lung, and heart conductivity.

Sofiene Mansouri (Mansouri, 2020) presented a comparison between ECG and bioimpedance measurement methods for non-invasive measurement of cardiac output using peripheral electrical impedance. He established a linear correlation between the two methods and found that the mean error of bioimpedance measurement in predicting cardiac output was 5.6%. EIT is highly effective in observing gastric emptying in patients receiving nasogastric liquid feeding.

Clare T. Soulsby and colleagues (Soulsby et al., 2006) aimed to compare gamma scintigraphy (GS) and EIT for measuring gastric emptying during nasogastric infusion, observing agreement between gastric emptying curves obtained from EIT and GS.

Marcos Gutierrez-Lopez and colleagues (Gutierrez-Lopez et al., 2019) proposed a new methodology based on electrical impedance for preclinical carcinoma localization in the breast, achieving measurements with electrodes arranged in a circular pattern around a breast phantom, resulting in an 83.33% success rate.

V. Cherepenin and colleagues (Cherepenin et al., 2001) designed a measurement system with 256 electrodes for the preliminary diagnosis of breast tumors, using the data obtained from measurements for image reconstruction and concluding that the system could be used for breast cancer diagnosis.

Some studies on skin cancer focus on distinguishing lesions on the skin from healthy tissue, while others aim to differentiate between benign and malignant lesions. Kamat and colleagues (Kamat et al., 2014) presented a portable bioimpedance measurement system using the AD5933 impedance converter, observing significant decreases in the MIX (magnitude) and IMIX (imaginary) values of tissue impedance in differentiated lesions compared to normal skin.

Peter Åberg and colleagues (Åberg et al., 2004) aimed to differentiate skin cancer from benign nevi using multi-frequency impedance spectra with a ring electrode model, showing that malignant melanoma could be distinguished from benign nevi with 100% sensitivity and 75% specificity, and non-melanoma skin cancers with 100% sensitivity and 87% specificity.

Hartinger and colleagues (Hartinger et al., 2012) designed an EIT system for skin cancer screening, developing a three-dimensional finite element model (FEM) of the skin to distinguish the electrical behaviors of malignant and benign lesions, and designing a 16-electrode handheld probe for the hardware component, finding significant correlation between simulation and hardware data.

The problem of low resolution due to the limited number of electrodes in EIT was addressed by Lu Yang and colleagues (Yang et al., 2023), who designed an EIT sensor with electrodes arranged in a circular pattern using a PCB, offering a solution to this problem.

Gurmeet Singh and colleagues (Singh et al., 2019) presented a system to improve resolution in EIT, proposing a multi-frequency electrical impedance system capable of generating real-time 2D images during continuous monitoring where impedance changes rapidly, concluding that the system design is suitable for clinical applications.

Ping Hua and colleagues (Hua et al., 1993) measured skin surface voltages by injecting current through an array of surface electrodes for EIT, using larger electrodes to reduce contact impedance, and employing FEM techniques to study the electrical distribution under the electrodes, finding that FEM models closely matched experimental values and could enhance image reconstruction performance for EIT.

Fred-Johan Pettersen and colleagues (Pettersen and Høgetveit, 2011) integrated an MRI scan of a human thigh into a simulation program (COMSOL MULTIPHYSICS) to calculate transfer impedance, defining the electrical properties of the tissue in the program, meshing, and simulating it, presenting the output data both numerically and graphically.

One issue with EIT is the lack of spatial sensitivity within the measured volume. Onic Islam Shuvo and Md. Naimul Islam (Shuvo and Islam, 2016) created a cylindrical phantom comprising homogeneous and inhomogeneous media, initially calculating spatial sensitivity for homogeneous media using simple geometric shapes analytically, and later using COMSOL MULTIPHYSICS

simulation program to present sensitivity analysis results based on FEM methods for inhomogeneous media, achieving successful results for the relevant region where sensitivity was maximized.

The studies in the literature generally focus on the imaging of different tissues or organs (lungs, heart, brain) using the EIT measurement method. Most recent studies aim to improve the resolution of obtained data, develop new methods to eliminate artifacts between the skin surface and electrodes, achieve image reconstruction using various FEM methods, or compare data obtained from experimental models with those from tissue models created in simulation environments. Although the studies to date demonstrate that the EIT measurement system is a viable alternative to non-invasive measurement techniques, further development is needed for its use in diagnosing various diseases. Considering the current increase in cancer cases, early diagnosis of cancer is crucial for initiating treatment processes earlier. There are studies in the literature that use or develop the EIT system for the diagnosis of breast, prostate, or skin cancer. Some of these studies involve the creation of actual experimental systems, while others utilize various simulation programs that allow for the modeling and electrical analysis of organs and tissues. The goal of these studies is to obtain higher precision data through the design differences of the created systems (such as the number of electrodes, electrode arrangement, measurement method).

3. THE SKIN

The skin is the largest organ in the human body in terms of weight and surface area. The skin provides homeostasis in the body. It regenerates when damaged and provides a protective effect against external threats. Being in direct contact with the external environment has given it a layered structure. This layered structure provides the skin with protective properties and an environment for various chemical reactions.

3.1. Structure of Skin

Skin is classified in three main ways: epidermis, dermis and subcutaneous tissue (hypodermis).

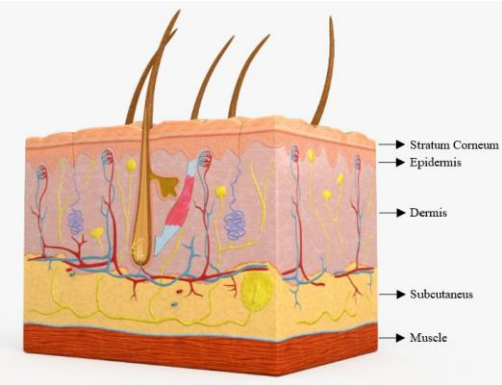

Figure 3.1. Layers of skin model

3.1.1. Epidermis

The epidermis is the uppermost layer of the skin and its thickness is approximately between 0.1 mm and 2 mm. The thickness of these layers varies depending on the part of the body. It consists of keratinocyte cells, a protein that provides resistance to the skin. Other cells found in greater density within the epidermis layer are as follows:

Stratum Corneum: It is the outermost layer of the epidermis. It is in direct contact with the external environment. It is approximately 0.02-0.03 mm thick. This layer consists of dead, flattened keratinocytes without nuclei. It prevents water loss by creating a protective barrier against environmental factors. It ensures that the layers below remain moist.

Melanocytes: They produce melanin, which gives the skin its color. Thus, they protect the skin from the harmful effects of ultraviolet (UV) radiation.

Langerhans Cells: They are a type of special white blood cells. They detect disease-causing cells and respond. These cells, which play an important role in the immune system response, protect the skin from infections.

Merkel Cells: Merkel cells, located in the basal layer of the epidermis, function as mechanoreceptors. They are associated with nerve endings.

Granstein Cells: These cells react exactly the opposite of the Langerhans cells. They prevent the skin from showing excessive sensitivity in the event of any immune defense.

3.1.2. Dermis

The dermis, which varies in thickness between 2 mm and 4 mm, acts as a skeleton for the skin, providing structural support and elasticity to the skin. Its lower layers consist of papillary and reticular layers.

Papillary Layer: It forms the upper layer of the dermis and is directly adjacent to the epidermis. It plays a role in the nutrient exchange between the epidermis and the dermis because it contains a large capillary network. It is associated with nerve endings and provides the sense of touch. It also contains plenty of elastic and collagen fibers. It also contains cells that respond to infection formation.

Reticular Layer: This layer, deeper than the dermis, has a network-like structure consisting of collagen and elastin fibers. It consists of dense and irregular connective tissue. The reticular layer provides strength and elasticity to the skin. Structures such as sweat glands, sebaceous glands and hair follicles are found in this layer.

3.1.3. Subcutaneous Tissue (Hypodermis)

As seen in Figure 3.1, subcutaneous tissue or hypodermis forms the deepest layer of the skin. It consists of loose connective tissue and fat. This layer acts as an insulating layer that protects the body against mechanical effects. The hypodermis also facilitates the movement of the skin on the structures in the lower layers.

3.2. Electrical Properties of Human Skin

The electrical properties of the skin are an integral part of its physiological functions and play an important role in various diagnostic and therapeutic applications. Electrical impedance, conductivity and permeability are the properties that constitute the electrical characteristics of the skin. These electrical properties of the skin show different responses depending on the frequency. Generally, the low-frequency region is affected by the extracellular environment. High frequencies are affected by the properties of the intracellular space. Since cell membranes have high capacitance, low-frequency and direct currents must pass around the cells, as seen in Figure 3.2. On the other hand, high-frequency currents can pass through cell membranes and other electronic barriers in the cell structure by polarization. The cell's internal and external environment changes like a simple capacitor, such as charged, uncharged and reversely charged. Therefore, the basic electrical properties of the tissue change as the frequency increases or decreases. (Aberg, 2004).

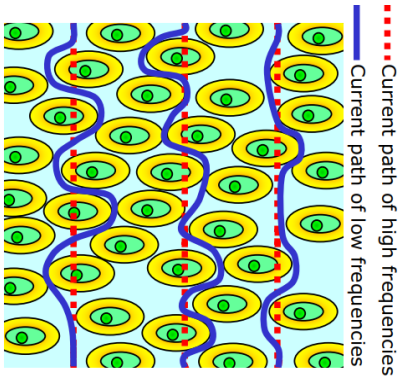

Figure 3.2. The path of current within the cell (Aberg, 2004)

3.2.1. Electrical Impedance

Electrical impedance is a measure of a material's resistance to electric current. The skin's electrical impedance is affected by factors such as skin moisture, skin layer thickness, and the properties of its cellular components. The Figure 3.3 shows the electrical equivalent model of the skin. Healthy skin is generally not very moist. This causes the skin to exhibit high impedance. The presence of insulating lipids in the skin is also one of the reasons for the skin's high impedance. The skin's electrical impedance varies with changes in humidity, temperature, or pathological conditions.

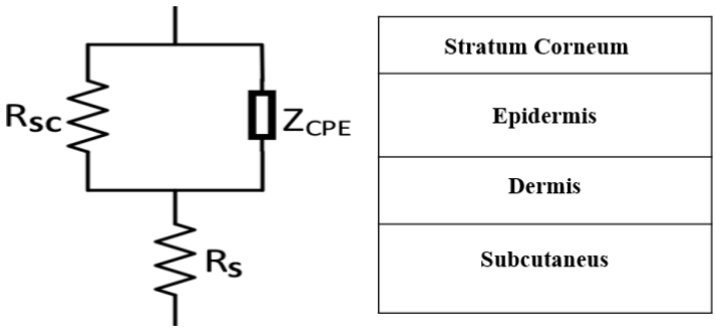

Figure 3.3. Electrical equivalent model of the skin

The electrical impedance decreases with increasing frequency; this situation is combined with the electrochemical properties of the skin and is expressed by regions called dielectric dispersion. These dispersions are shown in the Figure 3.4 with three major regions. α-dispersion is found in the frequency region between a few kHz-MHz. It generally represents the polarization characteristics of ionic molecules close to the membrane surface. Again, the frequency region between a few kHz and hundreds of MHz is expressed by β-dispersion and is related to structural changes and edema of cells. The region between MHz-GHz is γ-dispersion. It is affected by the conditions related to the dipole properties of polar molecules such as water. These three dispersions are classified as the main regions. However, especially considering that the electrical impedance of the skin has both real and imaginary parts, it is concluded that these three main distinctions are not completely separated and that there will be sub-region dispersions.

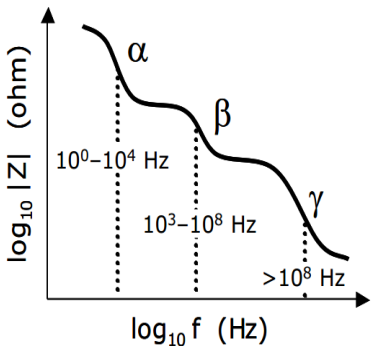

Figure 3.4. Frequency dependent dispersive properties of biological material (Aberg, 2004)

3.2.2. Electrical Conductivity

Conductivity is the opposite of impedance. It indicates the ability of a material to conduct electrical current. Increases in skin moisture content and conductive materials cause increased conductivity. This is used to assess skin health and detect abnormalities. These changes in conductivity are significant for bioimpedance-based diagnostic tools.

3.2.3. Electrical Permittivity

Permittivity refers to the ability of the skin to store and release electrical charge. This feature helps distinguish between healthy and abnormal tissues through changes in conductivity and permittivity.

3.3. Electrical Properties of Abnormal Human Skin Tissue

Tissues that exhibit abnormal and undesirable pathological properties in the skin exhibit different electrical properties compared to healthy skin. These differences serve as a litmus to diagnose abnormalities.

3.3.1. Impedance Changes in Pathological Conditions

The electrical properties of skin cancer or inflammatory abnormal tissues show different properties. For example, in tumors, the water density is quite high and their cellular components are differentiated compared to healthy tissue. This causes a lower impedance compared to normal skin. This change in impedance helps to distinguish malignant and benign lesions and to follow their progression.

3.3.2. Conductivity Variations

In pathological conditions such as inflammation, blood flow increases even more and edema occurs. This situation causes higher conductivity. As seen in Figure3.5, abnormal and healthy tissue show different properties at different frequencies. This change helps in the diagnosis and follow-up of inflammatory conditions and other abnormalities.

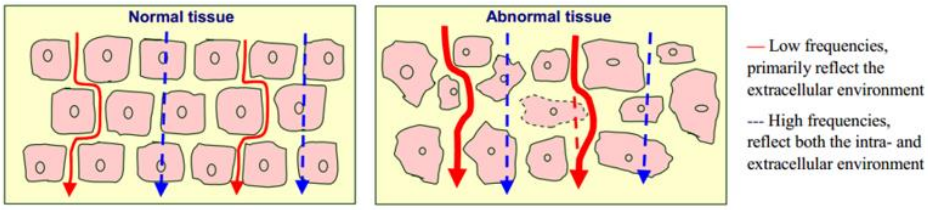

Figure 3.5. Current pathways in normal and abnormal tissue (Birgersson, 2012)

3.3.3. Permittivity and Tissue Analysis

The electrical conductivity of abnormal tissue in the skin is different from that of healthy tissue. These changes are observed. For example, abnormal tissue growth or inflammation can change the dielectric properties of the skin. Thus, these changes can be detected using electrical impedance imaging techniques. Understanding the structural and electrical properties of the skin is very important for developing accurate diagnosis and treatment techniques. Detailed examination of these properties provides alternative ways for non-invasive diagnostic methods. Thus, it allows disease detection and monitoring of disease progression.

4. ELECTRICAL IMPEDANCE TOMOGRAPHY

4.1. Introduction

Electrical Impedance Tomography (EIT) is an imaging technique used to create tomographic images of tissues inside the body using electrical impedance technique. This non-invasive method allows to follow physiological processes and visualize pathological conditions by evaluating the electrical properties of tissues. Advantages such as non-ionizing structure, portability and cost-effectiveness of EIT increase its preferability compared to traditional imaging techniques.

4.2. Method of Impedance Measurements

The basic principle of EIT is based on creating cross-sectional images by measuring the electrical impedance of the body or an organ. Impedance is defined as the resistance of a circuit to the flow of alternating current (AC). Impedance is a function of both resistance and reactance. In EIT, a series of electrodes are placed on the surface of the body or tissue. A small, alternating electric current is injected from the body surface through these electrodes. The resulting voltage distribution is then measured, and the impedance of the underlying tissues is calculated. The penetration of current through the skin and other biological material is related to frequency, the distance between the electrodes, the electrode size, and the physical properties of the examined tissue. In Figure 4.1, the depth of penetration of currents within the layers of the skin is roughly half the distance between the electrodes. In a double-layered structure, where the upper layer is less conductive and more capacitive than the lower layer, high frequencies penetrate deeper than low frequencies. (Aberg, 2004)

Electrode properties and their placement on the tissue affect the accuracy of impedance measurements. Therefore, electrode design is critical in an electrical impedance measurement system.

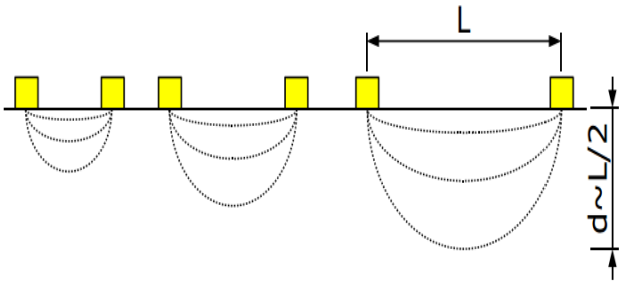

Figure 4.1. Depth of current penetration depend frequency (Aberg, 2004)

4.3. Electrode Configuration

The design of the electrodes plays an important role in the effectiveness and accuracy of EIT. Various electrode configurations are used according to some special conditions required for imaging:

Circular Arrangement: Electrodes are arranged in a circular pattern around the area of interest. This configuration is common for imaging cylindrical objects or body parts.

Array Arrangement: Electrodes are placed in a grid or array. This more complex arrangement provides detailed spatial resolution.

Flexible Arrangement: Used for irregularly shaped or dynamic surfaces (such as the body).

4.4. Data Collection

Data collection in EIT involves taking voltage measurements from multiple electrode pairs to capture positional changes in impedance. First, the EIT system is calibrated to ensure accurate and consistent measurements. Then, currents of different frequencies are sent from the electrodes to the body surface to create an impedance map of the body. The voltages obtained due to the currents of different frequencies sent from the different points where the electrodes are positioned are recorded. According to Ohm's law, impedance information is obtained from the current sent and the voltage obtained. Impedance data also includes magnitude and phase information.

4.5. Data Analysis

In EIT, data analysis involves processing impedance measurements to reconstruct the image. First, filtering and denoising steps are applied to improve the quality of the acquired data. Then, various algorithms are applied to transform impedance measurements into spatial distributions, and tissue properties such as conductivity and permittivity are estimated based on the impedance data. The following steps are aimed at reconstructing and enhancing the image.

4.6. Image Reconstruction

Image reconstruction is creating a visual of the internal tissue structure of the body based on the obtained impedance data. The back projection algorithms of X-ray CT inspire EIT image reconstruction. The image reconstruction process can be explained in a few simple steps, such as Algorithm Selection, Tomographic Imaging, and Visualization. Image reconstruction techniques are complex. Because the mathematical equations used in the algorithm must be better positioned and conditioned, this situation arises due to the Difference between the electrode to be measured and the reference center and the limited number of measurements, which limits the parameter estimates to be used in the image reconstruction. The algorithms used in EIT are divided into Absolute EIT and Difference EIT. Absolute EIT is a more complex problem due to the problems that may occur between body geometry and electrode shape and placement. On the other hand, Difference EIT is more stable since the errors between body geometry and electrode layout do not change as long as the difference measurements remain constant. In addition, being able to be expressed in a matrix format makes Difference EIT a more easily solvable problem.

The body has an internal conductivity distribution defined by the σ vector. With the help of some mappings, the x vector, a parameter defining σ, is estimated. The x parameter is usually at a lower spatial resolution than σ in the remote areas where the electrodes are positioned. $F(\sigma)$ estimates the measurements for a parameter value specified by the user for the Forward Problem. The measurement starts with an initial estimate of x_0, where x_{k+1} represents the iterative solution. In this case, estimating the measurement accuracy is not very specific. The error or data inconsistency is greater than the $y - F(\sigma)$ expression at this stage. Using this estimate and the error, the Δx update expressed as $x_1 = x_0 + \Delta x$ is repeated each time to reach the correct estimate. The update ends in the most optimal case. Based on the above explanations, the Figure 4.2 provides preliminary information for the image reconstruction stage.

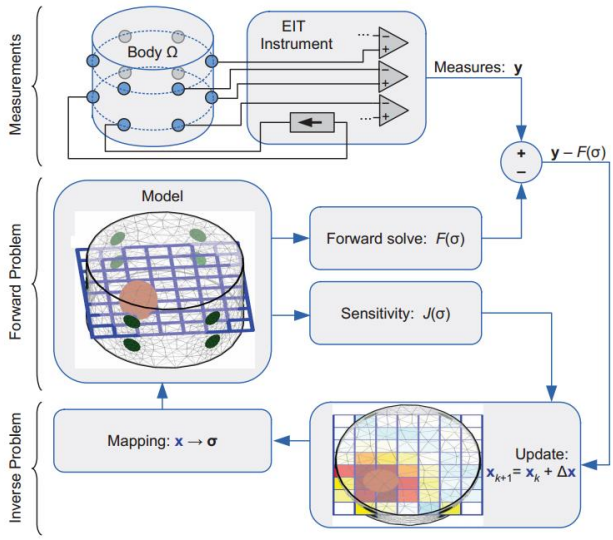

Figure 4.2. Schematic representation for image reconstruction (Holder, 2004)

4.7. Mathematic Models of EIT

The mathematical model used in EIT is related to the Forward and Inverse Model which will be explained in the following sections. This model expresses the relationship between the conductivity of points in a closed area and the corresponding potentials with some equations (Wu et al., 2021).

4.7.1. Maxwell's Equations

The current applied to the body with the electrodes creates an electromagnetic field. Maxwell's equations express the relationship between electric and magnetic fields. If **Ω** is defined as a closed region of three-dimensional space and **∂Ω** is defined as a finite subset of this field, then the conductivity of this field is σ. The scalar potential is **φ**, and the electric field is $\mathbf{E} = -\nabla\varphi$. The current density is $\mathbf{J} = -\sigma\nabla\varphi$, which is the continuity version of Ohm's law. If there are no internal current sources, this continuity is expressed by Kirchhoff's law $\nabla \cdot \sigma\nabla\varphi = 0$ (Holder, 2004).

The two fundamental parameters of Maxwell's equations are the electric field **E** and the magnetic field **H**. If these two parameters are considered vector functions of space, the fields produce electric displacement **D** and magnetic flux **B** fluxes when applied to a test material.

According to Faraday's Law, a magnetic field B is produced by electromagnetic induction. ($\vec{\mathrm{E}}$ is electric field)

$$\nabla \times \vec{\mathrm{E}} = -\frac{\partial \vec{B}}{\partial t} \tag{4.1}$$

According to Ampere's law, the displacement current includes $\partial D/\partial$t. (J is electric current density, D is electric displacement vector, $\partial D/\partial$t is displacement current)

$$\nabla \times \vec{H} = \frac{\partial \vec{D}}{\partial t} + \vec{j} \tag{4.2}$$

Where ε_0 is the electric constant, D is defined as:

$$D = \varepsilon_0 E \tag{4.3}$$

The relationship between the magnetic field B and H is related to the permeability. (μ_0 is the magnetic permeability constant)

$$B = \mu_0 H \tag{4.4}$$

According to Gauss's laws for the electric field E and magnetic fields B defined as:

$$\nabla . E = \frac{\rho}{\varepsilon_0} \tag{4.5}$$

$$\nabla . B = 0 \tag{4.6}$$

When the time-varying components of the electric field are ignored (electro quasi-static field) and σ is the conductivity, the equations can be expressed as follows:

$$\nabla \times E = 0 \tag{4.7}$$

$$\vec{j} = \sigma E \tag{4.8}$$

When equations (4.2) and (4.4) are combined, the following equation is obtained:

$$\nabla \times \vec{B} = \mu_0 \vec{j} \tag{4.9}$$

According to the Divergence theorem:

$$\nabla . \vec{j} = 0 \tag{4.10}$$

The electric field is also equal to the equation below, where φ is the electric potential.

$$E = -\nabla\varphi \tag{4.11}$$

When the necessary equations are made with the given equations, the following equation is finally obtained.

$$\nabla^2\varphi = -\frac{\nabla\sigma.\nabla\varphi}{\sigma} \tag{4.12}$$

Equation (4.12) describes the relationship between the Forward and Inverse Problems. If the conductivity σ is given and the electric potential φ is found, the Forward Model is obtained. If the electric potential φ is given and the conductivity σ is found, the Inverse Model is obtained.

4.8. EIT Forward Problem

The forward problem calculates the voltages inside an object when the conductivity inside the object is specified. As seen in Figure 4.3, the main objective of the forward problem is to calculate the voltage values at the electrodes connected to a TUT when the conductivity distribution is given. The forward problem is defined by applying current to one pair of electrodes and measuring the corresponding voltage from the remaining set of electrodes. Human body tissues generate impedance values when electric current is applied, which makes it possible to observe and monitor physiological functions based on the conductivity of tissues in the body.

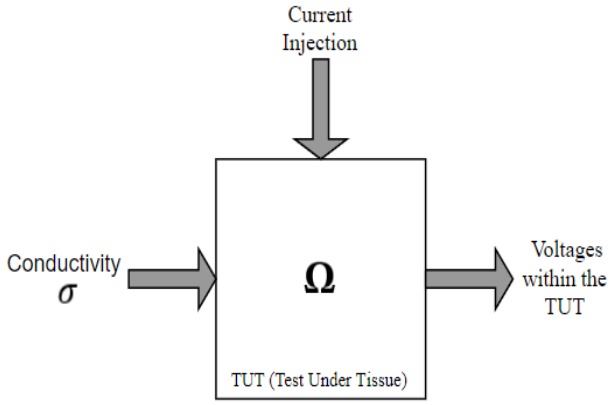

Figure 4.3. Forward model schematic for TUT

Two main approaches have been used for forward problem calculation in EIT: Analytical and Finite Element Models (FEM). Analytical models are helpful for regular shapes such as cylinders and help understand theoretical boundaries. For irregular geometries such as the patient's body, FEM has been the primary tool.

4.8.1. Finite Element Method (FEM)

Finite Element Analysis (FEA) is a numerical method used to solve engineering and physical problems. It is widely used to analyze systems with complex geometries and material properties. In the Finite Element Method (FEM), three-dimensional space is decomposed into (possibly irregular) polyhedrons called elements (e.g., tetrahedrons, prisms, or hexahedrons), and the unknown potential in each element is represented by a polynomial of constant order. As the elements become more numerous (as long as their interior angles remain finite) or the degree of the polynomial increases, it converges to the solution (or at least the weak solution) of the partial differential equation it represents (Strang and Fix, 1997). In 2D EIT, the tested area is divided into small triangular elements, while in 3D EIT, the tested area is divided into small polyhedral elements.

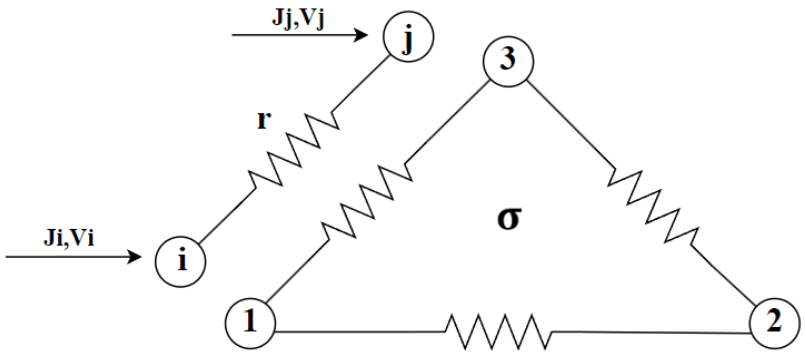

Figure 4.4. FEM equivalent circuit

In an electrical resistance network as in Figure 4.4, i and j are defined as a single resistive element. According to Ohm's law, the currents J_i and J_j can be defined as:

$$J_i = \frac{1}{r}(V_i - V_j) \tag{4.13}$$

$$J_j = \frac{1}{r}(V_j - V_i) \tag{4.14}$$

Equations (4.13) and (4.14) are written in matrix form.

$$\begin{pmatrix} J_i \\ J_j \end{pmatrix} = \frac{1}{r}\begin{pmatrix} 1 & -1 \\ -1 & 1 \end{pmatrix}\begin{pmatrix} V_i \\ V_j \end{pmatrix} \tag{4.15}$$

The given equations can be expressed in a general notation.

$$J = KV \tag{4.16}$$

The forward problem of EIT is used to obtain the electric potential from the conductivity distribution. The necessary mathematical equations are given in this section as a summary. Electrical potentials can be calculated using existing mathematical models. Thus, optimum models can be created for structures compared to accurate measurements' potential values. Along with Basic FEM, Complete Electrode Model (CEM), Conjugate Gradient (CG), and Krylov Subspace Methods also

provide solutions for the forward model. In this study, some FEM-based simulation programs have been used, which will be discussed in more detail in the following sections.

4.9. EIT Inverse Problem

Finding the conductivity distribution of a closed area by applying current to it and using the voltage values obtained is called the Inverse Problem.

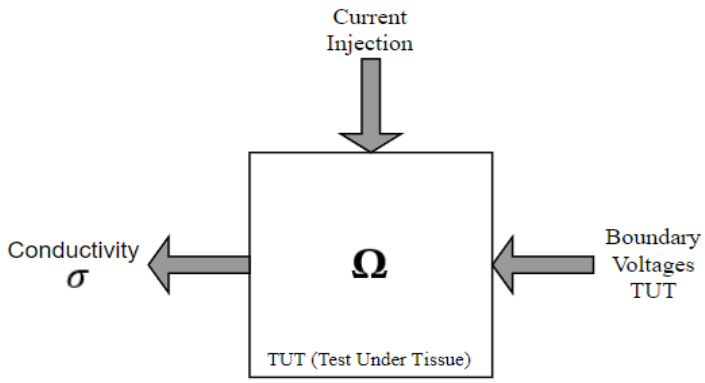

Figure 4.5. Inverse model schematic for TUT

In the system modeled in Figure 4.5, a body tissue (TUT) is defined as a closed area. By injecting current into this closed area and estimating the parameters of the system with the voltage values obtained, the conductivity distribution of the area is found. Understanding the relationship between the parameters and the data obtained from that domain is necessary. This situation necessitated the derivation of some equations. The mathematical equations explained in Section 4.7 solve the Inverse Problem. If a problem has a solution mathematically and is unique and stable, then this problem is well-positioned. However, the complexity of the geometry of some measurement systems reduces the number and quality of data obtained from that geometry. The Inverse Model to be created for these systems is ill-positioned and ill-conditioned. The fact that the solution for the EIT Inverse Problem is constantly dependent on the data creates complexity. The existence of parameters that cannot be estimated from the data obtained from the limit voltage measurements in EIT necessitated a high measurement sensitivity. Some methods have been developed to measure the sensitivity of the conductivity distribution. Some of the methods are Tikhonov Regularization (TR), (Tikhonov, 1963), (Phillips, 1962.), Filtered Backprojection (Jørgensen et al., 2021.), Singular Value Decomposition (SVD) (Aster, et al.,2004) , Selection of Hyperparameter, GREIT (Adler et al., 2009), and Total Variation (TV) Regularization (Borsic and Adler, 2012).

5. FEASIBILITY STUDY OF ELECTRICAL IMPEDANCE TOMOGRAPHY USING COMSOL MULTIPHYSICS

Electrical Impedance Tomography (EIT) is an imaging technique that uses techniques for imaging body structures and monitoring physiological processes with electrical impedance measurement methods. EIT is an important technique in medical diagnosis and physiological monitoring due to its non-invasive structure and real-time imaging.

COMSOL Multiphysics is a simulation software platform used to model complex physiological systems and analyze the model with various numerical calculations. Electrical, thermal, fluid and mechanical systems are defined in this simulation program. The program provides a realistic environment for solving partial differential equations (PDEs) that define these systems. The software allows model creation, parameter definition and visual presentation of the result. It also supports the integration of different physical environments such as electric fields, thermal effects and fluid dynamics. Thus, it allows comprehensive analysis of complex systems.

5.1. Software Architecture

Using EIT studies with COMSOL Multiphysics program offers significant advantages for the preliminary study and development of EIT systems. COMSOL's modeling and simulation capabilities allow modeling of biological structures, detailed analysis of the electrical impedance of tissues and the interaction of electrical fields with biological structures. Thus, the simulation program provides some conveniences before EIT studies are carried out.

Modeling Electrical Impedance: COMSOL Multiphysics creates models and performs detailed calculations by defining the electrical properties of the human body or specific tissues. This capability is important for simulating the propagation of electric currents in various biological materials and for testing the accuracy of impedance measurements.

Electrode Placement and Configuration: The software helps to model and simulate various electrode layouts to optimize the design of EIT systems. Thus, they can examine the effects of these electrode layouts on measurement accuracy and image quality.

Impedance Measurement Simulation: COMSOL can simulate the impedance measurement process by applying alternating currents across electrode pairs and calculating the resulting voltage distributions. This simulation provides insights into how impedance changes affect the measured data and helps develop data interpretation algorithms.

Image Reconstruction: The software also incorporates advanced image reconstruction techniques such as iterative algorithms and inverse problem solving methods. COMSOL simulates the reconstruction of tomographic images from impedance data.

Validation and Optimization: Iterative simulations provide a comparative presentation of theoretical and experimental data. The program allows this and is effective in optimizing the performance of EIT system designs.

The feasibility study of Electrical Impedance Tomography using COMSOL Multiphysics is an important part of the development and optimization of EIT systems.

5.2. Material and Method

5.2.1. Creating of Model

A three-layered binding model with a volume of 30x30x4 mm^3 was designed. The model consists of 1 mm thick epidermis, 2 mm thick dermis, and 1 mm thick subcutaneous layers. Eight electrode arrays with a radius of 0.25 mm were placed on the model. The same electrode array was rotated by 45° to create two more electrode arrays. Thus, 32 measurement electrodes were obtained to scan the skin surface 360°. An elliptical-shaped tissue with electrical properties different from healthy tissue was placed inside the skin model. As seen in Figure 5.1.b, the model represents unhealthy tissue containing abnormal tissue.

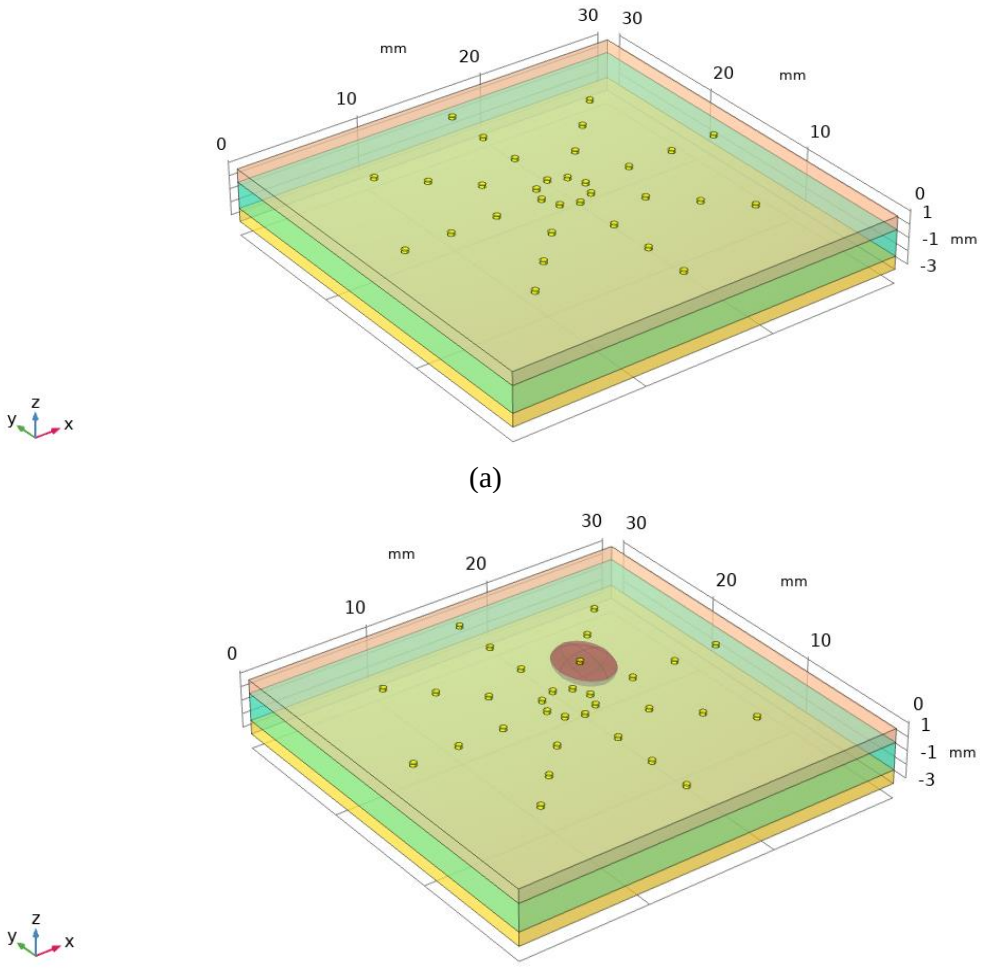

Figure 5.1. a) Healthy skin model b) Skin model with abnormal tissue

5.2.3. Definition of Electrical Parameters

In COMSOL, electrical conductivity is modeled using the Electric Fields and Currents Module. The conductivity value can be defined in the material properties and is used to analyze the electrical behavior in the model. Relative permittivity is simulated using the Electromagnetic Wave Module and AC/DC Module to simulate the dielectric properties of materials and the propagation of electromagnetic waves in the material.

This section defines the electrical conductivity and relative permittivity parameters for each skin layer and differentiated tissue material properties analytically depending on the frequency (Tissue Dielectric Properties, n.d.). Table 5.1 shows the frequency-dependent dielectric properties of the skin.

The material properties of the electrodes were determined to be constant (Au). Assuming that the electrical properties of the materials vary depending on the frequency, the frequency was created between 100 Hz and 1 MHz with a 100 kHz step interval.

Table 5.1. Defining electrical properties of materials

Material Name	**Electrical Conductivity**	**Relative Permitivity**
Epidermis	$(0.0002) \times frequency^2$	$(-0.0001) \times (frequency) + (1135)$
Dermis	$(0.02) \times frequency^2$	$(-0.01) \times (frequency) + (1135)$
Subcutaneus	$(0.2) \times frequency^2$	$(-0.1) \times (frequency) + (1135)$
Abnormal Tissue	$2000 \times frequency^2$	$(((-10)^{-15}) \times (frequency) + ((1135 \times (10)^{-10})$

The electrodes for measurements taken on the skin are defined as probes. Table 5.2 shows the defined electrodes. Each probe represents the measurement points.

Table 5.2. Defining of measuring electrode

Electrode Name	**Probe Name**	**Electrical Potential (V)**
Elektrode1	Domain Probe1	dom1 (V)
Elektrode2	Domain Probe2	dom2 (V)
Electrode3 . . .	Domain Probe3 . . .	dom3 (V) . . .
Electrode31	Domain Probe31	dom31 (V)
Electrode32	Domain Probe32	dom32 (V)

5.2.4. Creating Mesh

Mesh generation in the COMSOL Multiphysics program is one of the cornerstones of finite element analysis (FEA) processes. Mesh is a network of small elements obtained by discretizing the model's geometry and where calculations will be made. Mesh density can be adjusted according to the details of the analyzed region. The mesh generation process begins with an accurate and complete geometry definition being analyzed.

The complexity of the geometry affects the type of mesh and its density to be used. Increasing the density can increase the solution's accuracy but also increase the calculation time. The mesh density was selected to be dense for the designed model to provide a good solution. Figure 5.2.a. represents the mesh model of healthy skin tissue, while Figure 5.2.b. represents the mesh model of skin with abnormal tissue.

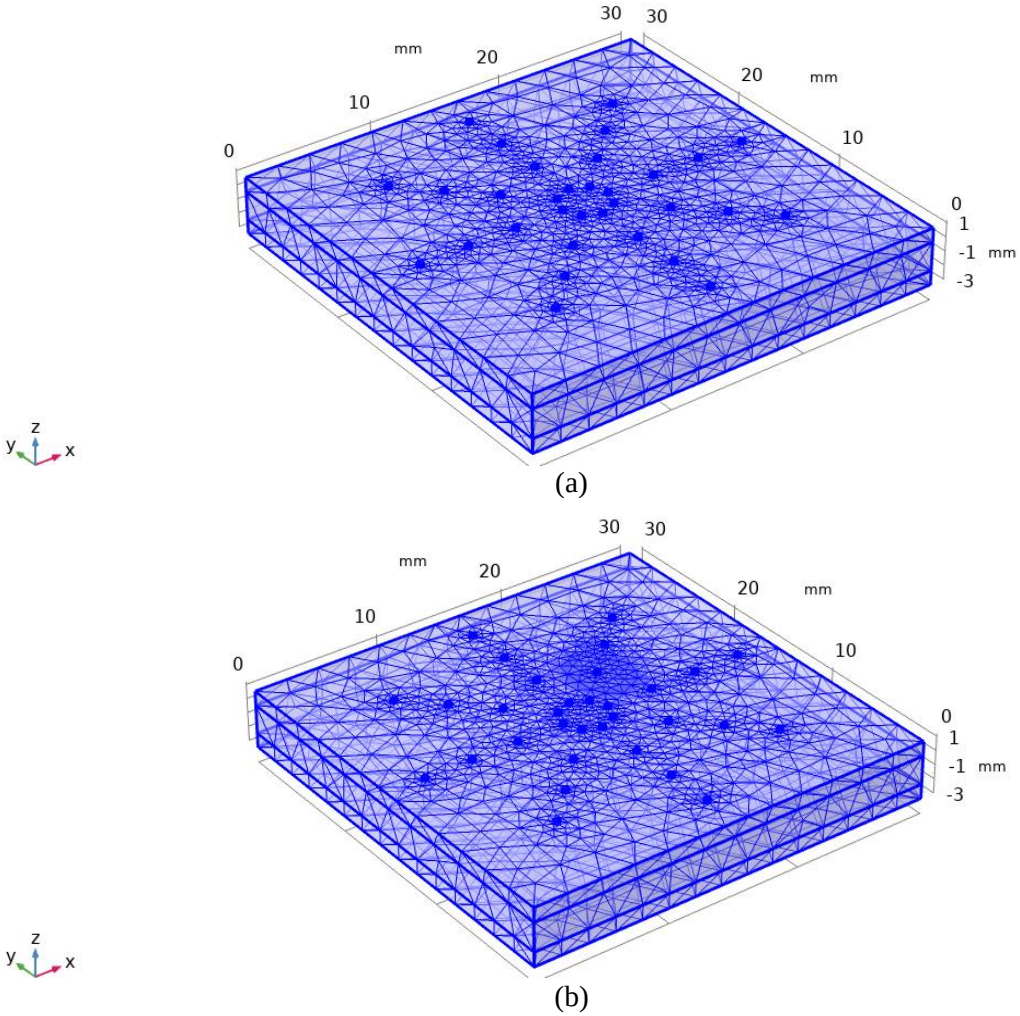

Figure 5.2. a) Mesh of healthy skin model b) Mesh of skin model with abnormal tissue

5.2.5. Measurement Procedure

The electrical study area is defined in the AC/DC module of the COMSOL MULTIPHYSIC program. In COMSOL Multiphysics, the Electric Currents and Study sections form the basis of electrical analysis. The Electric Currents module analyzes electrical current distributions and potential differences. This module allows the calculation of electric fields and current densities based on Ohm's law.

Ohm's Law: Describes the relationship between the applied voltage of an electric current and the electrical resistance of a material: $J=\sigma E$, where J is the current density, σ is the electrical conductivity, and E is the electric field.

Continuous Current (DC) and Alternating Current (AC): The module supports both DC and AC analyses. DC analyses examine constant voltage and current conditions, while AC analyses analyze time-varying sinusoidal voltages and currents.

Boundary Conditions: In electrical analyses, various boundary conditions, such as constant potential, insulating boundaries, and current sources, can be applied.

The Study section is the section that defines and manages the solution process of a model. The study includes the steps required to solve the mathematical expressions of the model and obtain the analysis results.

Physics Interfaces: Each study includes specific physics interfaces and interactive solution methods. For example, electric currents, heat transfer, and mechanical analyses can be considered together.

Solution Types:

Steady-State Solutions: Time-invariant solution of the system in its equilibrium state.

Time-Dependent (Transient) Solutions: Solutions that analyze dynamic processes that change over time.

Frequency Domain Solutions: Solutions based on frequency used in AC analysis.

According to the measurement method defined for the system, 8 Electric Currents were determined. Each of them represents a series of measurement electrodes. In this section, the boundary conditions of the electrodes and the alternating current to be applied to the electrodes were defined. (10 mA)

The next step consists of 8 different Electrical Study Modules that will provide electrical analysis. Figure 5.3 represents the electrical study areas from ES1 to ES8. Each sub-image (a-h) shows a different configuration of current injected pairs. Since the system varies with frequency, the Frequency Domain was selected in the Study Module. Frequencies were defined to indicate the step range. The simulation was run and the obtained data was recorded.

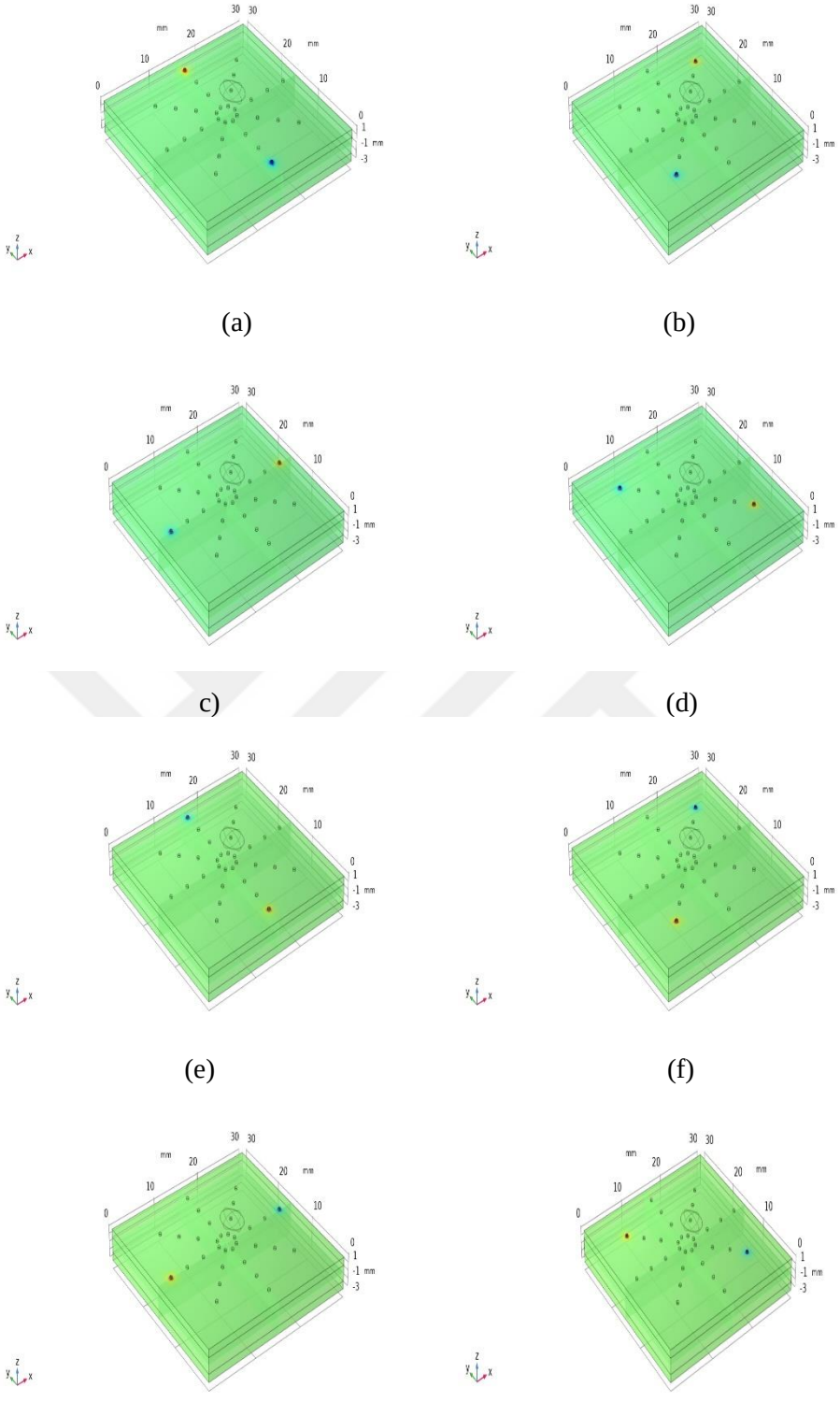

Figure 5.3. a) ES1 b) ES2 c) ES3 d) ES4 e) ES5 f) ES6 g) ES7 h) ES8

6. FEASIBILITY STUDY OF ELECTRICAL IMPEDANCE TOMOGRAPHY USING EIDORS

EIDORS (Electrical Impedance and Diffuse Optical Reconstruction Software) is an important software package used especially in EIT research. EIDORS is used to simulate, reconstruct, and visualize impedance tomography data. Being open source, EIDORS includes various electrode configurations, numerical algorithms, and visualization techniques required for research and applications.

EIDORS supports a wide range of electrode geometries, both 2D and 3D. It allows simulation and reconstruction of images based on specific measurement systems. EIDORS uses various advanced numerical algorithms, such as finite element methods (FEM) and Bayesian inference techniques for image reconstruction. It provides accurate and reliable reconstructions even in the presence of noise and uncertainties. It facilitates the interpretation and analysis of the results.

EIDORS is used in different scientific disciplines, such as flow measurement, material characterization, soil moisture monitoring, pollutant detection, lung ventilation monitoring, and brain imaging.

6.1. Software Architecture

EIDORS software consists of four main objects: data, image, forward model (fwd model), inverse model (inv model). Each object is represented by a structure. This section is to understand what these four general structures mean. All objects have a name and type attribute. The name is arbitrary; graphic functions display it and can also be used to distinguish objects in a user-specified function. The type is used to define the object type (e.g. data, image, etc.) (Adler and Lionheart, 2006).

6.1.1. Forward Model

The forward problem calculates the voltages inside the object if the conductivity inside the object is known. The main objective of the forward problem is to calculate the voltage values at the electrodes connected to the object given the conductivity distribution.Some numerical solutions are used to solve the forward problem. EIDORS provides this numerical solution with sensitivity mapping. These calculations are explained in more detail in sections 4.7 and 4.8. The Forward Model, in EIDORS, uses a finite element model (FEM) to represent electrode locations and properties and stimulation patterns.

6.1.2. Data

The EIDORS data object represents a measurement or simulation data frame. The data object contains two optional fields: configuration and forward model. Specifying the forward model allows

EIDORS to verify that the data has been interpreted correctly and reconstructed using the correct model. Configuration is a user-specified string that serves a similar function; the software can distinguish data objects by assigning a value to this field.

6.1.3. Inverse Model

In EIDORS, the inverse model object groups the information required to reconstruct images. This object distinguishes two basic reconstruction types:

Difference: Creates an image by calculating the difference between two data objects.

Static: Creates an image based on a single data object.

Solve: Contains a string or function pointer to the solver function. The provided functions are based on regular image reconstruction algorithms and require selecting an image prior and a hyperparameter.

Hyperparameter: Specifies the hyperparameter. For simple cases, a scalar value is provided in the value field. However, a hyperparameter selection strategy is specified as a function for more complex cases.

Image Priors: Image priors are usually used in two ways, with the regularization terms $\|\lambda \mathbf{Rx}\|$ or $\|\lambda \mathbf{x}\|_R$, where $\mathbf{x}$ is the vector of image element values. In the most common case, a quadratic norm is used, and these regularization terms can be expressed as $\lambda^2 \mathbf{x}^T \mathbf{Rx}$ or $\lambda^2 \mathbf{x}^T \mathbf{R}^T \mathbf{Rx}$, respectively. EIDORS solves this problem by defining two functions to calculate image priorities: R_prior and RtR _prior. The user can provide a value for one or both of these functions.

Parameters to the Image Priority Function: These parameters are specified using the name of the image priority function added to the inverse model object.

6.1.4. Image

The EIDORS image object represents the reconstructed or simulated conductivity values. This object contains the value of each image element in the finite element model (FEM).

6.2. Material and Method

In this thesis, before the electronic hardware is designed, the suitability of the proposed impedance mapping approach and electrode model for abnormal tissue detection is tested in the EIDORS environment. For this purpose, the physical shape and dimensions of the tissue to be measured are defined in a MATLAB environment. Abnormal tissue with different electrical properties is detected by entering coordinates at any location of the defined tissue. After this stage, the proposed electrode model should be placed on the tissue surface. In this step, the electrode model consists of electrodes whose structure, shape and dimensions are specified in the previous sections and placed on the tissue surface by entering the appropriate surface coordinates. Figure 6.1.a. shows the designed model. The current stimulation pattern and measurement pattern are defined,

respectively. The process of measuring the voltages coming from each electrode is defined. With this step, measurement data can now be obtained. Then, the finite element model (FEM) parameters are defined with the obtained data. As seen in Figure 6.2.b, after the mesh is created and the necessary analyses are performed, the forward model is obtained. The last step involves defining various reconstruction parameters and creating an inverse model using the data obtained from the forward model. Figure 6.1.c. represents the inverse model. The EIDORS code is given in Appendix B.

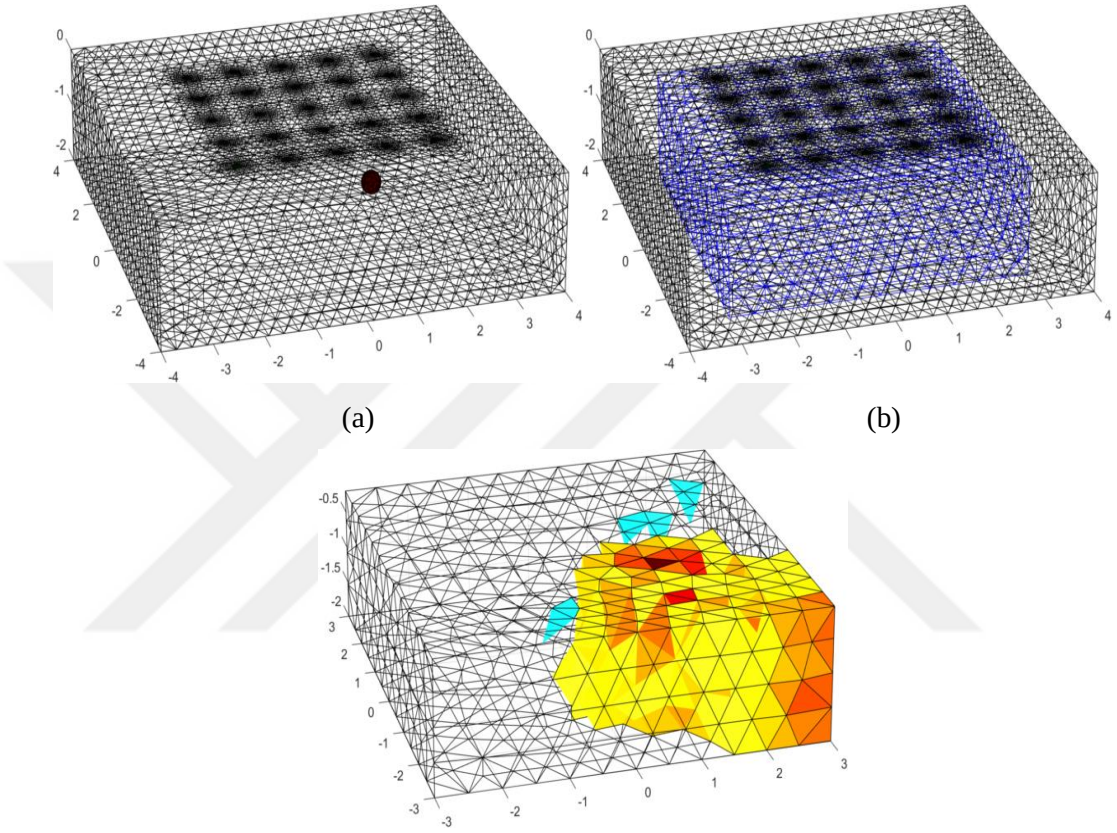

(a) (b)

(c)

Figure 6.1. a) Forward model of skin with abnormal tissue b) Mesh of skin with abnormal tissue in EIDORS c) Inverse model of skin with abnormal tissue

7. EXPERIMENTAL STUDY OF THE PROPOSED SYSTEM

7.1. Measurement of System Architecture

7.1.1. General Overview

In this section, an overview of the proposed electronic hardware is given. As seen in the Figure 7.1, the system is designed in blocks. These system blocks consists of a microcontroller, signal generator, VCCS circuit, output stage, and instrumentation amplifiers, which are explained in detail in the following sections.

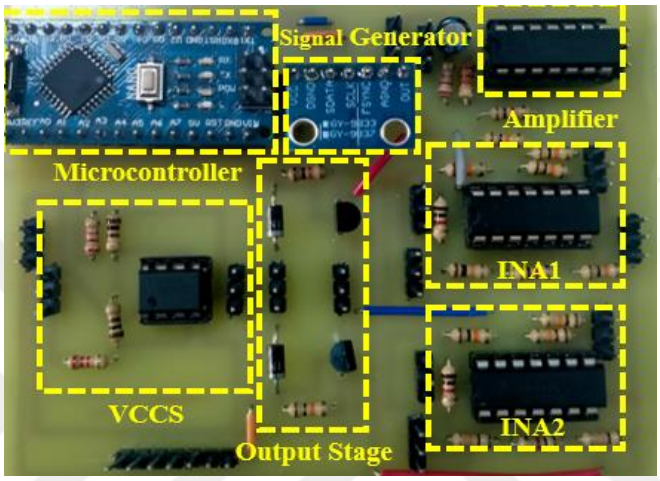

Figure 7.1. Electronic hardware of proposed model

Electrode Model

As seen in the Figure 7.2, in the first electrode array (electrode1 to electrode8), electrode1 is the source terminal while electrode8 is the ground for applied constant AC current (0.01A). The other electrodes are defined as the voltage measurement electrodes. The same measurement system is applied to the other seven electrode arrays rotating at a 45° angle (electrode9-electrode16, electrode17-electrode24, ..., electrode32-electrode25). Thus, with the proposed electrode system and the applied measurement method, a 360-degree scan is performed on the skin surface.

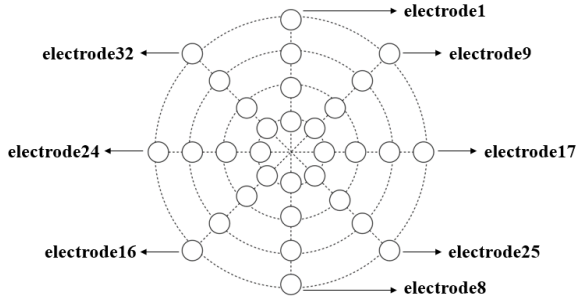

Figure 7.2. Electrode model of the proposed model

The geometry of the electrode model is designed to allow scanning at more frequent intervals on the skin surface. In this way, it aims to take more detailed measurements and detect abnormal

tissues more accurately and comprehensively. Each electrode represents a measurement point. The large number of electrodes ensures that the amount of data to be obtained from the skin surface is high and, therefore, the resolution is high. As a result, the designed electrode system and the applied measurement method are an extremely suitable and practical approach to analyze the skin surface's electrical properties in detail and detect abnormal tissues.

7.1.2. Electronic Hardware Definition

As seen in Figure 7.3, the EIT measurement system was designed and simulated in PSPICE environment while its PCB is designed in the EAGLE TCAD software.

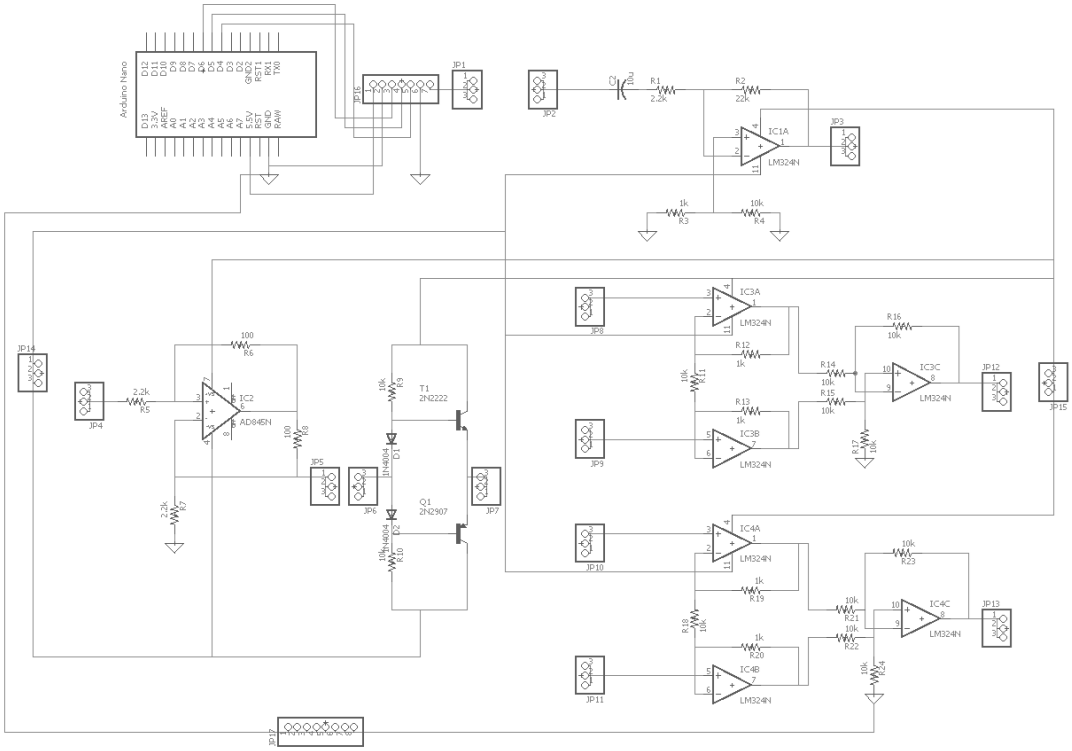

Figure 7.3. Electronic diagram of the measurement system

Signal Generation

AD9833 is used as Signal Generator. AD9833 is a programmable direct digital synthesizer (DDS) signal generator. This versatile device can produce sine, square, and triangle waveforms and operate over a wide frequency range. It is used with a microcontroller (e.g., Arduino or PIC). The microcontroller sends commands to AD9833 via the SPI interface, and AD9833 produces a signal at the set frequency and waveform.

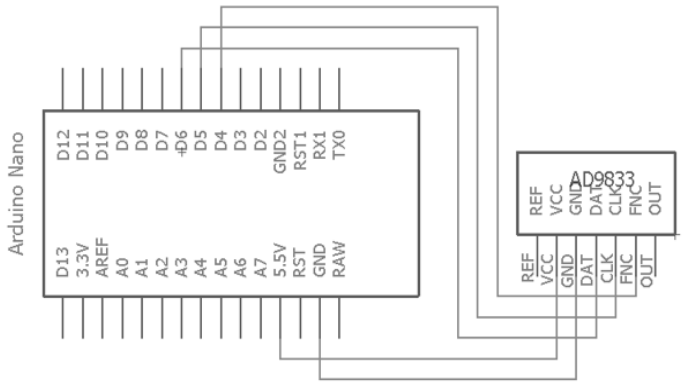

Figure 7.4. Arduino Nano-AD9833 pin configurations

The Signal Generator (AD9833), whose connections are given in Figure 7.4, produces a fixed sinusoidal signal with a frequency of 100 Hz and an amplitude of 0.3 V, controlled by the Microcontroller (Arduino Nano).

Amplifier

An amplifier circuit is a circuit that transfers the signal applied to its input to the output in an amplified form. The electronic circuit of an inverting amplifier is given in Figure 7.5.

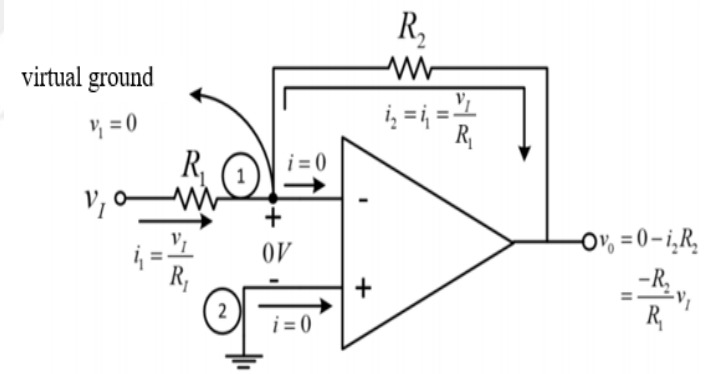

Figure 7.5. A simple inverting amplifier

In the measurement system, LM324 op-amp was used to amplify the voltage value produced by the signal generator. The resistance values were selected to amplify the gain of the amplifier by ten times. Thus, the output voltage value became 3V.

Voltage To Current Converter

In electronic circuit applications, input signal sources are usually in the form of a voltage source. If an output current is obtained depending on the input voltage in any circuit, it is called a voltage-controlled current source or voltage-current converter.

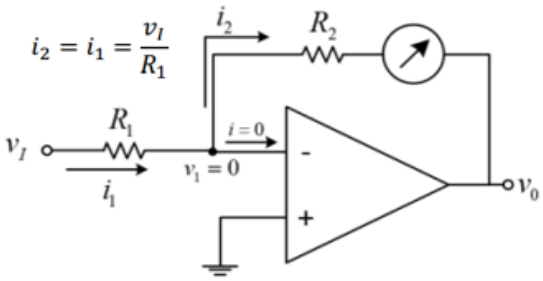

Figure 7.6. A simple voltage-current converter circuit

The expression in the image means that the i_2 current is directly connected to the V_I input voltage and is independent of the load resistance R_2. The resistance is shown as the load in the Figure 7.6 (İstanbullu and Avcı, 2020). However, depending on the circuit design, the load may also consist of different circuit elements such as capacitors, diodes, or transistors. However, in some cases, one end of the load to be connected to the circuit may need to be grounded. In this case, the circuit in the Figure 7.6 will not be suitable for such applications (İstanbullu and Avcı, 2020).

Howland Current Pump

The basic working principle of the circuit is to obtain a constant output current by controlling the input voltage and current with the op-amp's high open-loop gain and feedback mechanism. Considering the Howland current pump given in the Figure 7.7, one end of the load (Z_L) connected to the circuit is connected to the ground. In this case, the inverting terminal of the op-amp will not be a virtual ground.

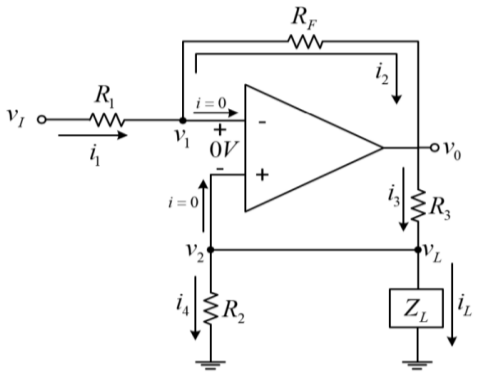

Figure 7.7. Howland current pump circuit

Based on the virtual short circuit discussion, $V_1 = V_2$. Thus, $V_1 = V_2 = V_L = i_L Z_L$ can be written. When the currents i_1 and i_2 are equalized, and the intermediate equations are solved, it is seen that the load current Z_L varies only with the input voltage, independent of the load impedance. If it is desired to send a constant current to a load independent of the load impedance or to draw current through the load, these operations can be performed with this circuit by simply changing the input voltage.

$$i_L = -v_1 \left(\frac{R_F}{R_1 R_3}\right) = \frac{-v_1}{R_2} \tag{7.1}$$

Since a constant current independent of the impedance is sent to the load with one end in the ground in the measurement system, the Howland Current Pump circuit was used. (LM741). The input signal of the Howland Current Pump circuit is the output signal of the amplifier. A constant current is obtained at the output of the circuit.

Output Stage

A push-pull circuit uses two active devices (BJTs or MOSFETs) to amplify the positive and negative half-cycles of the output signal separately. As shown in Figure 7.8, these devices are usually arranged in complementary order (an NPN and a PNP BJT or an N-channel and a P-channel MOSFET). Each device amplifies or transmits one half-cycle of the input signal.

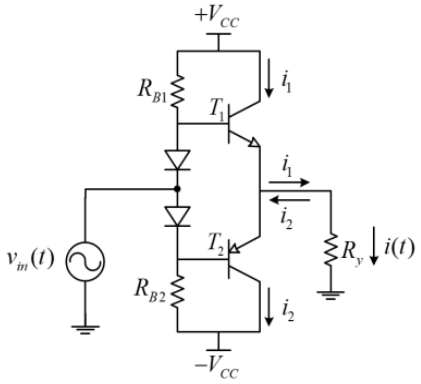

Figure 7.8. Push-Pull amplifier circuit

These amplifiers are used to provide voltage or current gain for the first and intermediate stages of a back-to-back amplifier circuit chain. Power gain is important for these stages. The Figure 7.9 shows that the push-pull circuit is connected just behind the Howland Current Pump circuit. These amplifiers function is to amplify small amplitude signals and pass them to the output stage.

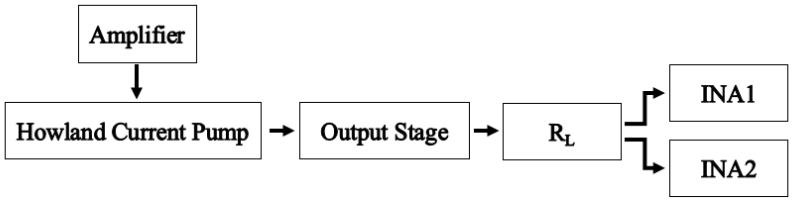

Figure 7.9. Output stage block diagram

INA

It is a difference amplifier used in cases where the signal to be amplified is very small and the Common mode signal is significant.

The primary difference amplifier mentioned earlier has disadvantages, such as the relatively small input resistance and difficulty adjusting the gain. In order to increase the input resistance of the circuit, a voltage follower (isolation amplifier) can be used for each input.

In the instrumentation amplifier in the Figure 7.10, choosing the $\frac{R_2}{R_1}$ and $\frac{R_4}{R_3}$ ratios as the same allows the gain of the circuit to changed with a single resistance value. A_1 and A_2 are the input stages, and A_3 is the amplifier stage.

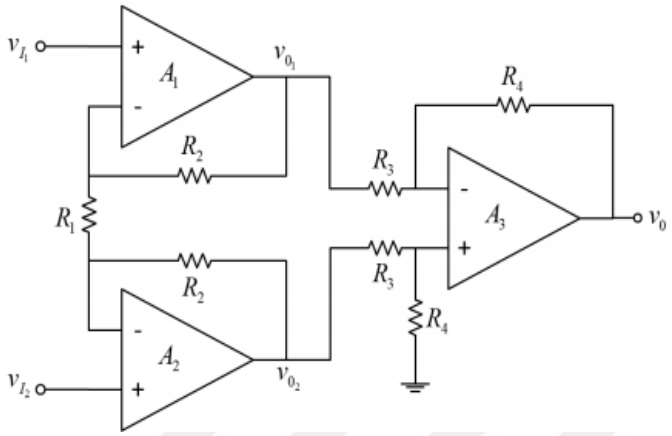

Figure 7.10. Instrumentation amplifier circuit

These amplifiers, the basic elements of modern analog data systems today, are produced as integrated circuits on a single chip with high linearity, low offset, and drift. Their gain is almost unchanged due to temperature changes. (INA128, AD522..).

Due to these features, instrumentation amplifiers are widely used to amplify bioelectric signals with small amplitude signals at the outputs of converters such as transducers and sensorsTwo instrumentation amplifiers, INA1 and INA2, were used in the measurement system. The voltage values obtained from the reference with the load representing the skin model were amplified 1.2 times and transferred to the output.

7.1.3. Resistive Phantom Model

Testing the accuracy of the hardware created is necessary before moving on to the image reconstruction phase. Phantoms are often preferred to evaluate the performance of EIT systems objectively (Gagnon et al., 2010). In the literature, two types of phantoms are described for this purpose: physical and mesh phantoms (G Hahn et al., 2000). Physical phantoms contain a conductive medium, usually an electrolyte solution, and can be visualized by an EIT system using surface electrodes. Mesh phantoms, on the other hand, consist of interconnected impedance elements arranged in a specific topology. While physical phantoms produce more realistic signals, mesh phantoms offer predictable, stable, and reproducible signals.

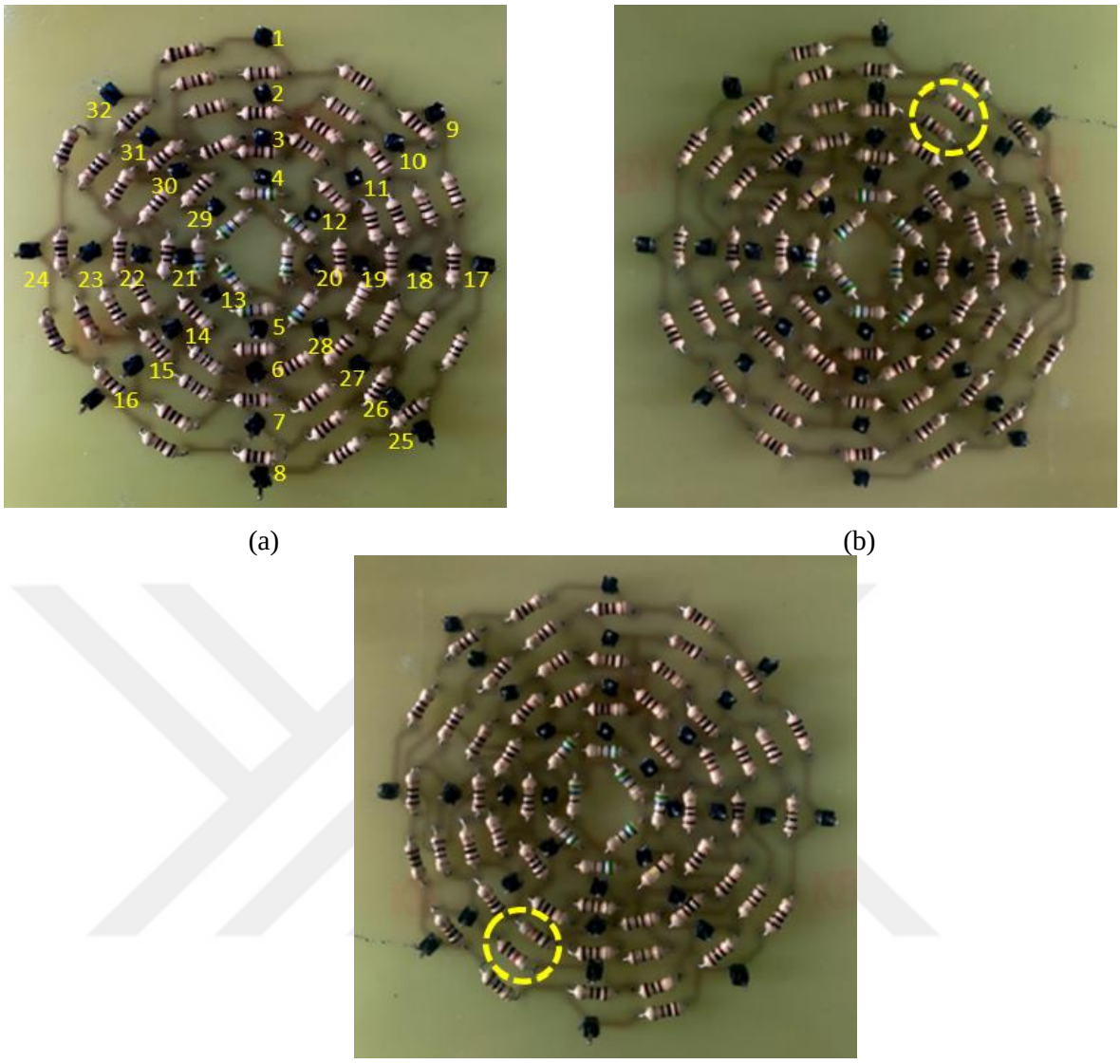

(a) (b)

(c)

Figure 7.11. a) Resistive model of healthy skin b) Resistive skin model with abnormal tissue between 2-10 electrode c) Resistive skin model with abnormal tissue between 7-15 electrode

In this study, a resistive network phantom representing the skin model was designed. Fifty-six resistors, each 100 Ω, were used. Thirty-two electrodes were numbered, as seen in Figure 7.11.a. The model in Figure 7.11.a. represents the homogeneous tissue that will be the measurement reference. Any abnormal tissue formed on the skin exhibits different electrical properties than healthy tissue (Birgersson et al., n.d.). The resistance values in the circular area in Figure 7.11.b. and Figure 7.11.c. are designed to differ from the other resistance values (1kΩ). This model represents the skin model with abnormal tissue inside.

7.1.4. Improved Resistive Phantom Model

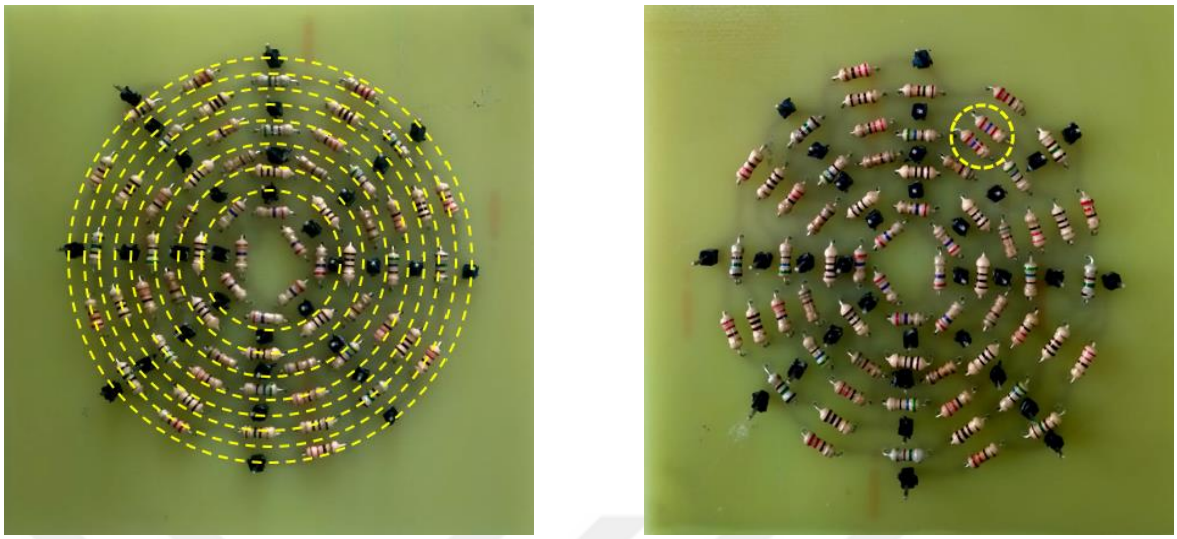

(a) (b)

Figure 7.12. a) Resistive model of healthy layered skin b) Resistive layered skin model with abnormal tissue between 2-10 electrode

The electrical properties of the lower layers of the skin (dermis and underlying tissues) are generally considered less resistive (more conductive) than the upper layers. In contrast, the upper layer (epidermis) is considered more resistive (less conductive). This is because the outermost layer of the epidermis, the stratum corneum, consists of dead cells and has a low water content.

This property causes it to have a high resistance and conduct electrical current poorly. The other epidermis layers (stratum lucidum, stratum granulosum, stratum spinosum, stratum basale) have lower resistance than the stratum corneum. However, they are generally more resistive than the epidermis, dermis, and the tissues beneath. In contrast, the dermis layer has a higher water content and contains collagen fibers, blood vessels, and nerves. These properties make the dermis more conductive. The hypodermis, or subcutaneous tissue, comprises fatty tissue and larger blood vessels. This layer can also conduct electrical current better. Figure 7.12. a) was designed according to this information. In the model, resistance values were determined so that the outermost ring represents the uppermost layer of the skin, and the innermost ring represents the lowermost layer of the skin. The magnitudes of the resistance values were selected to decrease from the outermost ring to the innermost ring. (220Ω-150Ω-100Ω-56Ω -22Ω-10Ω-5Ω-2Ω). Again, resistances with different values representing the abnormal tissue were added to the model. Thus, Figure 7.11.a was developed to represent the skin layers, and Figure 7.12.a was provided with a multi-layered structure.

8. CONCLUSIONS

8.1. Comsol Multiphysics Simulation Results

Volume plot: It shows the distributions within the model. It expresses the distribution of variables within the volume with colors.

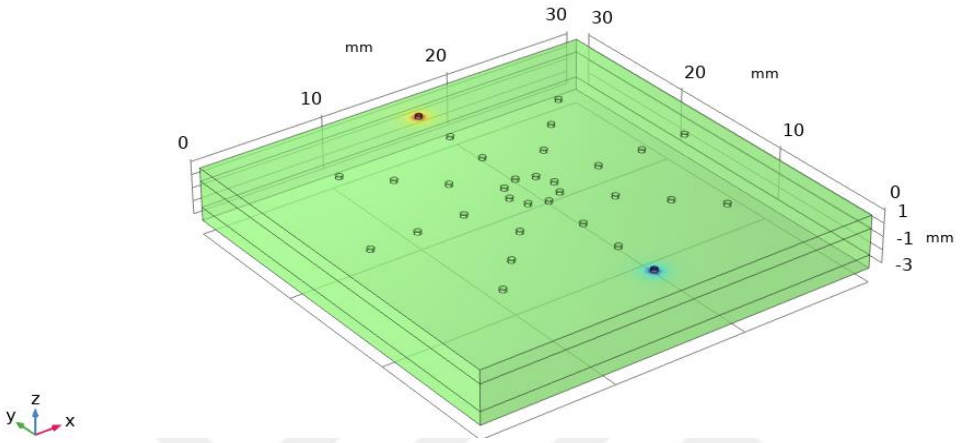

(a)

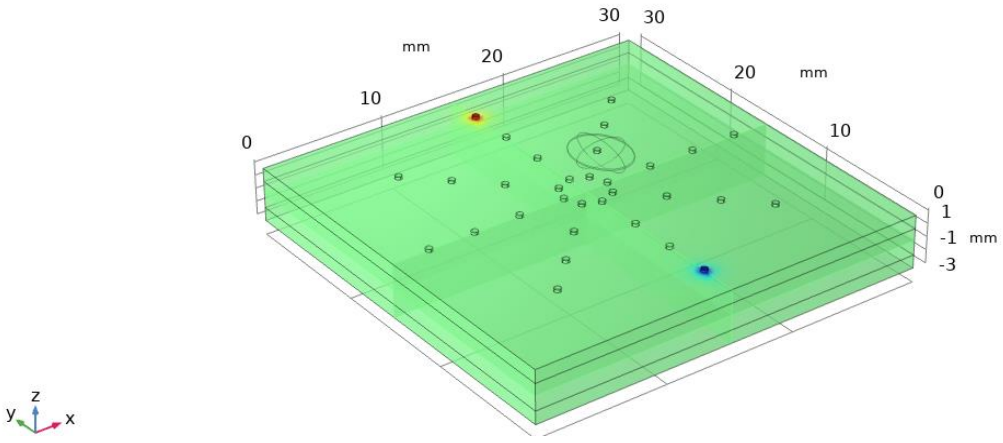

(b)

Figure 8.1. a) Electrical Study1 simulation of healthy skin model b) Electrical Study1 simulation of skin model with abnormal tissue

In Figure 8.1.a and 8.1.b, it is seen that the electric current flows from high potential (red region) to low potential (blue region). The blue area represents the area where the current is less intense. Accordingly, it is seen that the voltage distribution on the surface varies depending on the placement of the electrodes and the electrical properties of the skin tissue.

Arrow plot: Shows the direction and magnitude of vector quantities (e.g., speed, electric field) with arrows.

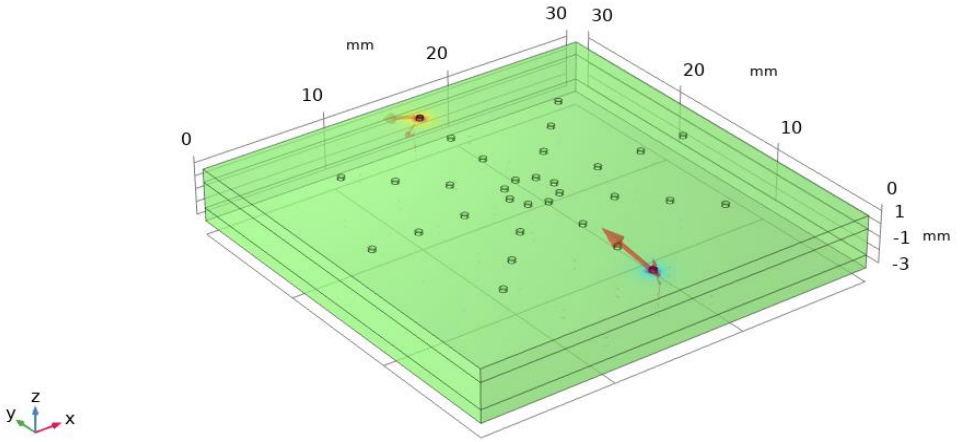

(a)

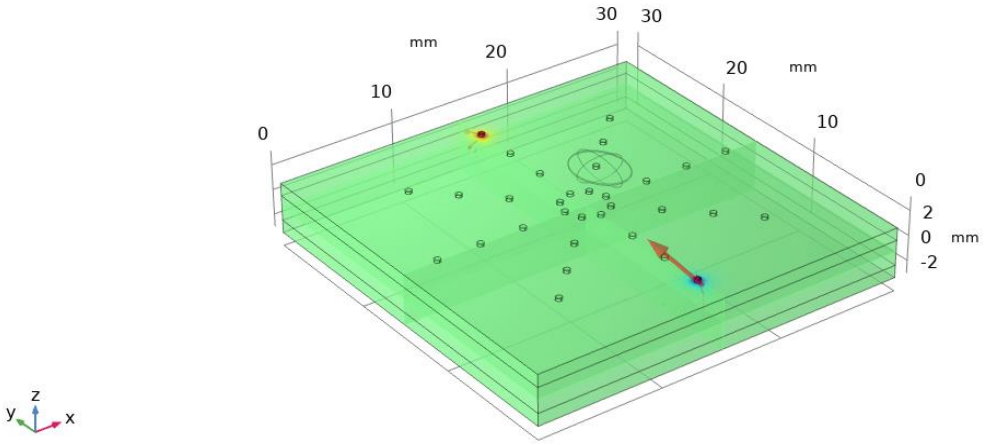

(b)

Figure 8.2. a) Arrow plot of healty skin model b) Arrow plot of skin model with abnormal tissue

The arrows in the simulation represent the direction and magnitude of the electrical current. In Figure 8.2.a and 8.2.b, it is seen that the electric current flows from high potential (red region) to low potential (blue region). The distance between the points where the electrodes are placed significantly affects the distribution of the current in the skin tissue. The positions of the electrodes, together with the electrical properties of the skin tissue, ensured that the voltage was distributed homogeneously or heterogeneously.

Surface plot: A graph showing the distribution of various physical quantities (such as temperature, pressure, voltage) on a two-dimensional surface of a model. This graph is necessary for the analysis of time-varying processes.

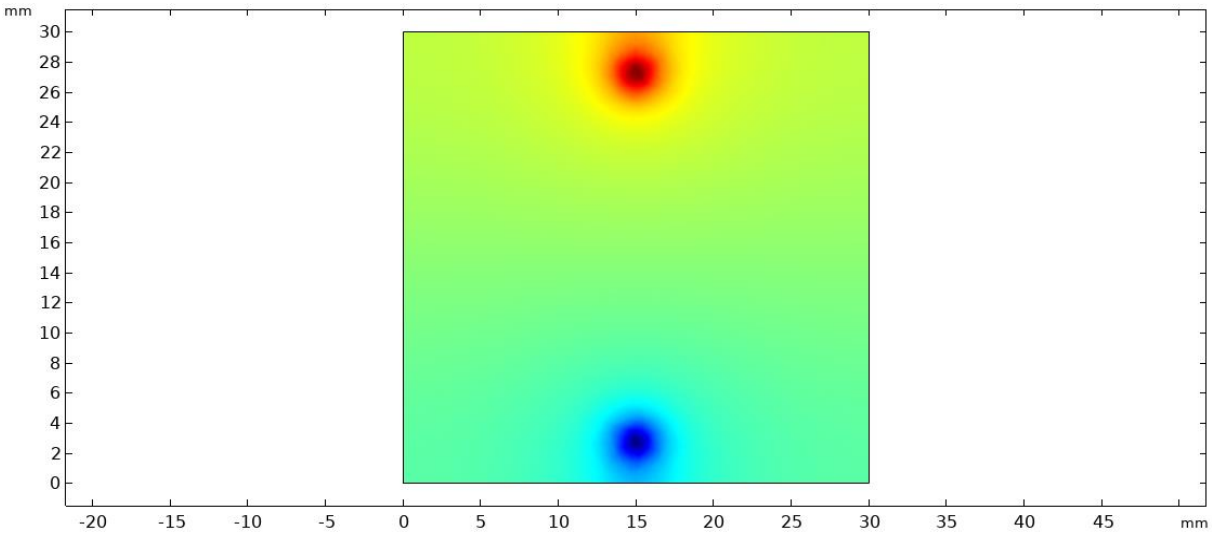

(a)

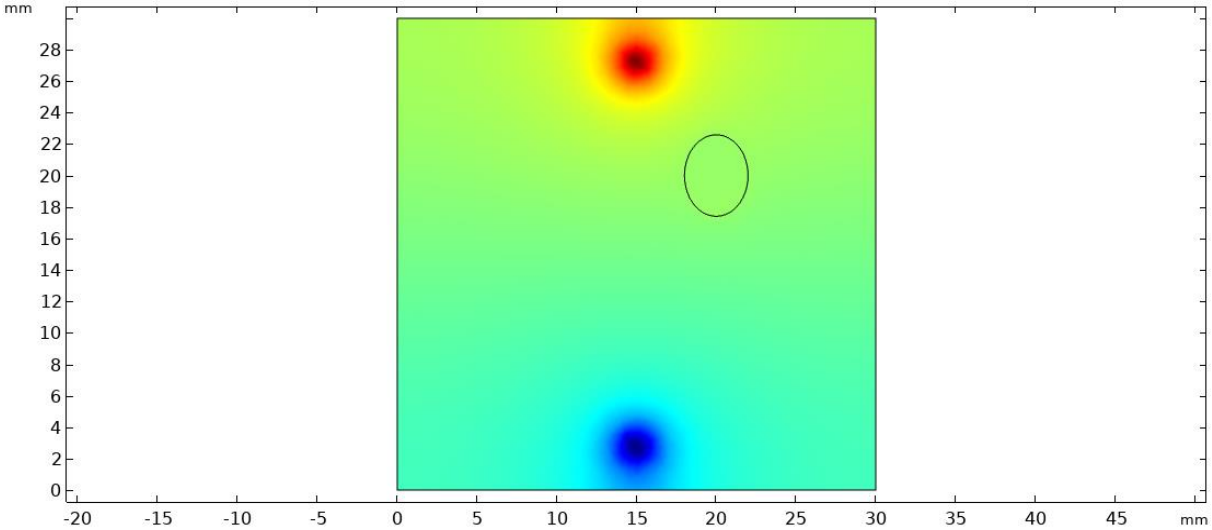

(b)

Figure 8.3. a) XY surface plot of healty skin model b) XY surface plot of skin model with abnormal tissue

The color differences in the surface plots in Figure 8.3.a and 8.3.b represent regions where electric currents are high and low, and therefore regions where electric potential is low and high. The images are XY planar sections obtained from the surface of the skin model with healthy and differentiated tissue. In the second image, the location and boundaries of the abnormal tissue are clearly seen.

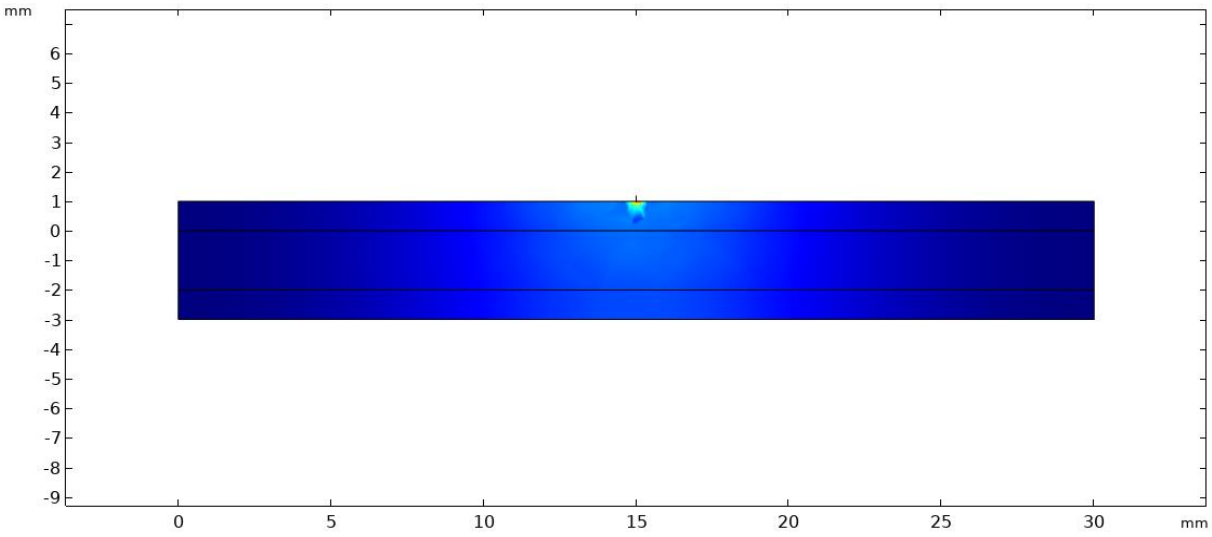

(a)

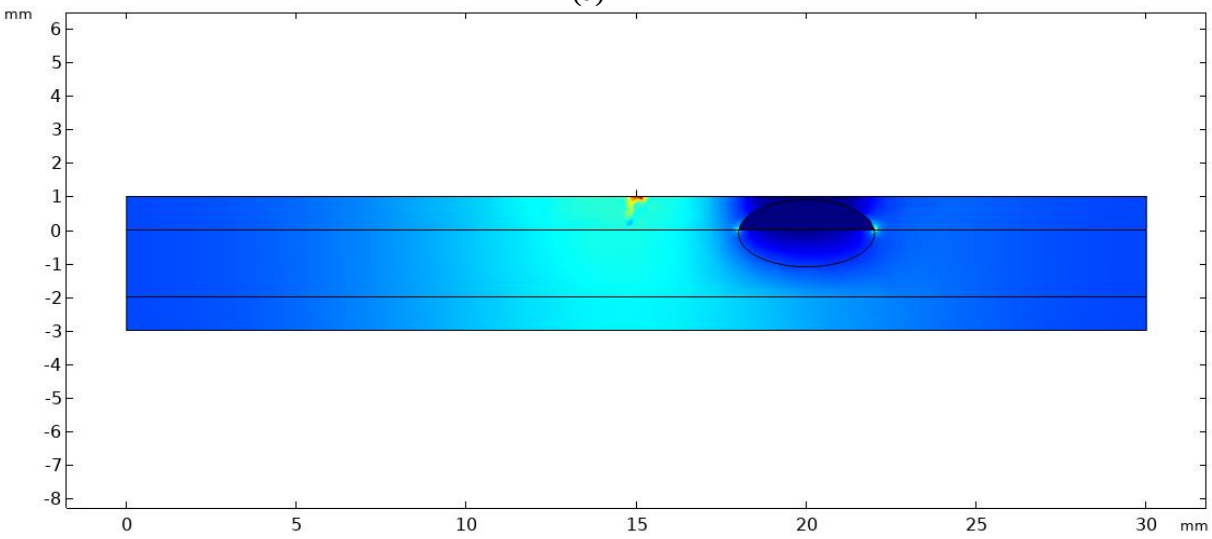

(b)

Figure 8.4. a) XZ surface plot of healty skin model b) XZ surface plot of skin model with abnormal tissue

The electric field surface graph obtained from the skin model simulation was recreated by taking a section from the XZ plane. Figure 8.4.a is the sectional image of the healthy skin tissue, and 8.4.b is the sectional image of the skin model with abnormal tissue.

Line graph: Line Graph is a graph that shows the variation of various physical quantities (e.g., temperature, pressure, voltage, current density, etc.) along a given line in a model. This graph is used to visualize and analyze simulation results in a single dimension.

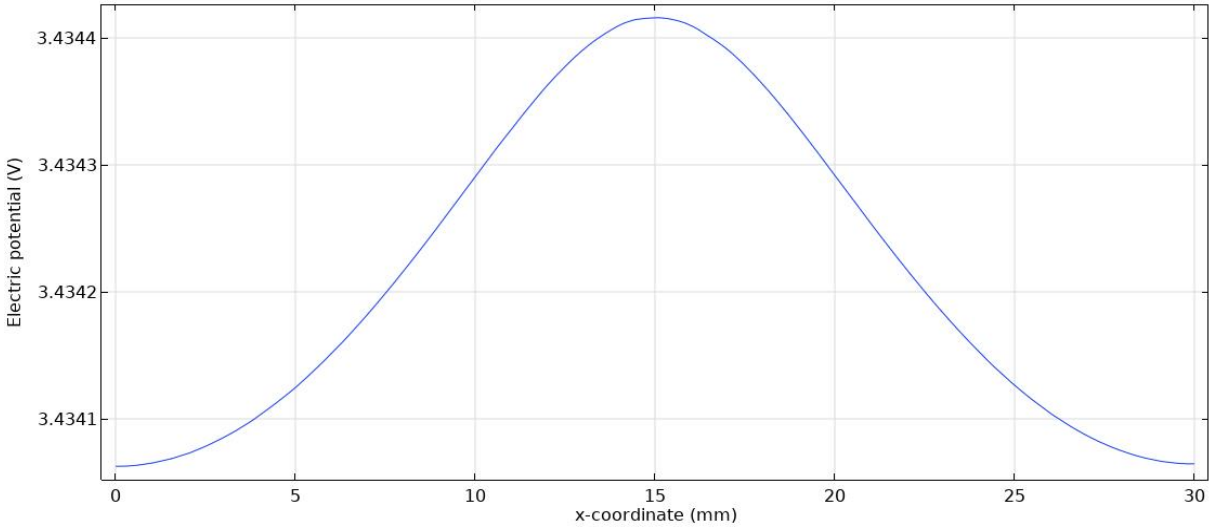

(a)

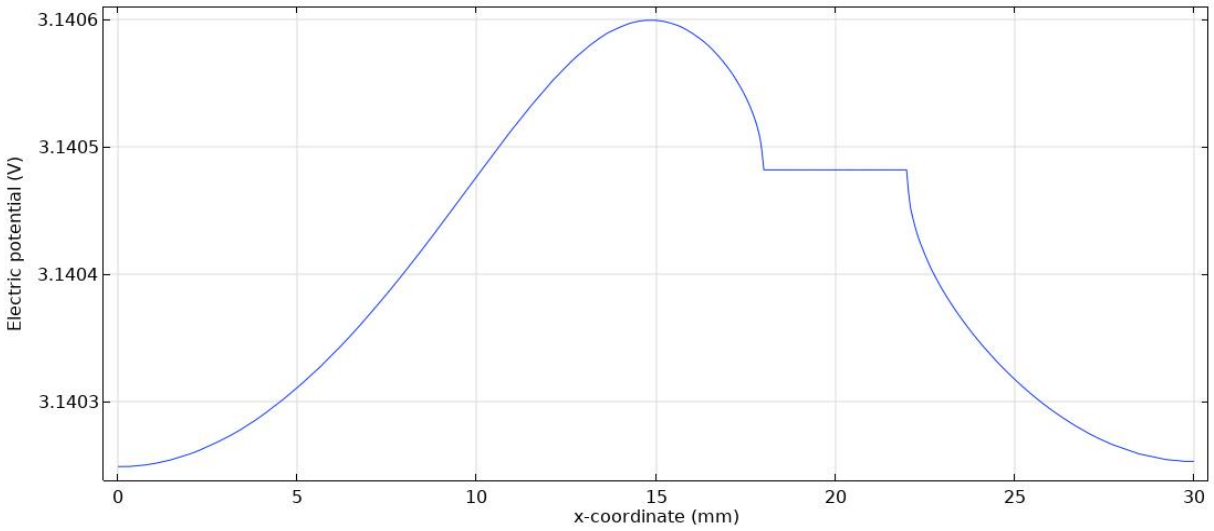

(b)

Figure 8.5. a) 1D plot of healty skin model b) 1D plot of skin model with abnormal tissue

In Figure 8.5.a and 8.5.b, the y-axis represents the electrical potential values and the x-axis represents the x-coordinate of the skin model (0-30 mm). Since the electrodes are positioned symmetrically, the electrical potential distribution in healthy tissue is expected to be symmetrical, and the results show that this assumption is correct. In Figure 8.5.b, the electrical potential difference at 20 mm and its surroundings is seen. This change in electrical potential indicates the presence of abnormal tissue that exhibits properties different from the typical electrical properties of the skin tissue.

All findings and details related to the subject should be given clearly under this title. A comparison and discussion of results from research with results obtained by others on the same topic

should be made. All findings and details related to the subject should be given clearly under this title. The results of the studies on the same subject should be compared and discussed with the findings obtained from the research.

8.2. EIDORS Simulation Results

As a result of the simulation performed in Section 6.2, forward and reverse models of abnormal tissue skin were obtained. The z-intersection image of the reverse model is given in Figure 8.6. The z-intersection of the model allows the visualization of the electrical distribution of abnormalities occurring at different depths of the skin model. By taking sections from different depths, the changing electrical properties of the skin layers can be visually examined, and pathological conditions can be detected.

Figure 8.6 is the image obtained from the simulated skin model at depths of 0.4-1-1.6 mm. EIDORS expresses the electrical conductivity or impedance distribution according to color codes. These colors allow us to understand how conductive or resistive the simulated model is.
In EIDORS; red, orange and yellow colors represent the low impedance region, blue and purple colors represent the high impedance region, and green tones represent the medium impedance region.

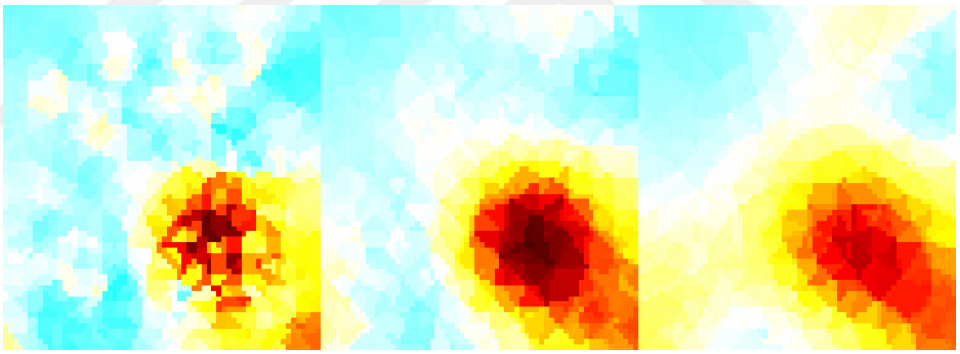

Figure 8.6. -0.4, -1.0, -1.6 mm z-intercepts image of skin with abnormal tissue

According to the cross-sectional view in Figure 8.6, it can be seen that a specific region is red and the areas outside that region are in blue tones. According to the information, the red region represents low impedance, and especially in the 1 mm cross-sectional image, an intense red region is seen. In the simulated model, abnormal tissue formation differs from the typical electrical properties of the skin. Accordingly, it is concluded that the electrical permitivity of the abnormal tissue is higher than the surrounding tissues.

8.3. Simulation and Experimental Data Results of Resistive Models

According to the determined measurement method, the data obtained from both models were recorded. This method's current injection-ground electrode pairs are 1-8, 9-16, 17-24, 25-32, 8-1, 16-9, 24-17, 32-25, respectively. In the same order, these measurements were named 'A-B-C-D-E-F-G-H.' Then, the difference between the data obtained from the model representing healthy tissue and the model with abnormal tissue was taken. Finally, these data were obtained graphically in MATLAB, with the x-axis being the electrode numbers (positions) and the y-axis being the difference voltage data.

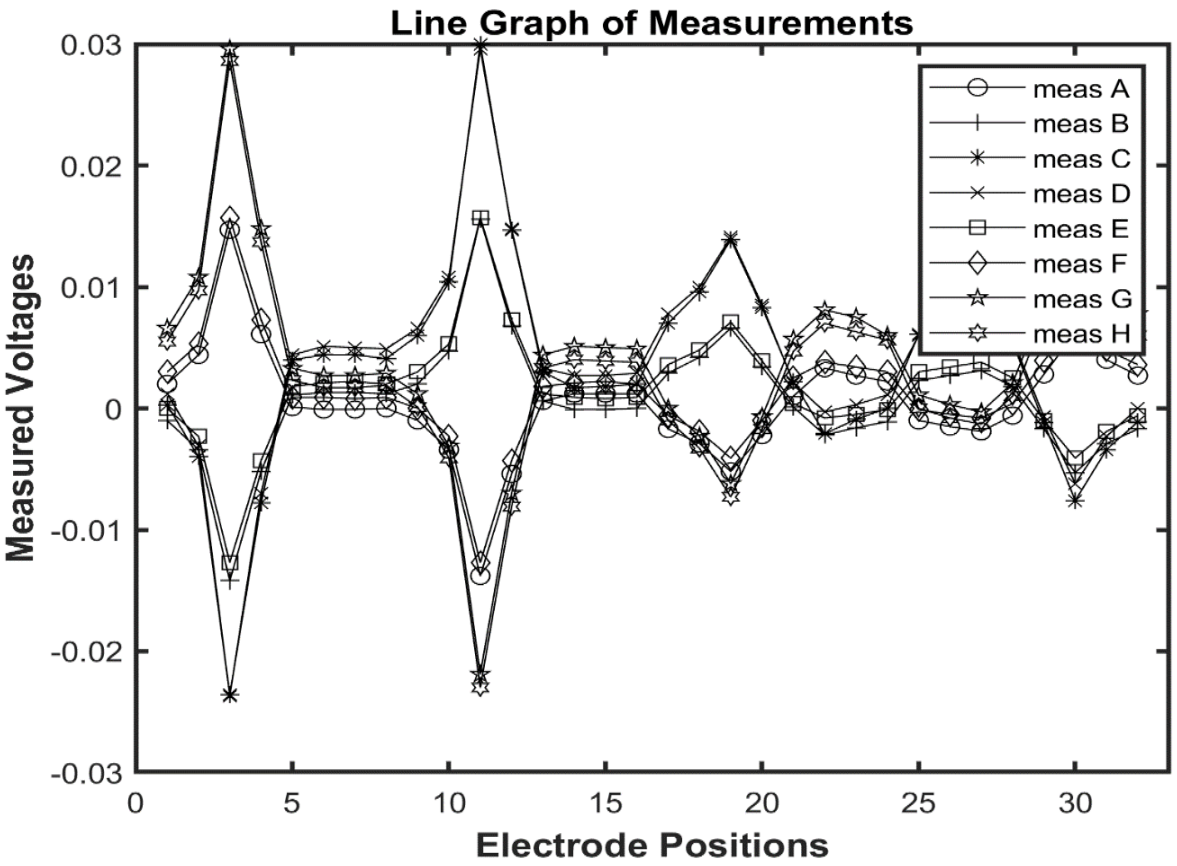

Figure 8.7. 1D plot of simulation result skin model with abnormal tissue between 2-10 electrodes

The data from the resistive model with healthy and abnormal tissue defined between electrodes 2-10 were obtained graphically in the MATLAB platform, as seen in Figure 8.7. According to the graph, maximum and minimum peaks are seen between electrodes 2-10. The peaks between the electrodes formed in the graph overlap with the abnormal tissue location defined in the model Figure 7.11.b. It was concluded that the presence and location of abnormal tissue are clearly seen in the graph.

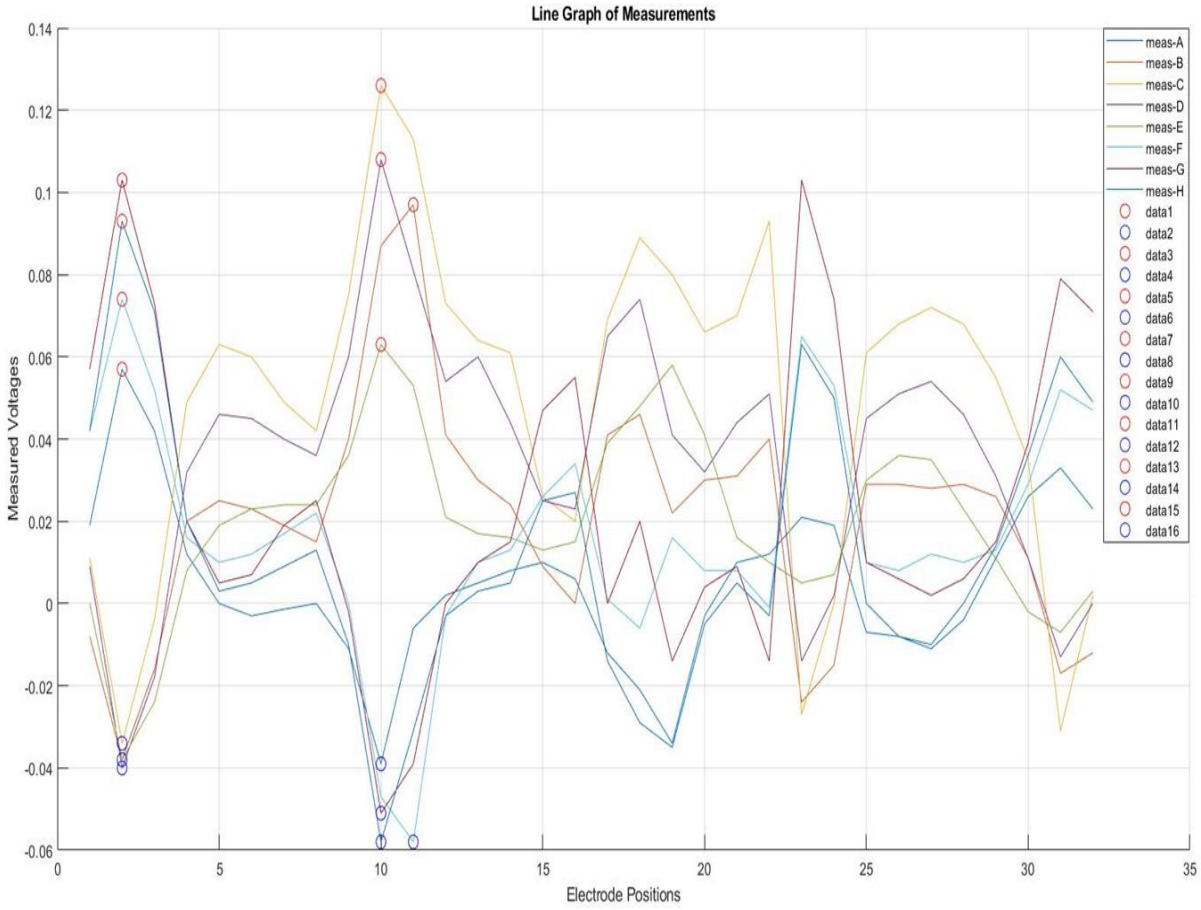

Figure 8.8. 1D plot of experimental result skin model with abnormal tissue between 2-10 electrodes

The experimental data of the resistive model with healthy and abnormal tissue defined between electrodes 2-10 were obtained graphically in the MATLAB platform as seen in Figure 8.8. According to the graph, maximum and minimum peaks are seen between electrodes 2-10. The peaks between the electrodes formed in the graph overlap with the abnormal tissue location defined in the model Figure 7.11.b. It was concluded that the presence and location of abnormal tissue are clearly seen in the graph. In addition, the data and graphs obtained from the simulation and experimental environment match.

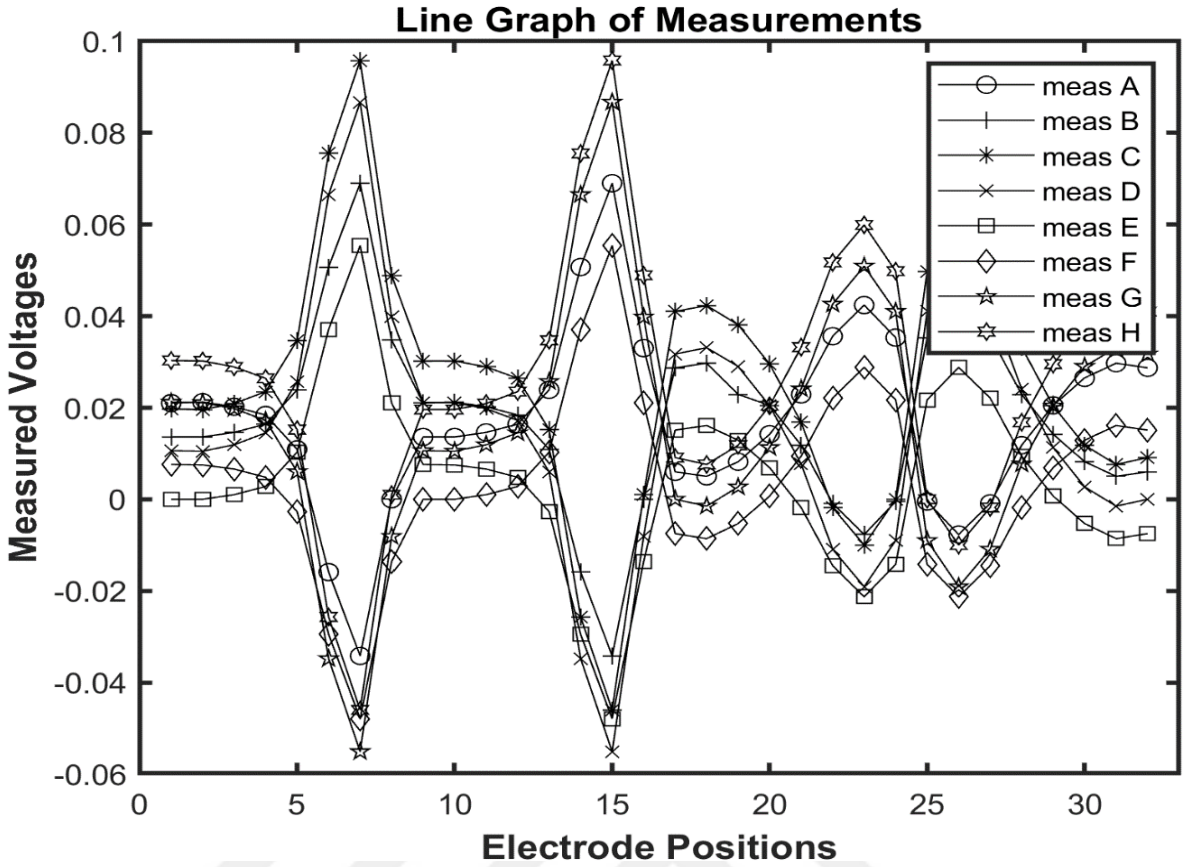

Figure 8.9. 1D plot of simulation result skin model with abnormal tissue between 7-15 electrodes

The data from the resistive model with healthy and abnormal tissue defined between electrodes 7-15 were obtained graphically in the MATLAB platform, as seen in Figure 8.9. According to the graph, maximum and minimum peaks are seen between electrodes 7-15. The peaks between the electrodes formed in the graph overlap with the abnormal tissue location defined in the model Figure 7.11.c. It was concluded that the presence and location of abnormal tissue are clearly seen in the graph.

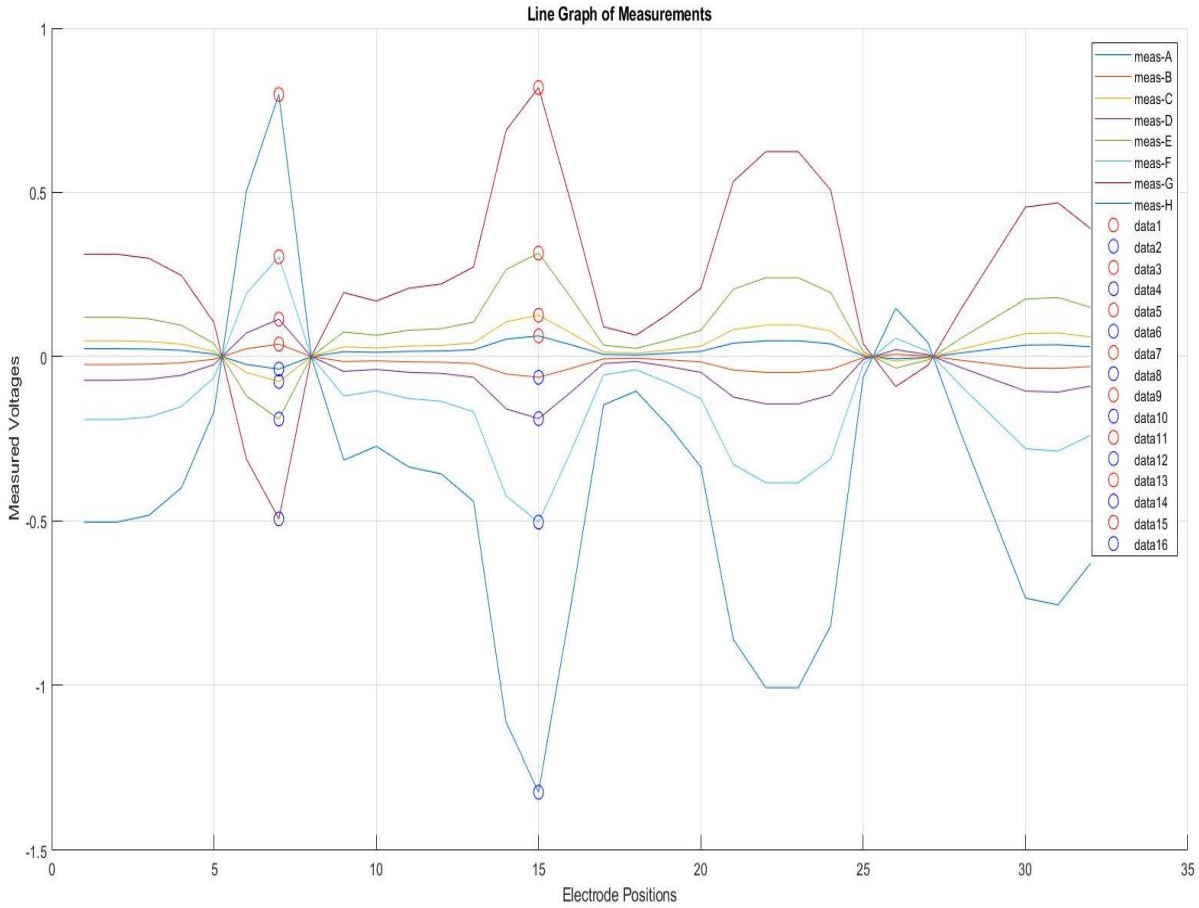

Figure 8.10. 1D plot of experimental result skin model with abnormal tissue between 7-15 electrodes

The experimental data of the resistive model with healthy and abnormal tissue defined between electrodes 7-15 were obtained graphically in the MATLAB platform as seen in Figure 8.10. According to the graph, maximum and minimum peaks are seen between electrodes 7-15. The peaks between the electrodes formed in the graph overlap with the abnormal tissue location defined in the model Figure 7.11.c. It was concluded that the presence and location of abnormal tissue are clearly seen in the graph. In addition, the data and graphs obtained from the simulation and experimental environment match.

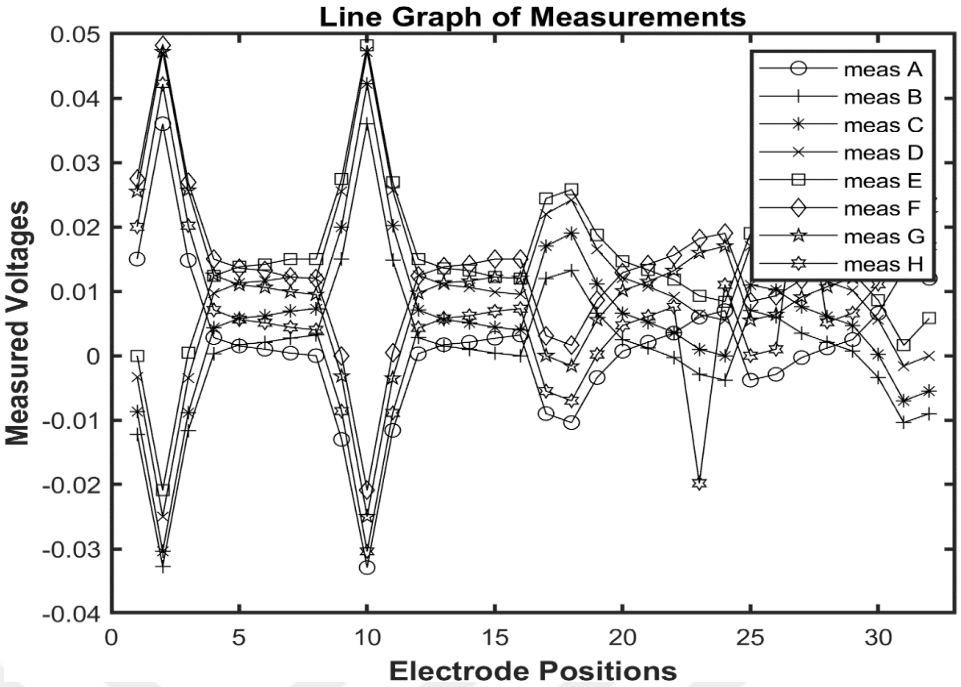

Figure 8.11. 1D plot of simulation result layered skin model with abnormal tissue between 2-10 electrodes

When the graph is examined, max and min peaks are seen between electrodes numbered 2-10. The peaks between the electrodes formed in the graph overlap with the abnormal tissue location defined in Figure 7.12.b. It was concluded that the presence and location of abnormal tissue is clearly seen in the graph.

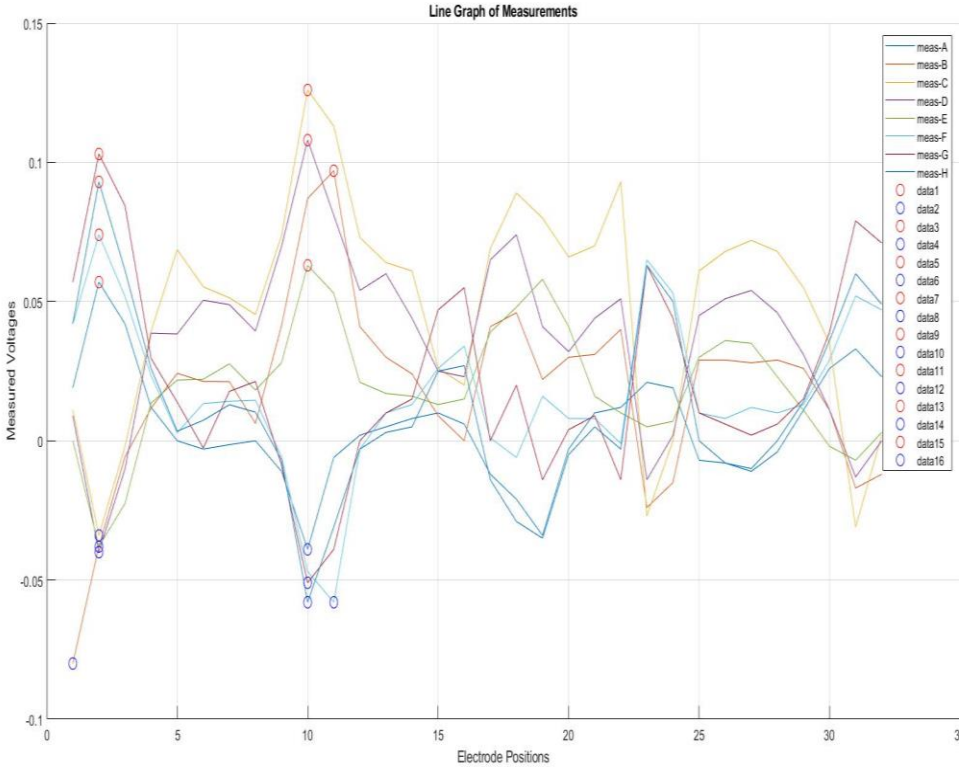

Figure 8.12. 1D plot of experimental result layered skin model with abnormal tissue between 2-10 electrodes

The experimental data of the layered resistive skin model with healthy and abnormal tissue defined between electrodes 2-10 were obtained graphically in the MATLAB platform as seen in Figure 8.12. According to the graph, maximum and minimum peaks are seen between electrodes 2-10. The peaks between the electrodes formed in the graph overlap with the abnormal tissue location defined in the model Figure 7.12.b. It was concluded that the presence and location of abnormal tissue are clearly seen in the graph. In addition, the data and graphs obtained from the simulation and experimental environment match.

8.4. Image Generation from Resistive Phantom Data

When creating an image, it can be thought of as consisting of points or elements with a certain value. The value of the element is related to the color or intensity of the image. In technical terms, the grid is called a "matrix" and each point in the grid is called a "pixel". The size of the grid determines the resolution of the image. The size of an image can vary greatly; for example, it can be a square of 128×128, 256×256, or 512×512 pixels. In general, the dimensions of an image can be m-times-n, where 'm' pixels are in the vertical direction and 'n' pixels are in the horizontal direction (Reyes-Aldasoro, 2015). The intensity level of each pixel is the basic information that makes up an image. The intensity values of the pixels are also used to perform operations such as segmentation or filtering. The intensity level of a grayscale image defines how bright or dark a pixel at that location should be. The 'uint8' data type assigns an integer value (without decimals) between 0 and 255 to represent the brightness of a pixel. A value of 0 represents black, and a value of 255 represents white. Using intensities, relationships between the intensities of neighboring pixels and their relative changes allow for interpretation of texture analysis.

This study used the data obtained from the different resistive models designed to create images on the MATLAB platform. The image size is 10x10 pixels square. The differences in gray tones in the image indicate the differences in the data. The algorithm created aims to mark the abnormal tissue's location, defined in the resistive model with a red ring in the image. The MATLAB code is given in Appendix A.

Figure 8.13 is 2D MATLAB images of the resistive skin model with abnormal tissue between electrodes 2-10.

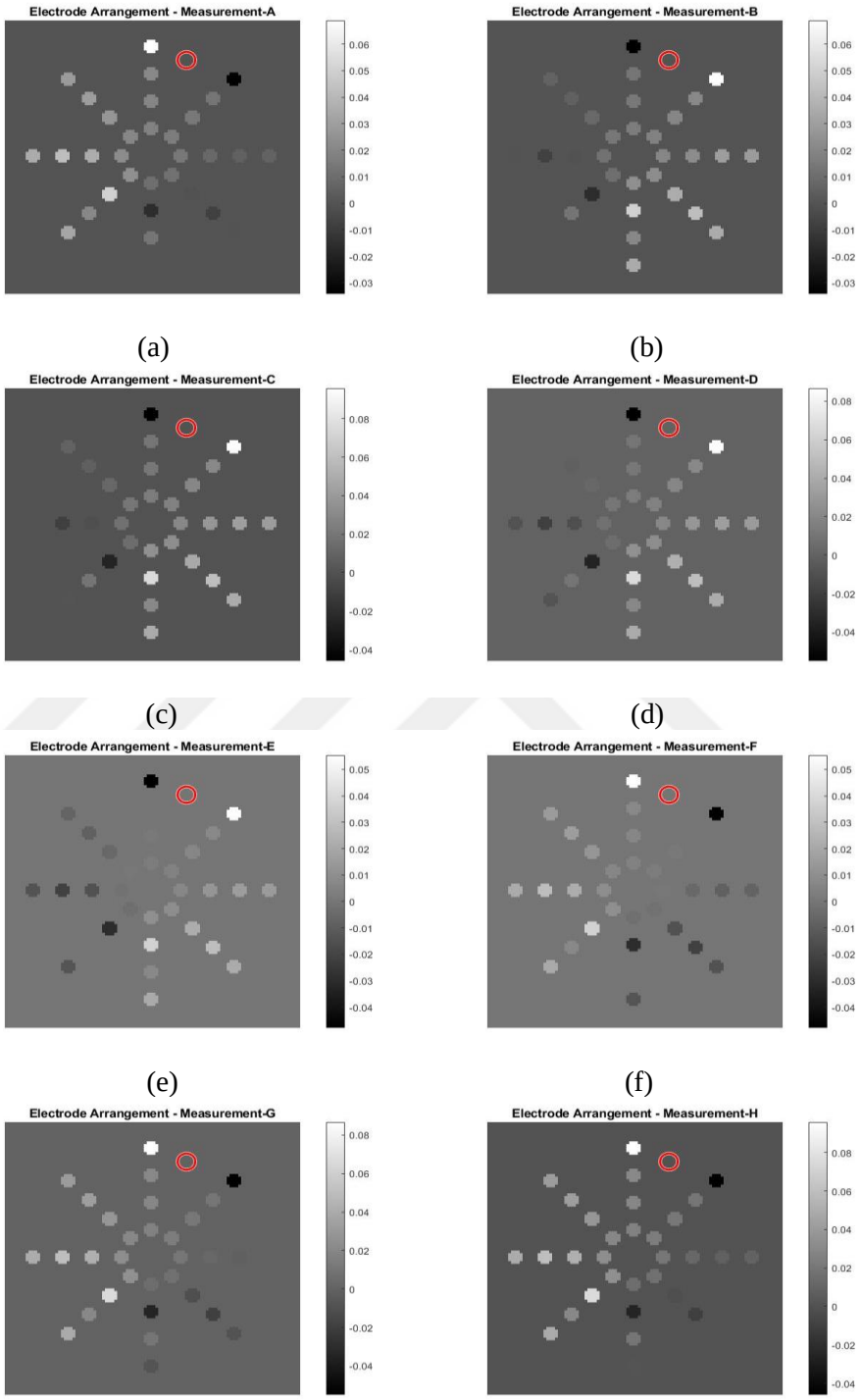

Figure 8.13. a) Image of measurement-A b) Image of measurement-B c) Image of measurement-C d) Image of measurement-D e) Image of measurement-E f) Image of measurement-F g) Image of measurement-G h) Image of measurement-H

Figures 8.14 is 2D MATLAB images of the resistive skin model with abnormal tissue between electrodes 7-15.

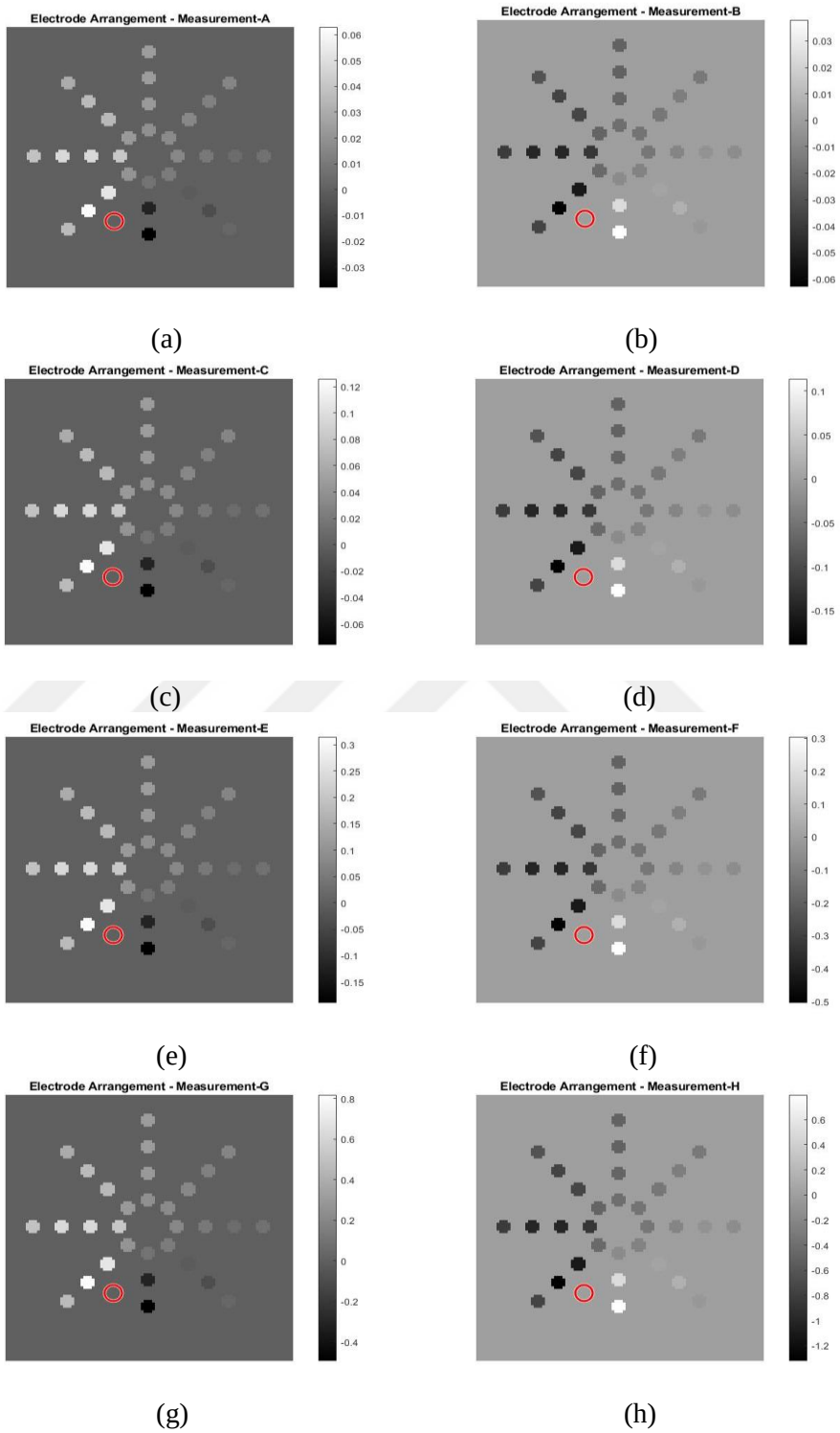

Figure 8.14. a) Image of measurement-A b) Image of measurement-B c) Image of measurement-C d) Image of measurement-D e) Image of measurement-E f) Image of measurement-F g) Image of measurement-G h) Image of measurement-H

Figures 8.15 is 2D MATLAB images of the resistive layer skin model with abnormal tissue between electrodes 2-10.

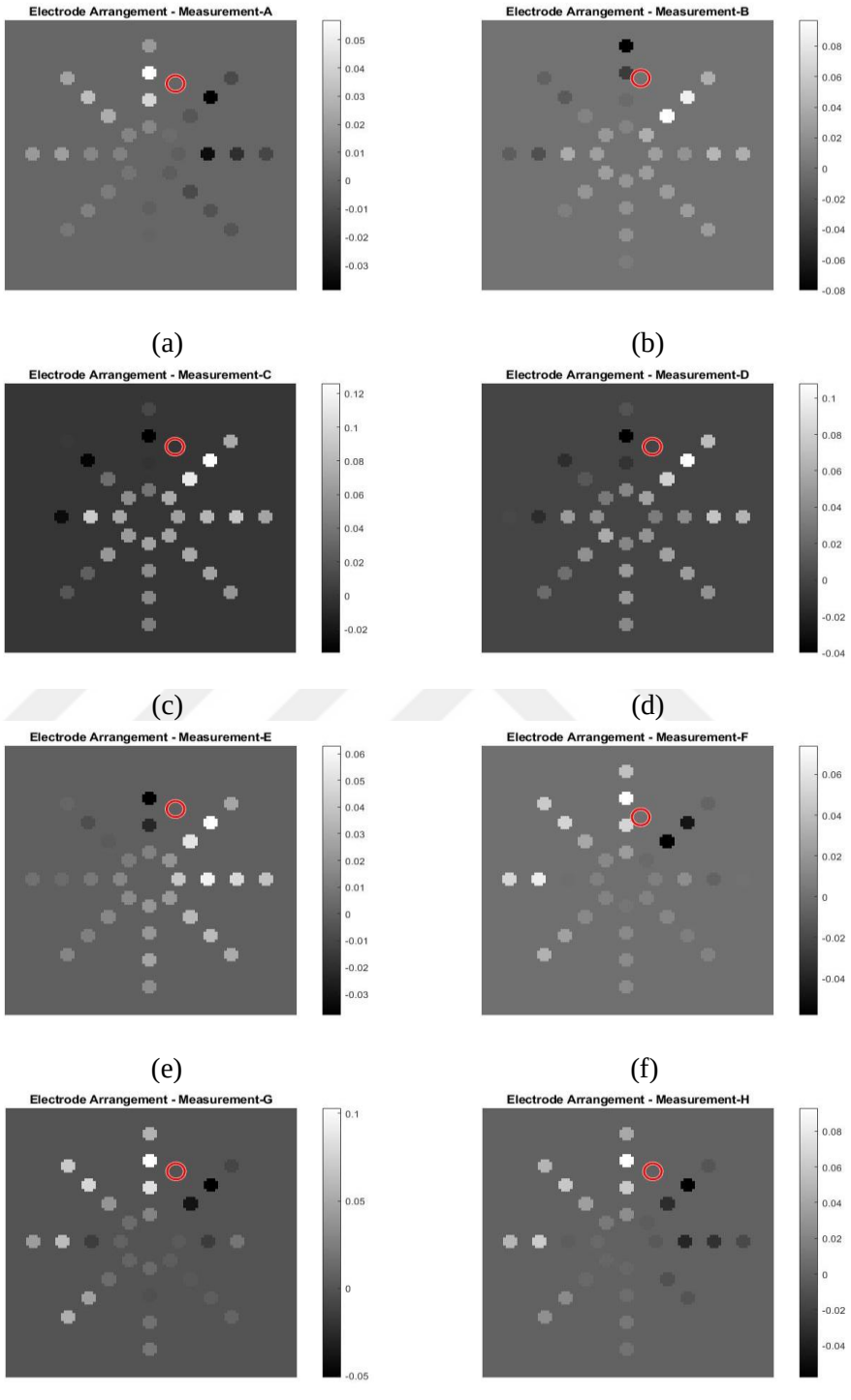

Figure 8.15. a) Image of measurement-A b) Image of measurement-B c) Image of measurement-C d) Image of measurement-D e) Image of measurement-E f) Image of measurement-F g) Image of measurement-G h) Image of measurement-H

This thesis includes the novel electrode design and measurement system developed for detecting abnormal tissues formed on the skin with the EIT technique. It also presents a study that compares the simulation and experimental results of the proposed system.

First, a realistic three-layer skin tissue model was constructed on the COMSOL and EIDORS platforms. Electrical parameters such as electrical conductivity and permittivity were defined for the skin tissue. The novel electrode design was placed on the skin. The aim was to scan the skin tissue 360° from the surface with the geometry of the electrode design and the stimulation pattern method. Then, the electrical working areas were defined, and the models were simulated.

In the COMSOL simulation, a healthy skin model of 30x30x4 mm3 was first simulated and the measurements were recorded. Then, a differentiated tissue was defined in the same model. It was simulated again. According to the 3D simulation result, the location of the differentiated tissue is shown in Figures 8.1 and 8.2. In Figure 8.3, an elliptical abnormal tissue presence with a center at (20,20) coordinates and an approximate surface size of 2x2.5 mm2 is seen according to the 2D-XY surface graph. In Figure 8.4, when the 2D-XZ graph is examined, it is seen that the abnormal tissue is approximately 2 mm deep from the skin surface. Figure 8.5 expresses the electrical potential of the healthy and abnormal skin model changing along the x coordinate. When the 1D graph is examined, the electrical potential decreases in the range of 18-22 mm. According to this information, it is concluded that an abnormal tissue with a lower impedance than the normal tissue has formed inside the healthy skin tissue.

In the simulation performed in EIDORS, an EIT study was conducted with a skin model and an electrode arrangement placed on the surface. The model was created, stimulation patterns were defined, and a mesh was created using the FEA method. The data obtained from the forward model was used to make the inverse model expressing the electrical conductivity distribution of the skin model. Z-intercepts were created at 0.4, 1, and 1.6 mm depths from the inverse model surface obtained using the Difference EIT method. Figure 8.6 is the z-intercept image obtained from different layers of the skin. The red region in this image differs from the surrounding color tones. This color difference in the EIDORS platform means that that region has a lower impedance. According to the simulation's cross-sectional image, it is concluded that an abnormal tissue formation with lower impedance is observed compared to the surrounding tissues. In this sense, the EIDORS platform allows sections to be taken from different points to diagnose and follow up on abnormal tissue in the body. This feature of EIDORS, which enables studies on the EIT technique, provides consistent results regarding the diagnosis and location of abnormal tissue formed in the body. The system was simulated in the experimental environment and implemented in the laboratory environment. Resistive phantoms representing the electrical properties of the skin tissue, healthy and containing different resistance values in some regions, were created. Resistive models were first simulated in the PSPICE environment. The difference in the data obtained from resistive phantoms representing models containing healthy and differentiated tissue was taken. Figure 8.7 shows the 1D graph of 8

measurement data obtained using the difference method. When the graph is examined, peaks are seen around electrodes numbered 2-10.

The difference data obtained from the same model in the laboratory environment is shown in Figure 8.8. It is seen that the data peaks between electrodes numbered 2-10. The region representing the abnormal tissue in the resistive model was taken to a different position, and the data was re-recorded. Figures 8.9 and 8.10 are the graphs obtained from the data. When the graphs are examined, peaks are seen between electrodes numbered 7-15. The data obtained from the resistive model representing layered skin tissue is given in Figures 8.11 and 8.12. As seen in the graphs, peaks are again seen between electrodes numbered 2-10. It was also observed that the difference in data obtained from the resistive model representing layered skin was lower than the other models.

The data obtained from the integrated resistive skin tissues and EIT system were also used to create images in MATLAB. The algorithm developed to create images is aimed at detecting abnormal tissue. The red circles in Figures 8.13, 8.14, and 8.15 show the locations of abnormal tissue.

According to the comments made on these graphs, it is concluded that the data obtained from the EIT system implemented in the laboratory environment and the data obtained as a result of the simulation in the computer environment are consistent.

As a result, abnormal tissue detection studies of the non-invasive, comfortable, and low-cost EIT technique, which allows the diagnosis and follow-up of abnormal tissues formed on the skin, were performed in this study. The studies were tested on different platforms (COMSOL, EIDORS), and the results obtained showed that this electrical impedance-based technique detects abnormal tissues on the skin with high accuracy and reliability. The study contributes to EIT studies in the biomedical and medical fields. The number of data obtained for this electrical impedance-based imaging technique and the specificity of the measurement system affect the image quality so that it can be obtained at the correct rate. The small amount of data received is one of the problems with the EIT technique. The electrode design and measurement method proposed in this study effectively solves this problem. Although the non-invasive measurements made from the skin surface are the advantages of this system, issues that will affect the values of the data, such as skin-electrode interface problems and artifacts, are the disadvantages of this system. The solutions to these problems will be the subject of future studies.

REFERENCES

Åberg, P., 2004. Skin Cancer As Seen By. PhD Thesis, Karolinska Institutet, Sweden, 73p

Åberg, P., Nicander, I., Hansson, J., Geladi, P., Holmgren, U., and Ollmar, S., 2004. Skin cancer identification using multifrequency electrical impedance - A potential screening tool. IEEE Transactions on Biomedical Engineering, *51*(12), 2097–2102. https://doi.org/10.1109/TBME.2004.836523

Adler, A., and Lionheart, W. R. B., 2006. Uses and abuses of EIDORS: An extensible software base for EIT. Physiological Measurement, 27(5). https://doi.org/10.1088/0967-3334/27/5/S03

Ang, V., Rahiman, M. H. F., Rahim, R. A., Aw, S. R., Wahab, Y. A., Thomas, W. K. T., and Siow, L. T., 2017. Forward problem studies of electrical resistance tomography system on concrete materials. AIP Conference Proceedings, 1808. https://doi.org/10.1063/1.4975242

Birgersson, U., Birgersson, E., Aberg, P., and Nicander, I. (n.d.). Non-invasive bioimpedance of intact skin : mathematical modeling and experiments. 1. https://doi.org/10.1088/0967-3334/32/1/001

Braun, F., Proença, M., Adler, A., Riedel, T., Thiran, J. P., and Solà, J., 2018. Accuracy and reliability of noninvasive stroke volume monitoring via ECG-gated 3D electrical impedance tomography in healthy volunteers. PLoS ONE, *13*(1), 1–19. https://doi.org/10.1371/journal.pone.0191870

Cherepenin V, Karpov, A., Korjenevsky, A., Kornienko V, Mazaletskaya, A., Mazourov, D., and Meister, D., 2001. A 3D electrical impedance tomography (EIT) system for breast cancer detection. Physiological Measurement, 22(1), 9–18. https://doi.org/10.1088/0967-3334/22/1/302

G Hahn, M Beer, I Frerichs, T Dudykevych, T Schröder, and G Hellige., 2000. A simple method to check the dynamic performance of electrical impedance tomography systems. Physiological Measurement, 21(1), 53. https://doi.org/10.1088/0967-3334/21/1/307

Gagnon, H., Cousineau, M., Adler, A., and Hartinger, A. E., 2010. A resistive mesh phantom for assessing the performance of EIT systems. IEEE Transactions on Biomedical Engineering, 57(9), 2257–2266. https://doi.org/10.1109/TBME.2010.2052618

Gutierrez-Lopez, M., Prado-Olivarez, J., Diaz-Carmona, J., Herrera-Ramírez, C. A., Gutierrez-Gnecchi, J. A., & Medina-Sánchez, C. G., 2019. Electrical impedance-based methodology for locating carcinoma emulators on breast models. Journal of Sensors. https://doi.org/10.1155/2019/8587191

Hartinger, A. E., Guardo, R., and Gagnon, H., 2012. EIT system and reconstruction algorithm adapted for skin cancer imaging. 2012 11th International Conference on Information Science, Signal Processing and Their Applications, ISSPA, 798–803. https://doi.org/10.1109/ISSPA.2012.6310662

Hua, P., Woo, E. J., Webster, J. G., and Tompkins, W. J., 1993. Finite Element Modeling of Impedance in Electrical-Skin Contact Impedance in Electrical Impedance Tomography. IEEE Transactions on Biomedical Engineering, 40(4), 335–343. https://doi.org/10.1109/10.222326

İstanbullu, M., and Avcı, M., 2020. Mikroelektronik Laboratuvar Uygulamaları 2. Adana, 258s

Kamat, D. K., Chavan, A. P., and Patil, P. M., 2014. Bio-Impedance Measurement System for Analysis of Skin Diseases. International Journal of Application or Innovation in Engineering & Management, 3(2), 92–96.

Mansouri, S., 2020. Determination of Cardiac Output by Peripheral Electrical Bioimpedance. IEEJ Transactions on Electrical and Electronic Engineering, 15(9), 1321–1326. https://doi.org/10.1002/tee.23199

McDermott, B., O'Halloran, M., Porter, E., and Santorelli, A., 2018. Brain haemorrhage detection using a SVM classifier with electrical impedance tomography measurement frames. PLoS ONE, 13(7), 1–26. https://doi.org/10.1371/journal.pone.0200469

Mellenthin, M. M., Mueller, J. L., de Camargo, E. D. L. B., de Moura, F. S., Rattis Santos, T. B., Lima, R. G., Hamilton, S. J., Muller, P. A., and Alsaker, M., 2019. The ACE1 Electrical Impedance Tomography System for Thoracic Imaging. IEEE Transactions on Instrumentation and Measurement, 68(9), 3137–3150. https://doi.org/10.1109/TIM.2018.2874127

Pettersen, F. J., and Høgetveit, J. O., 2011. From 3D tissue data to impedance using Simpleware ScanFE+IP and COMSOL Multiphysics - A tutorial. Journal of Electrical Bioimpedance, 2(1), 13–32. https://doi.org/10.5617/jeb.173

Reyes-Aldasoro, C. C., 2015. Introduction to Images. In Biomedical Image Analysis Recipes in MATLAB® (pp. 45–70). John Wiley & Sons, Ltd. https://doi.org/https://doi.org/10.1002/9781118657546.ch2

Shi, X., Li, W., You, F., Huo, X., Xu, C., Ji, Z., Liu, R., Liu, B., Li, Y., Fu, F., and Dong, X., 2018. High-precision electrical impedance tomography data acquisition system for brain imaging. IEEE Sensors Journal, 18(14), 5974–5984. https://doi.org/10.1109/JSEN.2018.2836336

Shuvo, O. I., and Islam, M. N., 2016. Sensitivity Analysis of the Tetrapolar Electrical Impedance Measurement Systems Using COMSOL Multiphysics for the non-uniform and Inhomogeneous Medium. Dhaka University Journal of Science, *64*(1), 7–13. https://doi.org/10.3329/dujs.v64i1.28517

Singh, G., Anand, S., Lall, B., Srivastava, A., and Singh, V., 2019. A Low-Cost Portable Wireless Multi-frequency Electrical Impedance Tomography System. Arabian Journal for Science and Engineering, 44(3), 2305–2320. https://doi.org/10.1007/s13369-018-3435-4

Soleimani, M., and Rymarczyk, T., 2023. Ultrasound Tomography for Lung Imaging: An Experimental Phantom Study. IEEE Sensors Journal, 23(8), 8769–8775. https://doi.org/10.1109/JSEN.2023.3252340

Soulsby, C. T., Khela, M., Yazaki, E., Evans, D. F., Hennessy, E., & Powell-Tuck, J., 2006. Measurements of gastric emptying during continuous nasogastric infusion of liquid feed: Electric impedance tomography versus gamma scintigraphy. Clinical Nutrition, 25(4), 671–680. https://doi.org/10.1016/j.clnu.2005.11.015

Strang, G., and Fix, G. J., 1997. An analysis of the finite element method. Prentice-Hall, Inc.

Tissue Dielectric Properties. (n.d.). https://itis.swiss/virtual-population/tissue-properties/database/dielectric-properties/

Yang, L., Wu, H., Liu, K., Chen, B., Huang, S., & Yao, J., 2023. A Multicircle Planar Electrical Impedance Tomography Sensor for 3-D Miniature Imaging. IEEE Sensors Journal, 23(9), 9697–9706. https://doi.org/10.1109/JSEN.2023.3262266

CURRICULUM VITAE

Büşra OĞUZHAN, graduated from Kilis Mehmet Zelzele Science High School in 2014, completed her undergraduate education in Biomedical Engineering at Çukurova University and has a master's degree in Biomedical Engineering at Çukurova University.

APPENDICES

APPENDEX A: MATLAB Code for Image Generation

```
% Impedance measurement data
[ load empedance_data;];
%%
% Electrode array matrix
matrix_size = 100;
pixel_radius = 2.5;
radii = [40, 30, 20, 10];
center = matrix_size / 2;
theta = linspace(0, 2*pi, 9);
theta(end) = [];
electrodes = {
[1, 9, 17, 25, 8, 16, 24, 32],
[2, 10, 18, 26, 7, 15, 23, 31],
[3, 11, 19, 27, 6, 14, 22, 30],
[4, 12, 20, 28, 5, 13, 21, 29]
};
rotation_angle = -pi/2;
% Visualize impedance data for each measurement
figure;
hold on;
colors = lines(8); % Color palette
for i = 1:8
plot(1:32, empedance_data(:, i), 'Color', colors(i, :), 'DisplayName', ['Measurement-', char('A'+i1)]);
end
legend show;
xlabel('Electrode Number');
ylabel('Impedance');
title('Impedance Measurement Data');
grid on;
% Locating and marking electrodes with maximum and minimum impedance levels
for i = 1:8
[~, max_idx] = max(empedance_data(:, i));
[~, min_idx] = min(empedance_data(:, i));
plot(max_idx, empedance_data(max_idx, i), 'ro', 'MarkerSize', 8);
plot(min_idx, empedance_data(min_idx, i), 'bo', 'MarkerSize', 8);
end
```

```
hold off;
%%
% Creating electrode layout matrix for each measurement
electrode_matrices = cell(1, 8);
for k = 1:8
electrode_matrix = zeros(matrix_size);
for i = 1:length(radii)
radius = radii(i);
for j = 1:length(theta)
elektrot_no = electrodes{i}(j);
x = round(center + radius * cos(theta(j) + rotation_angle));
y = round(center + radius * sin(theta(j) + rotation_angle));
for dx = -ceil(pixel_radius):ceil(pixel_radius)
for dy = -ceil(pixel_radius):ceil(pixel_radius)
if dx^2 + dy^2 <= pixel_radius^2
x_coord = round(x + dx);
y_coord = round(y + dy);
if x_coord > 0 && x_coord <= matrix_size && y_coord > 0 && y_coord <= matrix_size
electrode_matrix(y_coord, x_coord) = empedance_data(electrode_no, k);
end
end
end
end
end
end
electrode_matrices{k} = electrode_matrix;
end
%%
% Marking maximum and minimum impedance levels on electrode layout matrices
for k = 1:8
electrode_matrix = electrode_matrices{k};
[~, max_idx] = max(empedance_data(:, k));
[~, min_idx] = min(empedance_data(:, k));
[max_y, max_x] = find(electrode_matrix == empedance_data(max_idx, k), 1);
[min_y, min_x] = find(electrode_matrix == empedance_data(min_idx, k), 1);

% Calculating the midpoint
```

```
mid_x = round((max_x + min_x) / 2);
mid_y = round((max_y + min_y) / 2);
% Electrode layout matrix visualization
figure;
imagesc(electrode_matrix);
colormap(gray);
colorbar;
title(['Electrode Arrangement - Measurement-', char('A'+k-1)]);
axis equal;
axis off;
% Marked with a red circle
hold on;
viscircles([mid_x, mid_y], 3, 'EdgeColor', 'r');
hold off;
end
```

APPENDEX B: MATLAB Code for EIDORS Simulation

```
clearvars;
tic;
shape_str = ['solid top    = plane(0,0,0;0,0,1);\n'...
             'solid block  = orthobrick(-15,-15,-1;15,15,0) -maxh=0.3;\n'
...
             'solid mainobj= top and block ;\n'];
elec_pos = [ %electrode array = A
             0          ,        12.25,  0,   0,  0,  1;
             0          ,         8.75,  0,   0,  0,  1;
             0          ,         5.25,  0,   0,  0,  1;
             0          ,         1.75,  0,   0,  0,  1;
             0          ,        -1.75,  0,   0,  0,  1;
             0          ,        -5.25,  0,   0,  0,  1;
             0          ,        -8.75,  0,   0,  0,  1;
             0          ,       -12.25,  0,   0,  0,  1;
             %electrode array = B
             8.66205807 ,  8.66205807 ,  0,   0,  0,  1;
             6.187184335,  6.187184335,  0,   0,  0,  1;
             3.712310601,  3.712310601,  0,   0,  0,  1;
             1.237436867,  1.237436867,  0,   0,  0,  1;
            -1.237436867, -1.237436867,  0,   0,  0,  1;
            -3.712310601, -3.712310601,  0,   0,  0,  1;
            -6.187184335, -6.187184335,  0,   0,  0,  1;
            -8.66205807 , -8.66205807 ,  0,   0,  0,  1;
             %electrode array = C
            12.25       ,            0,  0,   0,  0,  1;
             8.75       ,            0,  0,   0,  0,  1;
             5.25       ,            0,  0,   0,  0,  1;
             1.75       ,            0,  0,   0,  0,  1;
            -1.75       ,            0,  0,   0,  0,  1;
            -5.25       ,            0,  0,   0,  0,  1;
            -8.75       ,            0,  0,   0,  0,  1;
            -12.25      ,            0,  0,   0,  0,  1;
             %electrode array = D
             8.66205807 ,  -8.66205807,  0,   0,  0,  1;
             6.187184335, -6.187184335,  0,   0,  0,  1;
             3.712310601, -3.712310601,  0,   0,  0,  1;
             1.237436867, -1.237436867,  0,   0,  0,  1;
            -1.237436867,  1.237436867,  0,   0,  0,  1;
            -3.712310601,  3.712310601,  0,   0,  0,  1;
```

```
            -6.187184335,  6.187184335,  0,   0,  0,  1;
            -8.66205807 ,  8.66205807 ,  0,   0,  0,  1;
            ];
elec_shape=[0.25];
elec_obj = 'top';
fmdl = ng_mk_gen_models(shape_str, elec_pos, elec_shape, elec_obj);
figure
show_fem(fmdl)
stim(1).stim_pattern=
[0.01;0;0;0;0;0;0;0.01;0;0;0;0;0;0;0;0;0;0;0;0;0;0;0;0;0;0;0;0;0;0;0;0;0;0;0;0;0;0;0;0;0];
%1-8
stim(1).meas_pattern =
[0,0,0,0,0,0,0,0,0,0,0,0,0,0,0,0,0,0,0,0,0,0,0,0,0,0,0,0,0,0,0,0,0,0,0,0,0,0,0,0,0,0,0,0        %1
 0,1,0,0,0,0,0,-1,0,0,0,0,0,0,0,0,0,0,0,0,0,0,0,0,0,0,0,0,0,0,0,0,0,0,0,0,0,0,0,0,0,0,0       %2
 0,0,1,0,0,0,0,-1,0,0,0,0,0,0,0,0,0,0,0,0,0,0,0,0,0,0,0,0,0,0,0,0,0,0,0,0,0,0,0,0,0,0,0       %3
 0,0,0,1,0,0,0,-1,0,0,0,0,0,0,0,0,0,0,0,0,0,0,0,0,0,0,0,0,0,0,0,0,0,0,0,0,0,0,0,0,0,0,0       %4
 0,0,0,0,1,0,0,-1,0,0,0,0,0,0,0,0,0,0,0,0,0,0,0,0,0,0,0,0,0,0,0,0,0,0,0,0,0,0,0,0,0,0,0       %5
 0,0,0,0,0,1,0,-1,0,0,0,0,0,0,0,0,0,0,0,0,0,0,0,0,0,0,0,0,0,0,0,0,0,0,0,0,0,0,0,0,0,0,0       %6
 0,0,0,0,0,0,1,-1,0,0,0,0,0,0,0,0,0,0,0,0,0,0,0,0,0,0,0,0,0,0,0,0,0,0,0,0,0,0,0,0,0,0,0       %7
 0,0,0,0,0,0,0,0,0,0,0,0,0,0,0,0,0,0,0,0,0,0,0,0,0,0,0,0,0,0,0,0,0,0,0,0,0,0,0,0,0,0,0,0      %8
 0,0,0,0,0,0,0,0,1,0,0,0,0,0,0,-1,0,0,0,0,0,0,0,0,0,0,0,0,0,0,0,0,0,0,0,0,0,0,0,0,0,0,0       %9
 0,0,0,0,0,0,0,0,0,1,0,0,0,0,0,-1,0,0,0,0,0,0,0,0,0,0,0,0,0,0,0,0,0,0,0,0,0,0,0,0,0,0,0      %10
 0,0,0,0,0,0,0,0,0,0,1,0,0,0,0,-1,0,0,0,0,0,0,0,0,0,0,0,0,0,0,0,0,0,0,0,0,0,0,0,0,0,0,0      %11
 0,0,0,0,0,0,0,0,0,0,0,1,0,0,0,-1,0,0,0,0,0,0,0,0,0,0,0,0,0,0,0,0,0,0,0,0,0,0,0,0,0,0,0      %12
 0,0,0,0,0,0,0,0,0,0,0,0,1,0,0,-1,0,0,0,0,0,0,0,0,0,0,0,0,0,0,0,0,0,0,0,0,0,0,0,0,0,0,0      %13
 0,0,0,0,0,0,0,0,0,0,0,0,0,1,0,-1,0,0,0,0,0,0,0,0,0,0,0,0,0,0,0,0,0,0,0,0,0,0,0,0,0,0,0      %14
 0,0,0,0,0,0,0,0,0,0,0,0,0,0,1,-1,0,0,0,0,0,0,0,0,0,0,0,0,0,0,0,0,0,0,0,0,0,0,0,0,0,0,0      %15
 0,0,0,0,0,0,0,0,0,0,0,0,0,0,0,0,0,0,0,0,0,0,0,0,0,0,0,0,0,0,0,0,0,0,0,0,0,0,0,0,0,0,0,0      %16
 0,0,0,0,0,0,0,0,0,0,0,0,0,0,0,0,1,0,0,0,0,0,0,-1,0,0,0,0,0,0,0,0,0,0,0,0,0,0,0,0,0,0,0      %17
 0,0,0,0,0,0,0,0,0,0,0,0,0,0,0,0,0,1,0,0,0,0,0,-1,0,0,0,0,0,0,0,0,0,0,0,0,0,0,0,0,0,0,0      %18
 0,0,0,0,0,0,0,0,0,0,0,0,0,0,0,0,0,0,1,0,0,0,0,-1,0,0,0,0,0,0,0,0,0,0,0,0,0,0,0,0,0,0,0      %19
 0,0,0,0,0,0,0,0,0,0,0,0,0,0,0,0,0,0,0,1,0,0,0,-1,0,0,0,0,0,0,0,0,0,0,0,0,0,0,0,0,0,0,0      %20
 0,0,0,0,0,0,0,0,0,0,0,0,0,0,0,0,0,0,0,0,1,0,0,-1,0,0,0,0,0,0,0,0,0,0,0,0,0,0,0,0,0,0,0      %21
 0,0,0,0,0,0,0,0,0,0,0,0,0,0,0,0,0,0,0,0,0,1,0,-1,0,0,0,0,0,0,0,0,0,0,0,0,0,0,0,0,0,0,0      %22
 0,0,0,0,0,0,0,0,0,0,0,0,0,0,0,0,0,0,0,0,0,0,1,-1,0,0,0,0,0,0,0,0,0,0,0,0,0,0,0,0,0,0,0      %23
 0,0,0,0,0,0,0,0,0,0,0,0,0,0,0,0,0,0,0,0,0,0,0,0,0,0,0,0,0,0,0,0,0,0,0,0,0,0,0,0,0,0,0,0      %24
 0,0,0,0,0,0,0,0,0,0,0,0,0,0,0,0,0,0,0,0,0,0,0,0,0,1,0,0,0,0,0,0,-1,0,0,0,0,0,0,0,0,0,0,0     %25
 0,0,0,0,0,0,0,0,0,0,0,0,0,0,0,0,0,0,0,0,0,0,0,0,0,0,1,0,0,0,0,0,-1,0,0,0,0,0,0,0,0,0,0,0     %26
 0,0,0,0,0,0,0,0,0,0,0,0,0,0,0,0,0,0,0,0,0,0,0,0,0,0,0,1,0,0,0,0,-1,0,0,0,0,0,0,0,0,0,0,0     %27
 0,0,0,0,0,0,0,0,0,0,0,0,0,0,0,0,0,0,0,0,0,0,0,0,0,0,0,0,1,0,0,0,-1,0,0,0,0,0,0,0,0,0,0,0     %28
 0,0,0,0,0,0,0,0,0,0,0,0,0,0,0,0,0,0,0,0,0,0,0,0,0,0,0,0,0,1,0,0,-1,0,0,0,0,0,0,0,0,0,0,0     %29
```

```
 0,0,0,0,0,0,0,0,0,0,0,0,0,0,0,0,0,0,0,0,0,0,0,0,0,0,0,0,0,1,0,-1      %30
 0,0,0,0,0,0,0,0,0,0,0,0,0,0,0,0,0,0,0,0,0,0,0,0,0,0,0,0,0,0,0,1,-1      %31
 0,0,0,0,0,0,0,0,0,0,0,0,0,0,0,0,0,0,0,0,0,0,0,0,0,0,0,0,0,0,0,0,0];     %32
stim(2).stim_pattern=
[0;0;0;0;0;0;0;0;0.01;0;0;0;0;0;0;0.01;0;0;0;0;0;0;0;0;0;0;0;0;0;0;0];
%9-16
stim(2).meas_pattern}
[1,0,0,0,0,0,0,0,0,0,0,0,0,0,0,0,0,0,0,0,0,0,0,0,0,0,0,0,0,0,0,0,0        %1
 0,1,0,0,0,0,0,0,-1,0,0,0,0,0,0,0,0,0,0,0,0,0,0,0,0,0,0,0,0,0,0,0,0,0       %2
 0,0,1,0,0,0,0,0,-1,0,0,0,0,0,0,0,0,0,0,0,0,0,0,0,0,0,0,0,0,0,0,0,0,0       %3
 0,0,0,1,0,0,0,0,-1,0,0,0,0,0,0,0,0,0,0,0,0,0,0,0,0,0,0,0,0,0,0,0,0,0       %4
 0,0,0,0,1,0,0,0,-1,0,0,0,0,0,0,0,0,0,0,0,0,0,0,0,0,0,0,0,0,0,0,0,0,0       %5
 0,0,0,0,0,1,0,0,-1,0,0,0,0,0,0,0,0,0,0,0,0,0,0,0,0,0,0,0,0,0,0,0,0,0       %6
 0,0,0,0,0,0,1,0,-1,0,0,0,0,0,0,0,0,0,0,0,0,0,0,0,0,0,0,0,0,0,0,0,0,0       %7
 0,0,0,0,0,0,0,0,0,0,0,0,0,0,0,0,0,0,0,0,0,0,0,0,0,0,0,0,0,0,0,0,0,0        %8
 0,0,0,0,0,0,0,0,0,0,0,0,0,0,0,0,0,0,0,0,0,0,0,0,0,0,0,0,0,0,0,0,0,0        %9
 0,0,0,0,0,0,0,0,0,1,0,0,0,0,0,-1,0,0,0,0,0,0,0,0,0,0,0,0,0,0,0,0,0      %10
 0,0,0,0,0,0,0,0,0,0,1,0,0,0,0,-1,0,0,0,0,0,0,0,0,0,0,0,0,0,0,0,0,0      %11
 0,0,0,0,0,0,0,0,0,0,0,1,0,0,0,-1,0,0,0,0,0,0,0,0,0,0,0,0,0,0,0,0,0      %12
 0,0,0,0,0,0,0,0,0,0,0,0,1,0,0,-1,0,0,0,0,0,0,0,0,0,0,0,0,0,0,0,0,0      %13
 0,0,0,0,0,0,0,0,0,0,0,0,0,1,0,-1,0,0,0,0,0,0,0,0,0,0,0,0,0,0,0,0,0      %14
 0,0,0,0,0,0,0,0,0,0,0,0,0,0,1,-1,0,0,0,0,0,0,0,0,0,0,0,0,0,0,0,0,0      %15
 0,0,0,0,0,0,0,0,0,0,0,0,0,0,0,0,0,0,0,0,0,0,0,0,0,0,0,0,0,0,0,0,0,0      %16
 0,0,0,0,0,0,0,0,0,0,0,0,0,0,0,0,1,0,0,0,0,0,0,-1,0,0,0,0,0,0,0,0,0      %17
 0,0,0,0,0,0,0,0,0,0,0,0,0,0,0,0,0,1,0,0,0,0,0,-1,0,0,0,0,0,0,0,0,0      %18
 0,0,0,0,0,0,0,0,0,0,0,0,0,0,0,0,0,0,1,0,0,0,0,-1,0,0,0,0,0,0,0,0,0      %19
 0,0,0,0,0,0,0,0,0,0,0,0,0,0,0,0,0,0,0,1,0,0,0,-1,0,0,0,0,0,0,0,0,0      %20
 0,0,0,0,0,0,0,0,0,0,0,0,0,0,0,0,0,0,0,0,1,0,0,-1,0,0,0,0,0,0,0,0,0      %21
 0,0,0,0,0,0,0,0,0,0,0,0,0,0,0,0,0,0,0,0,0,1,0,-1,0,0,0,0,0,0,0,0,0      %22
 0,0,0,0,0,0,0,0,0,0,0,0,0,0,0,0,0,0,0,0,0,0,1,-1,0,0,0,0,0,0,0,0,0      %23
 0,0,0,0,0,0,0,0,0,0,0,0,0,0,0,0,0,0,0,0,0,0,0,0,0,0,0,0,0,0,0,0,0,0      %24
 0,0,0,0,0,0,0,0,0,0,0,0,0,0,0,0,0,0,0,0,0,0,0,0,0,1,0,0,0,0,0,0,-1      %25
 0,0,0,0,0,0,0,0,0,0,0,0,0,0,0,0,0,0,0,0,0,0,0,0,0,0,1,0,0,0,0,0,-1      %26
 0,0,0,0,0,0,0,0,0,0,0,0,0,0,0,0,0,0,0,0,0,0,0,0,0,0,0,1,0,0,0,0,-1      %27
 0,0,0,0,0,0,0,0,0,0,0,0,0,0,0,0,0,0,0,0,0,0,0,0,0,0,0,0,1,0,0,0,-1      %28
 0,0,0,0,0,0,0,0,0,0,0,0,0,0,0,0,0,0,0,0,0,0,0,0,0,0,0,0,0,1,0,0,-1      %29
 0,0,0,0,0,0,0,0,0,0,0,0,0,0,0,0,0,0,0,0,0,0,0,0,0,0,0,0,0,0,1,0,-1      %30
 0,0,0,0,0,0,0,0,0,0,0,0,0,0,0,0,0,0,0,0,0,0,0,0,0,0,0,0,0,0,0,1,-1      %31
 0,0,0,0,0,0,0,0,0,0,0,0,0,0,0,0,0,0,0,0,0,0,0,0,0,0,0,0,0,0,0,0,0];     %32
stim(3).stim_pattern =
```

```
[0;0;0;0;0;0;0;0;0;0;0;0;0;0;0;0;0.01;0;0;0;0;0;0;-0.01;0;0;0;0;0;0;0;0];
%17-24
stim(3).meas_pattern =
[1,0,0,0,0,0,0,-1,0,0,0,0,0,0,0,0,0,0,0,0,0,0,0,0,0,0,0,0,0,0,0,0,0,0,0       %1
 0,1,0,0,0,0,0,0,-1,0,0,0,0,0,0,0,0,0,0,0,0,0,0,0,0,0,0,0,0,0,0,0,0,0,0,0       %2
 0,0,1,0,0,0,0,0,-1,0,0,0,0,0,0,0,0,0,0,0,0,0,0,0,0,0,0,0,0,0,0,0,0,0,0,0       %3
 0,0,0,1,0,0,0,0,-1,0,0,0,0,0,0,0,0,0,0,0,0,0,0,0,0,0,0,0,0,0,0,0,0,0,0,0       %4
 0,0,0,0,1,0,0,0,-1,0,0,0,0,0,0,0,0,0,0,0,0,0,0,0,0,0,0,0,0,0,0,0,0,0,0,0       %5
 0,0,0,0,0,1,0,0,-1,0,0,0,0,0,0,0,0,0,0,0,0,0,0,0,0,0,0,0,0,0,0,0,0,0,0,0       %6
 0,0,0,0,0,0,1,0,-1,0,0,0,0,0,0,0,0,0,0,0,0,0,0,0,0,0,0,0,0,0,0,0,0,0,0,0       %7
 0,0,0,0,0,0,0,0,0,0,0,0,0,0,0,0,0,0,0,0,0,0,0,0,0,0,0,0,0,0,0,0,0,0,0,0       %8
 0,0,0,0,0,0,0,0,1,0,0,0,0,0,0,0,-1,0,0,0,0,0,0,0,0,0,0,0,0,0,0,0,0,0,0,0      %9
 0,0,0,0,0,0,0,0,0,1,0,0,0,0,0,0,-1,0,0,0,0,0,0,0,0,0,0,0,0,0,0,0,0,0,0,0     %10
 0,0,0,0,0,0,0,0,0,0,1,0,0,0,0,0,-1,0,0,0,0,0,0,0,0,0,0,0,0,0,0,0,0,0,0,0     %11
 0,0,0,0,0,0,0,0,0,0,0,1,0,0,0,0,-1,0,0,0,0,0,0,0,0,0,0,0,0,0,0,0,0,0,0,0     %12
 0,0,0,0,0,0,0,0,0,0,0,0,1,0,0,0,-1,0,0,0,0,0,0,0,0,0,0,0,0,0,0,0,0,0,0,0     %13
 0,0,0,0,0,0,0,0,0,0,0,0,0,1,0,0,-1,0,0,0,0,0,0,0,0,0,0,0,0,0,0,0,0,0,0,0     %14
 0,0,0,0,0,0,0,0,0,0,0,0,0,0,1,0,-1,0,0,0,0,0,0,0,0,0,0,0,0,0,0,0,0,0,0,0     %15
 0,0,0,0,0,0,0,0,0,0,0,0,0,0,0,1,-1,0,0,0,0,0,0,0,0,0,0,0,0,0,0,0,0,0,0,0     %16
 0,0,0,0,0,0,0,0,0,0,0,0,0,0,0,0,0,0,0,0,0,0,0,0,0,0,0,0,0,0,0,0,0,0,0,0      %17
 0,0,0,0,0,0,0,0,0,0,0,0,0,0,0,0,0,1,0,0,0,0,0,-1,0,0,0,0,0,0,0,0,0,0,0,0     %18
 0,0,0,0,0,0,0,0,0,0,0,0,0,0,0,0,0,0,1,0,0,0,0,-1,0,0,0,0,0,0,0,0,0,0,0,0     %19
 0,0,0,0,0,0,0,0,0,0,0,0,0,0,0,0,0,0,0,1,0,0,0,-1,0,0,0,0,0,0,0,0,0,0,0,0     %20
 0,0,0,0,0,0,0,0,0,0,0,0,0,0,0,0,0,0,0,0,1,0,0,-1,0,0,0,0,0,0,0,0,0,0,0,0     %21
 0,0,0,0,0,0,0,0,0,0,0,0,0,0,0,0,0,0,0,0,0,1,0,-1,0,0,0,0,0,0,0,0,0,0,0,0     %22
 0,0,0,0,0,0,0,0,0,0,0,0,0,0,0,0,0,0,0,0,0,0,1,-1,0,0,0,0,0,0,0,0,0,0,0,0     %23
 0,0,0,0,0,0,0,0,0,0,0,0,0,0,0,0,0,0,0,0,0,0,0,0,0,0,0,0,0,0,0,0,0,0,0,0      %24
 0,0,0,0,0,0,0,0,0,0,0,0,0,0,0,0,0,0,0,0,0,0,0,0,0,0,0,0,1,0,0,0,0,0,0,-1     %25
 0,0,0,0,0,0,0,0,0,0,0,0,0,0,0,0,0,0,0,0,0,0,0,0,0,0,0,0,0,1,0,0,0,0,0,-1     %26
 0,0,0,0,0,0,0,0,0,0,0,0,0,0,0,0,0,0,0,0,0,0,0,0,0,0,0,0,0,0,1,0,0,0,0,-1     %27
 0,0,0,0,0,0,0,0,0,0,0,0,0,0,0,0,0,0,0,0,0,0,0,0,0,0,0,0,0,0,0,1,0,0,0,-1     %28
 0,0,0,0,0,0,0,0,0,0,0,0,0,0,0,0,0,0,0,0,0,0,0,0,0,0,0,0,0,0,0,0,1,0,0,-1     %29
 0,0,0,0,0,0,0,0,0,0,0,0,0,0,0,0,0,0,0,0,0,0,0,0,0,0,0,0,0,0,0,0,0,1,0,-1     %30
 0,0,0,0,0,0,0,0,0,0,0,0,0,0,0,0,0,0,0,0,0,0,0,0,0,0,0,0,0,0,0,0,0,0,1,-1     %31
 0,0,0,0,0,0,0,0,0,0,0,0,0,0,0,0,0,0,0,0,0,0,0,0,0,0,0,0,0,0,0,0,0,0,0,0];    %32
stim(4).stim_pattern =
[0;0;0;0;0;0;0;0;0;0;0;0;0;0;0;0;0;0;0;0;0;0;0;0;0;0;0;0;0.01;0;0;0;0;0;0;-0.01];
%25-32
stim(4).meas_pattern =
[1,0,0,0,0,0,0,-1,0,0,0,0,0,0,0,0,0,0,0,0,0,0,0,0,0,0,0,0,0,0,0,0,0,0,0,0,0       %1
 0,1,0,0,0,0,0,0,-1,0,0,0,0,0,0,0,0,0,0,0,0,0,0,0,0,0,0,0,0,0,0,0,0,0,0,0,0       %2
```

```
 0,0,1,0,0,0,0,- 1,0,0,0,0,0,0,0,0,0,0,0,0,0,0,0,0,0,0,0,0,0,0,0,0,0,0,0,0,0      %3
 0,0,0,1,0,0,0,-1,0,0,0,0,0,0,0,0,0,0,0,0,0,0,0,0,0,0,0,0,0,0,0,0,0,0,0,0,0      %4
 0,0,0,0,1,0,0,-1,0,0,0,0,0,0,0,0,0,0,0,0,0,0,0,0,0,0,0,0,0,0,0,0,0,0,0,0,0      %5
 0,0,0,0,0,1,0,-1,0,0,0,0,0,0,0,0,0,0,0,0,0,0,0,0,0,0,0,0,0,0,0,0,0,0,0,0,0      %6
 0,0,0,0,0,0,1,-1,0,0,0,0,0,0,0,0,0,0,0,0,0,0,0,0,0,0,0,0,0,0,0,0,0,0,0,0,0      %7
 0,0,0,0,0,0,0,0,0,0,0,0,0,0,0,0,0,0,0,0,0,0,0,0,0,0,0,0,0,0,0,0,0,0,0,0,0,0      %8
 0,0,0,0,0,0,0,0,1,0,0,0,0,0,0,-1,0,0,0,0,0,0,0,0,0,0,0,0,0,0,0,0,0,0,0,0,0      %9
 0,0,0,0,0,0,0,0,0,1,0,0,0,0,0,-1,0,0,0,0,0,0,0,0,0,0,0,0,0,0,0,0,0,0,0,0,0     %10
 0,0,0,0,0,0,0,0,0,0,1,0,0,0,0,-1,0,0,0,0,0,0,0,0,0,0,0,0,0,0,0,0,0,0,0,0,0     %11
 0,0,0,0,0,0,0,0,0,0,0,1,0,0,0,-1,0,0,0,0,0,0,0,0,0,0,0,0,0,0,0,0,0,0,0,0,0     %12
 0,0,0,0,0,0,0,0,0,0,0,0,1,0,0,-1,0,0,0,0,0,0,0,0,0,0,0,0,0,0,0,0,0,0,0,0,0     %13
 0,0,0,0,0,0,0,0,0,0,0,0,0,1,0,-1,0,0,0,0,0,0,0,0,0,0,0,0,0,0,0,0,0,0,0,0,0     %14
 0,0,0,0,0,0,0,0,0,0,0,0,0,0,1,-1,0,0,0,0,0,0,0,0,0,0,0,0,0,0,0,0,0,0,0,0,0     %15
 0,0,0,0,0,0,0,0,0,0,0,0,0,0,0,0,0,0,0,0,0,0,0,0,0,0,0,0,0,0,0,0,0,0,0,0,0,0     %16
 0,0,0,0,0,0,0,0,0,0,0,0,0,0,0,0,1,0,0,0,0,0,0,-1,0,0,0,0,0,0,0,0,0,0,0,0,0,0     %17
 0,0,0,0,0,0,0,0,0,0,0,0,0,0,0,0,0,1,0,0,0,0,0,-1,0,0,0,0,0,0,0,0,0,0,0,0,0,0     %18
 0,0,0,0,0,0,0,0,0,0,0,0,0,0,0,0,0,0,1,0,0,0,0,-1,0,0,0,0,0,0,0,0,0,0,0,0,0,0     %19
 0,0,0,0,0,0,0,0,0,0,0,0,0,0,0,0,0,0,0,1,0,0,0,-1,0,0,0,0,0,0,0,0,0,0,0,0,0,0     %20
 0,0,0,0,0,0,0,0,0,0,0,0,0,0,0,0,0,0,0,0,1,0,0,-1,0,0,0,0,0,0,0,0,0,0,0,0,0,0     %21
 0,0,0,0,0,0,0,0,0,0,0,0,0,0,0,0,0,0,0,0,0,1,0,-1,0,0,0,0,0,0,0,0,0,0,0,0,0,0     %22
 0,0,0,0,0,0,0,0,0,0,0,0,0,0,0,0,0,0,0,0,0,0,1,-1,0,0,0,0,0,0,0,0,0,0,0,0,0,0     %23
 0,0,0,0,0,0,0,0,0,0,0,0,0,0,0,0,0,0,0,0,0,0,0,0,0,0,0,0,0,0,0,0,0,0,0,0,0,0     %24
 0,0,0,0,0,0,0,0,0,0,0,0,0,0,0,0,0,0,0,0,0,0,0,0,0,0,0,0,0,0,0,0,0,0,0,0,0,0     %25
 0,0,0,0,0,0,0,0,0,0,0,0,0,0,0,0,0,0,0,0,0,0,0,0,0,0,0,0,0,0,0,0,0,0,0,0,0,-1    %26
 0,0,0,0,0,0,0,0,0,0,0,0,0,0,0,0,0,0,0,0,0,0,0,0,0,0,0,0,0,0,0,0,0,0,0,0,0,-1    %27
 0,0,0,0,0,0,0,0,0,0,0,0,0,0,0,0,0,0,0,0,0,0,0,0,0,0,0,0,0,0,0,0,0,0,0,0,0,-1    %28
 0,0,0,0,0,0,0,0,0,0,0,0,0,0,0,0,0,0,0,0,0,0,0,0,0,0,0,0,0,0,0,0,0,0,0,0,0,-1    %29
 0,0,0,0,0,0,0,0,0,0,0,0,0,0,0,0,0,0,0,0,0,0,0,0,0,0,0,0,0,0,0,0,0,0,0,0,0,-1    %30
 0,0,0,0,0,0,0,0,0,0,0,0,0,0,0,0,0,0,0,0,0,0,0,0,0,0,0,0,0,0,0,0,0,0,0,0,0,-1    %31
 0,0,0,0,0,0,0,0,0,0,0,0,0,0,0,0,0,0,0,0,0,0,0,0,0,0,0,0,0,0,0,0,0,0,0,0,0,0];   %32
stim(5).stim_pattern =
[-0.01;0;0;0;0;0;0;0.01;0;0;0;0;0;0;0;0;0;0;0;0;0;0;0;0;0;0;0;0;0;0;0;0;0;0;0];
%8-1
stim(5).meas_pattern =
[0,0,0,0,0,0,0,0,0,0,0,0,0,0,0,0,0,0,0,0,0,0,0,0,0,0,0,0,0,0,0,0,0,0,0,0,0,0      %1
 1,1,0,0,0,0,0,0,0,0,0,0,0,0,0,0,0,0,0,0,0,0,0,0,0,0,0,0,0,0,0,0,0,0,0,0,0,0      %2
 1,0,1,0,0,0,0,0,0,0,0,0,0,0,0,0,0,0,0,0,0,0,0,0,0,0,0,0,0,0,0,0,0,0,0,0,0,0      %3
 1,0,0,1,0,0,0,0,0,0,0,0,0,0,0,0,0,0,0,0,0,0,0,0,0,0,0,0,0,0,0,0,0,0,0,0,0,0      %4
 1,0,0,0,1,0,0,0,0,0,0,0,0,0,0,0,0,0,0,0,0,0,0,0,0,0,0,0,0,0,0,0,0,0,0,0,0,0      %5
 1,0,0,0,0,1,0,0,0,0,0,0,0,0,0,0,0,0,0,0,0,0,0,0,0,0,0,0,0,0,0,0,0,0,0,0,0,0      %6
 1,0,0,0,0,0,1,0,0,0,0,0,0,0,0,0,0,0,0,0,0,0,0,0,0,0,0,0,0,0,0,0,0,0,0,0,0,0      %7
```

```
 0,0,0,0,0,0,0,0,0,0,0,0,0,0,0,0,0,0,0,0,0,0,0,0,0,0,0,0,0,0,0,0        %8
 0,0,0,0,0,0,0,0,0,0,0,0,0,0,0,0,0,0,0,0,0,0,0,0,0,0,0,0,0,0,0,0        %9
 0,0,0,0,0,0,0,0,-1,1,0,0,0,0,0,0,0,0,0,0,0,0,0,0,0,0,0,0,0,0,0,0      %10
 0,0,0,0,0,0,0,0,-1,0,1,0,0,0,0,0,0,0,0,0,0,0,0,0,0,0,0,0,0,0,0,0      %11
 0,0,0,0,0,0,0,0,-1,0,0,1,0,0,0,0,0,0,0,0,0,0,0,0,0,0,0,0,0,0,0,0      %12
 0,0,0,0,0,0,0,0,-1,0,0,0,1,0,0,0,0,0,0,0,0,0,0,0,0,0,0,0,0,0,0,0      %13
 0,0,0,0,0,0,0,0,-1,0,0,0,0,1,0,0,0,0,0,0,0,0,0,0,0,0,0,0,0,0,0,0      %14
 0,0,0,0,0,0,0,0,-1,0,0,0,0,0,1,0,0,0,0,0,0,0,0,0,0,0,0,0,0,0,0,0      %15
 0,0,0,0,0,0,0,0,-1,0,0,0,0,0,0,1,0,0,0,0,0,0,0,0,0,0,0,0,0,0,0,0      %16
 0,0,0,0,0,0,0,0,0,0,0,0,0,0,0,0,0,0,0,0,0,0,0,0,0,0,0,0,0,0,0,0       %17
 0,0,0,0,0,0,0,0,0,0,0,0,0,0,0,0,-1,1,0,0,0,0,0,0,0,0,0,0,0,0,0,0      %18
 0,0,0,0,0,0,0,0,0,0,0,0,0,0,0,0,-1,0,1,0,0,0,0,0,0,0,0,0,0,0,0,0      %19
 0,0,0,0,0,0,0,0,0,0,0,0,0,0,0,0,-1,0,0,1,0,0,0,0,0,0,0,0,0,0,0,0      %20
 0,0,0,0,0,0,0,0,0,0,0,0,0,0,0,0,-1,0,0,0,1,0,0,0,0,0,0,0,0,0,0,0      %21
 0,0,0,0,0,0,0,0,0,0,0,0,0,0,0,0,-1,0,0,0,0,1,0,0,0,0,0,0,0,0,0,0      %22
 0,0,0,0,0,0,0,0,0,0,0,0,0,0,0,0,-1,0,0,0,0,0,1,0,0,0,0,0,0,0,0,0      %23
 0,0,0,0,0,0,0,0,0,0,0,0,0,0,0,0,-1,0,0,0,0,0,0,1,0,0,0,0,0,0,0,0      %24
 0,0,0,0,0,0,0,0,0,0,0,0,0,0,0,0,0,0,0,0,0,0,0,0,0,0,0,0,0,0,0,0       %25
 0,0,0,0,0,0,0,0,0,0,0,0,0,0,0,0,0,0,0,0,0,0,0,0,-1,1,0,0,0,0,0,0      %26
 0,0,0,0,0,0,0,0,0,0,0,0,0,0,0,0,0,0,0,0,0,0,0,0,-1,0,1,0,0,0,0,0      %27
 0,0,0,0,0,0,0,0,0,0,0,0,0,0,0,0,0,0,0,0,0,0,0,0,-1,0,0,1,0,0,0,0      %28
 0,0,0,0,0,0,0,0,0,0,0,0,0,0,0,0,0,0,0,0,0,0,0,0,-1,0,0,0,1,0,0,0      %29
 0,0,0,0,0,0,0,0,0,0,0,0,0,0,0,0,0,0,0,0,0,0,0,0,-1,0,0,0,0,1,0,0      %30
 0,0,0,0,0,0,0,0,0,0,0,0,0,0,0,0,0,0,0,0,0,0,0,0,-1,0,0,0,0,0,1,0      %31
 0,0,0,0,0,0,0,0,0,0,0,0,0,0,0,0,0,0,0,0,0,0,0,0,-1,0,0,0,0,0,0,1];    %32
stim(6).stim_pattern =
[0;0;0;0;0;0;0;0;-0.01;0;0;0;0;0;0;0.01;0;0;0;0;0;0;0;0;0;0;0;0;0;0;0;0];
%16-9
stim(6).meas_pattern =
[0,0,0,0,0,0,0,0,0,0,0,0,0,0,0,0,0,0,0,0,0,0,0,0,0,0,0,0,0,0,0,0        %1
 1,1,0,0,0,0,0,0,0,0,0,0,0,0,0,0,0,0,0,0,0,0,0,0,0,0,0,0,0,0,0,0        %2
 1,0,1,0,0,0,0,0,0,0,0,0,0,0,0,0,0,0,0,0,0,0,0,0,0,0,0,0,0,0,0,0        %3
 1,0,0,1,0,0,0,0,0,0,0,0,0,0,0,0,0,0,0,0,0,0,0,0,0,0,0,0,0,0,0,0        %4
 1,0,0,0,1,0,0,0,0,0,0,0,0,0,0,0,0,0,0,0,0,0,0,0,0,0,0,0,0,0,0,0        %5
 1,0,0,0,0,1,0,0,0,0,0,0,0,0,0,0,0,0,0,0,0,0,0,0,0,0,0,0,0,0,0,0        %6
 1,0,0,0,0,0,1,0,0,0,0,0,0,0,0,0,0,0,0,0,0,0,0,0,0,0,0,0,0,0,0,0        %7
 1,0,0,0,0,0,0,1,0,0,0,0,0,0,0,0,0,0,0,0,0,0,0,0,0,0,0,0,0,0,0,0        %8
 0,0,0,0,0,0,0,0,0,0,0,0,0,0,0,0,0,0,0,0,0,0,0,0,0,0,0,0,0,0,0,0        %9
 0,0,0,0,0,0,0,0,-1,1,0,0,0,0,0,0,0,0,0,0,0,0,0,0,0,0,0,0,0,0,0,0      %10
 0,0,0,0,0,0,0,0,-1,0,1,0,0,0,0,0,0,0,0,0,0,0,0,0,0,0,0,0,0,0,0,0      %11
 0,0,0,0,0,0,0,0,-1,0,0,1,0,0,0,0,0,0,0,0,0,0,0,0,0,0,0,0,0,0,0,0      %12
```

```
 0,0,0,0,0,0,0,0,-1,0,0,0,1,0,0,0,0,0,0,0,0,0,0,0,0,0,0,0,0,0,0,0,0,0,0,0,0,0      %13
 0,0,0,0,0,0,0,0,-1,0,0,0,0,1,0,0,0,0,0,0,0,0,0,0,0,0,0,0,0,0,0,0,0,0,0,0,0,0      %14
 0,0,0,0,0,0,0,0,-1,0,0,0,0,0,1,0,0,0,0,0,0,0,0,0,0,0,0,0,0,0,0,0,0,0,0,0,0,0      %15
 0,0,0,0,0,0,0,0,0,0,0,0,0,0,0,0,0,0,0,0,0,0,0,0,0,0,0,0,0,0,0,0,0,0,0,0,0,0      %16
 0,0,0,0,0,0,0,0,0,0,0,0,0,0,0,0,0,0,0,0,0,0,0,0,0,0,0,0,0,0,0,0,0,0,0,0,0,0      %17
 0,0,0,0,0,0,0,0,0,0,0,0,0,0,0,0,0,-1,1,0,0,0,0,0,0,0,0,0,0,0,0,0,0,0,0,0,0,0      %18
 0,0,0,0,0,0,0,0,0,0,0,0,0,0,0,0,0,-1,0,1,0,0,0,0,0,0,0,0,0,0,0,0,0,0,0,0,0,0      %19
 0,0,0,0,0,0,0,0,0,0,0,0,0,0,0,0,0,-1,0,0,1,0,0,0,0,0,0,0,0,0,0,0,0,0,0,0,0,0      %20
 0,0,0,0,0,0,0,0,0,0,0,0,0,0,0,0,0,-1,0,0,0,1,0,0,0,0,0,0,0,0,0,0,0,0,0,0,0,0      %21
 0,0,0,0,0,0,0,0,0,0,0,0,0,0,0,0,0,-1,0,0,0,0,1,0,0,0,0,0,0,0,0,0,0,0,0,0,0,0      %22
 0,0,0,0,0,0,0,0,0,0,0,0,0,0,0,0,0,-1,0,0,0,0,0,1,0,0,0,0,0,0,0,0,0,0,0,0,0,0      %23
 0,0,0,0,0,0,0,0,0,0,0,0,0,0,0,0,0,-1,0,0,0,0,0,0,1,0,0,0,0,0,0,0,0,0,0,0,0,0      %24
 0,0,0,0,0,0,0,0,0,0,0,0,0,0,0,0,0,0,0,0,0,0,0,0,0,0,0,0,0,0,0,0,0,0,0,0,0,0      %25
 0,0,0,0,0,0,0,0,0,0,0,0,0,0,0,0,0,0,0,0,0,0,0,0,0,0,0,0,0,0,0,0,0,-1,1,0,0,0,0,0,0      %26
 0,0,0,0,0,0,0,0,0,0,0,0,0,0,0,0,0,0,0,0,0,0,0,0,0,0,0,0,0,0,0,0,0,-1,0,1,0,0,0,0,0      %27
 0,0,0,0,0,0,0,0,0,0,0,0,0,0,0,0,0,0,0,0,0,0,0,0,0,0,0,0,0,0,0,0,0,-1,0,0,1,0,0,0,0      %28
 0,0,0,0,0,0,0,0,0,0,0,0,0,0,0,0,0,0,0,0,0,0,0,0,0,0,0,0,0,0,0,0,0,-1,0,0,0,1,0,0,0      %29
 0,0,0,0,0,0,0,0,0,0,0,0,0,0,0,0,0,0,0,0,0,0,0,0,0,0,0,0,0,0,0,0,0,-1,0,0,0,0,1,0,0      %30
 0,0,0,0,0,0,0,0,0,0,0,0,0,0,0,0,0,0,0,0,0,0,0,0,0,0,0,0,0,0,0,0,0,-1,0,0,0,0,0,1,0      %31
 0,0,0,0,0,0,0,0,0,0,0,0,0,0,0,0,0,0,0,0,0,0,0,0,0,0,0,0,0,0,0,0,0,-1,0,0,0,0,0,0,1];    %32
stim(7).stim_pattern =
[0;0;0;0;0;0;0;0;0;0;0;0;0;0;0;0;-0.01;0;0;0;0;0;0;0.01;0;0;0;0;0;0;0];
%24-17
stim(7).meas_pattern =
[0,0,0,0,0,0,0,0,0,0,0,0,0,0,0,0,0,0,0,0,0,0,0,0,0,0,0,0,0,0,0,0,0,0,0,0,0,0       %1
 1,1,0,0,0,0,0,0,0,0,0,0,0,0,0,0,0,0,0,0,0,0,0,0,0,0,0,0,0,0,0,0,0,0,0,0,0,0       %2
 1,0,1,0,0,0,0,0,0,0,0,0,0,0,0,0,0,0,0,0,0,0,0,0,0,0,0,0,0,0,0,0,0,0,0,0,0,0       %3
 1,0,0,1,0,0,0,0,0,0,0,0,0,0,0,0,0,0,0,0,0,0,0,0,0,0,0,0,0,0,0,0,0,0,0,0,0,0       %4
 1,0,0,0,1,0,0,0,0,0,0,0,0,0,0,0,0,0,0,0,0,0,0,0,0,0,0,0,0,0,0,0,0,0,0,0,0,0       %5
 1,0,0,0,0,1,0,0,0,0,0,0,0,0,0,0,0,0,0,0,0,0,0,0,0,0,0,0,0,0,0,0,0,0,0,0,0,0       %6
 1,0,0,0,0,0,1,0,0,0,0,0,0,0,0,0,0,0,0,0,0,0,0,0,0,0,0,0,0,0,0,0,0,0,0,0,0,0       %7
 1,0,0,0,0,0,0,1,0,0,0,0,0,0,0,0,0,0,0,0,0,0,0,0,0,0,0,0,0,0,0,0,0,0,0,0,0,0       %8
 0,0,0,0,0,0,0,0,0,0,0,0,0,0,0,0,0,0,0,0,0,0,0,0,0,0,0,0,0,0,0,0,0,0,0,0,0,0       %9
 0,0,0,0,0,0,0,0,-1,1,0,0,0,0,0,0,0,0,0,0,0,0,0,0,0,0,0,0,0,0,0,0,0,0,0,0,0,0      %10
 0,0,0,0,0,0,0,0,-1,0,1,0,0,0,0,0,0,0,0,0,0,0,0,0,0,0,0,0,0,0,0,0,0,0,0,0,0,0      %11
 0,0,0,0,0,0,0,0,-1,0,0,1,0,0,0,0,0,0,0,0,0,0,0,0,0,0,0,0,0,0,0,0,0,0,0,0,0,0      %12
 0,0,0,0,0,0,0,0,-1,0,0,0,1,0,0,0,0,0,0,0,0,0,0,0,0,0,0,0,0,0,0,0,0,0,0,0,0,0      %13
 0,0,0,0,0,0,0,0,-1,0,0,0,0,1,0,0,0,0,0,0,0,0,0,0,0,0,0,0,0,0,0,0,0,0,0,0,0,0      %14
 0,0,0,0,0,0,0,0,-1,0,0,0,0,0,1,0,0,0,0,0,0,0,0,0,0,0,0,0,0,0,0,0,0,0,0,0,0,0      %15
 0,0,0,0,0,0,0,0,-1,0,0,0,0,0,0,1,0,0,0,0,0,0,0,0,0,0,0,0,0,0,0,0,0,0,0,0,0,0      %16
 0,0,0,0,0,0,0,0,0,0,0,0,0,0,0,0,0,0,0,0,0,0,0,0,0,0,0,0,0,0,0,0,0,0,0,0,0,0      %17
```

```
 0,0,0,0,0,0,0,0,0,0,0,0,0,0,0,0,-1,1,0,0,0,0,0,0,0,0,0,0,0,0,0,0      %18
 0,0,0,0,0,0,0,0,0,0,0,0,0,0,0,0,-1,0,1,0,0,0,0,0,0,0,0,0,0,0,0,0      %19
 0,0,0,0,0,0,0,0,0,0,0,0,0,0,0,0,-1,0,0,1,0,0,0,0,0,0,0,0,0,0,0,0      %20
 0,0,0,0,0,0,0,0,0,0,0,0,0,0,0,0,-1,0,0,0,1,0,0,0,0,0,0,0,0,0,0,0      %21
 0,0,0,0,0,0,0,0,0,0,0,0,0,0,0,0,-1,0,0,0,0,1,0,0,0,0,0,0,0,0,0,0      %22
 0,0,0,0,0,0,0,0,0,0,0,0,0,0,0,0,-1,0,0,0,0,0,1,0,0,0,0,0,0,0,0,0      %23
 0,0,0,0,0,0,0,0,0,0,0,0,0,0,0,0,0,0,0,0,0,0,0,0,0,0,0,0,0,0,0,0       %24
 0,0,0,0,0,0,0,0,0,0,0,0,0,0,0,0,0,0,0,0,0,0,0,0,0,0,0,0,0,0,0,0       %25
 0,0,0,0,0,0,0,0,0,0,0,0,0,0,0,0,0,0,0,0,0,0,0,0,0,0,-1,1,0,0,0,0,0,0  %26
 0,0,0,0,0,0,0,0,0,0,0,0,0,0,0,0,0,0,0,0,0,0,0,0,0,0,-1,0,1,0,0,0,0,0  %27
 0,0,0,0,0,0,0,0,0,0,0,0,0,0,0,0,0,0,0,0,0,0,0,0,0,0,-1,0,0,1,0,0,0,0  %28
 0,0,0,0,0,0,0,0,0,0,0,0,0,0,0,0,0,0,0,0,0,0,0,0,0,0,-1,0,0,0,1,0,0,0  %29
 0,0,0,0,0,0,0,0,0,0,0,0,0,0,0,0,0,0,0,0,0,0,0,0,0,0,-1,0,0,0,0,1,0,0  %30
 0,0,0,0,0,0,0,0,0,0,0,0,0,0,0,0,0,0,0,0,0,0,0,0,0,0,-1,0,0,0,0,0,1,0  %31
 0,0,0,0,0,0,0,0,0,0,0,0,0,0,0,0,0,0,0,0,0,0,0,0,0,0,-1,0,0,0,0,0,0,1]; %32
stim(8).stim_pattern =
[0;0;0;0;0;0;0;0;0;0;0;0;0;0;0;0;0;0;0;0;0;0;0;0;0;0;0;0;0;0;0;-0.01;0;0;0;0;0;0;0.01];
%32-25
stim(8).meas_pattern =
[0,0,0,0,0,0,0,0,0,0,0,0,0,0,0,0,0,0,0,0,0,0,0,0,0,0,0,0,0,0,0,0       %1
 1,1,0,0,0,0,0,0,0,0,0,0,0,0,0,0,0,0,0,0,0,0,0,0,0,0,0,0,0,0,0,0       %2
 1,0,1,0,0,0,0,0,0,0,0,0,0,0,0,0,0,0,0,0,0,0,0,0,0,0,0,0,0,0,0,0       %3
 1,0,0,1,0,0,0,0,0,0,0,0,0,0,0,0,0,0,0,0,0,0,0,0,0,0,0,0,0,0,0,0       %4
 1,0,0,0,1,0,0,0,0,0,0,0,0,0,0,0,0,0,0,0,0,0,0,0,0,0,0,0,0,0,0,0       %5
 1,0,0,0,0,1,0,0,0,0,0,0,0,0,0,0,0,0,0,0,0,0,0,0,0,0,0,0,0,0,0,0       %6
 1,0,0,0,0,0,1,0,0,0,0,0,0,0,0,0,0,0,0,0,0,0,0,0,0,0,0,0,0,0,0,0       %7
 1,0,0,0,0,0,0,1,0,0,0,0,0,0,0,0,0,0,0,0,0,0,0,0,0,0,0,0,0,0,0,0       %8
 0,0,0,0,0,0,0,0,0,0,0,0,0,0,0,0,0,0,0,0,0,0,0,0,0,0,0,0,0,0,0,0       %9
 0,0,0,0,0,0,0,0,-1,1,0,0,0,0,0,0,0,0,0,0,0,0,0,0,0,0,0,0,0,0,0,0      %10
 0,0,0,0,0,0,0,0,-1,0,1,0,0,0,0,0,0,0,0,0,0,0,0,0,0,0,0,0,0,0,0,0      %11
 0,0,0,0,0,0,0,0,-1,0,0,1,0,0,0,0,0,0,0,0,0,0,0,0,0,0,0,0,0,0,0,0      %12
 0,0,0,0,0,0,0,0,-1,0,0,0,1,0,0,0,0,0,0,0,0,0,0,0,0,0,0,0,0,0,0,0      %13
 0,0,0,0,0,0,0,0,-1,0,0,0,0,1,0,0,0,0,0,0,0,0,0,0,0,0,0,0,0,0,0,0      %14
 0,0,0,0,0,0,0,0,-1,0,0,0,0,0,1,0,0,0,0,0,0,0,0,0,0,0,0,0,0,0,0,0      %15
 0,0,0,0,0,0,0,0,-1,0,0,0,0,0,0,1,0,0,0,0,0,0,0,0,0,0,0,0,0,0,0,0      %16
 0,0,0,0,0,0,0,0,0,0,0,0,0,0,0,0,0,0,0,0,0,0,0,0,0,0,0,0,0,0,0,0       %17
 0,0,0,0,0,0,0,0,0,0,0,0,0,0,0,0,-1,1,0,0,0,0,0,0,0,0,0,0,0,0,0,0      %18
 0,0,0,0,0,0,0,0,0,0,0,0,0,0,0,0,-1,0,1,0,0,0,0,0,0,0,0,0,0,0,0,0      %19
 0,0,0,0,0,0,0,0,0,0,0,0,0,0,0,0,-1,0,0,1,0,0,0,0,0,0,0,0,0,0,0,0      %20
 0,0,0,0,0,0,0,0,0,0,0,0,0,0,0,0,-1,0,0,0,1,0,0,0,0,0,0,0,0,0,0,0      %21
 0,0,0,0,0,0,0,0,0,0,0,0,0,0,0,0,-1,0,0,0,0,1,0,0,0,0,0,0,0,0,0,0      %22
```

```
 0,0,0,0,0,0,0,0,0,0,0,0,0,0,0,-1,0,0,0,0,0,1,0,0,0,0,0,0,0,0,0      %23
 0,0,0,0,0,0,0,0,0,0,0,0,0,0,0,0,-1,0,0,0,0,0,0,1,0,0,0,0,0,0,0,0      %24
 0,0,0,0,0,0,0,0,0,0,0,0,0,0,0,0,0,0,0,0,0,0,0,0,0,0,0,0,0,0,0,0,0      %25
 0,0,0,0,0,0,0,0,0,0,0,0,0,0,0,0,0,0,0,0,0,0,0,0,0,0,0,-1,1,0,0,0,0,0,0      %26
 0,0,0,0,0,0,0,0,0,0,0,0,0,0,0,0,0,0,0,0,0,0,0,0,0,0,0,-1,0,1,0,0,0,0,0      %27
 0,0,0,0,0,0,0,0,0,0,0,0,0,0,0,0,0,0,0,0,0,0,0,0,0,0,0,-1,0,0,1,0,0,0,0      %28
 0,0,0,0,0,0,0,0,0,0,0,0,0,0,0,0,0,0,0,0,0,0,0,0,0,0,0,-1,0,0,0,1,0,0,0      %29
 0,0,0,0,0,0,0,0,0,0,0,0,0,0,0,0,0,0,0,0,0,0,0,0,0,0,0,-1,0,0,0,0,1,0,0      %30
 0,0,0,0,0,0,0,0,0,0,0,0,0,0,0,0,0,0,0,0,0,0,0,0,0,0,0,-1,0,0,0,0,0,1,0      %31
 0,0,0,0,0,0,0,0,0,0,0,0,0,0,0,0,0,0,0,0,0,0,0,0,0,0,0,0,0,0,0,0,0,0,0];     %32
fmdl.stimulation = stim;
img= mk_image(fmdl,1);
img.elem_data(fmdl.mat_idx{1}) = 2;
figure
show_fem(img); view(-16,22); set(gca,'Projection','perspective');
vi = fwd_solve(img);
img.elem_data(:) = 1;
vh = fwd_solve(img);
shape_str = ['solid top    = plane(0,0,0;0,0,1);\n'...
             'solid block  = orthobrick(-15,-15,-1;15,15,0) -maxh=0.3;\n'
...
             'solid mainobj= top and block;\n'...];
imdl = ng_mk_gen_models(shape_str, elec_pos, elec_shape, elec_obj);
imdl.stimulation = stim;
%inverse model: a smaller region directly over the electrodes with
coarser mesh
shape_str = 'solid mainobj= orthobrick(-14,-14,-1;14,14,-0.1) maxh=0.5;';
cmdl = ng_mk_gen_models(shape_str, [], [], '');
%define the mapping between the two meshes
c2f= mk_coarse_fine_mapping( imdl, cmdl);
% set the reconstruction parameters
inv3d= select_imdl(imdl, {'Basic GN dif'});
inv3d.solve= @inv_solve_diff_GN_one_step;
inv3d.hyperparameter.value = .03;
inv3d.RtR_prior= @prior_laplace;
inv3d.fwd_model.coarse2fine = c2f;
inv3d.rec_model = cmdl
figure
hh= show_fem(cmdl); set(hh,'EdgeColor',[0,0,1]);
hold on; show_fem(imdl); hold off
view(-16,22); set(gca,'Projection','perspective')
```

```
imgr = inv_solve(inv3d, vh, vi);
figure
show_fem(imgr); view(-16,22); set(gca,'Projection','perspective');
print_convert surface_sim04b.png '-density 150'
% Set levels for z-intercepts of -0.4,-1.0,-1.6
levels= [inf,inf,-0.9,1,1; inf,inf,-0.5,2,1; inf,inf,-0.2,3,1];
figure
show_slices(imgr,levels)
% % Try a different prior
inv3d.RtR_prior= @prior_noser;
inv3d.prior_use_fwd_not_rec = 1;
inv3d.hyperparameter.value = .8;
imgr = inv_solve(inv3d, vh, vi);
figure
show_fem(imgr); view(30,30); set(gca,'Projection','perspective')
print_convert surface_sim04c.png '-density 100'
% % % Set levels for z-intercepts of -0.4,-1.0,-1.6
levels= [inf,inf,-0.9,1,1; inf,inf,-0.5,2,1; inf,inf,-0.2,3,1];
figure
show_slices(imgr,levels)
print_convert surface_sim04d.png '-density 150'
toc
```